

FACULDADE DE ENGENHARIA DA UNIVERSIDADE DO PORTO

# Underwater Optical Communication an Approach Based on LED

**Bernardo Miguel Carvalho Silva**

FINAL VERSION



Masters in Electrical and Computers Engineering

Supervisor: Nuno Alexandre Lopes Moreira da Cruz

Co-Supervisors: José Carlos dos Santos Alves, Luís Manuel de Sousa Pessoa

October 30, 2015



A Dissertação intitulada

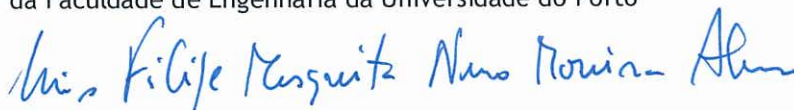
“Underwater Optical Communication: An Approach Based on LED”

foi aprovada em provas realizadas em 23-10-2015

o júri



Presidente Professor Doutor António José de Pina Martins  
Professor Auxiliar do Departamento de Engenharia Eletrotécnica e de Computadores  
da Faculdade de Engenharia da Universidade do Porto



Professor Doutor Luís Filipe Mesquita Nero Moreira Alves  
Professor Auxiliar do Departamento de Eletrónica, Telecomunicações e Informática  
Universidade de Aveiro



Mestre Nuno Alexandre Lopes Moreira da Cruz  
Assistente do Departamento de Engenharia Eletrotécnica e de Computadores da  
Faculdade de Engenharia da Universidade do Porto

O autor declara que a presente dissertação (ou relatório de projeto) é da sua exclusiva autoria e foi escrita sem qualquer apoio externo não explicitamente autorizado. Os resultados, ideias, parágrafos, ou outros extratos tomados de ou inspirados em trabalhos de outros autores, e demais referências bibliográficas usadas, são corretamente citados.



Autor - Bernardo Miguel Carvalho Silva





# Abstract

One of the major obstacles in the use of underwater robots on a large scale is the difficulty in communicating with the platforms during missions, since the most common methods of communication (via radio or other electromagnetic waves) used in commercial systems use signals that are strongly attenuated in water. Alternatively, acoustic-based solutions have long been the default wireless communication method for underwater applications, since they allow reasonable ranges. However, due to the severe limitations in bandwidth and the slow data rates with high latency, these are not the most efficient solutions. Summing up, using acoustics, applications such as monitoring and controlling remote operations are not practical.

In this project, it is intended to take advantage of the recent developments of the light emitting diode (LED), (specially with the higher light output and more precise tuning of the wavelength) and the photo-sensor technology. These will be used to develop an improved communication module, in response to the growing demand of robotic solutions for the marine environment that features a high speed communication system at short ranges, where low power, low complexity and small dimensions are pretended.

Using high brightness blue, cyan and green LED based transmitters and a blue/green enhanced photo-diode based receivers, the main goal is to achieve, with an abundant number of tests in all sort of conditions and environments, data transmission rates up to 1 Mbps over 5 meters with the capability of transmitting in sea and river waters.

The final step consists of the creation of an operational platform, to test multiple combinations of Tx/Rx configurations and relative orientations, and, using the information obtained through the tests, tune up the system, so its maximum efficiency can be reached, matching up all the delineated objectives.



# Acknowledgments

Começo este capítulo de Agradecimentos por dizer que apesar de ter feito questão de escrever esta dissertação em Inglês, porque achei que seria muito mais interessante um trabalho científico que demarca o final do percurso académico na faculdade, ser legível e ter visibilidade a um público mais abrangente nacional e internacional, escrevo estas palavras de agradecimento e de reconhecimento no bom e velho Português, pois estas palavras são dedicadas a algumas pessoas que me marcaram mais e que me ajudaram ao longo deste percurso. Apesar de aparentemente mais leigas, estas palavras tal como estas pessoas, para mim são as referências mais especiais.

Após esta introdução, começa propriamente os ditos agradecimentos, e queria começar por agradecer a quem originou este tema e este trabalho e também quem o apoiou, por isso aos meus orientadores Professor Nuno Cruz e Dr. Luís Pessoa. Obrigado por terem colocado este desafio, e obrigado por toda a disponibilidade, conselhos e troca de experiências. Não teria conseguido assimilar todo o trabalho sem a vossa ajuda. Ao Professor Nuno Cruz que desde o início, foi um dos fatores mais preponderantes na escolha desta dissertação, porque pela minha experiência no meu percurso académico, assumi de imediato que com o Professor iria conseguir trabalhar de forma mais autónoma, mas se precisasse de qualquer tipo de apoio, sabia que podia contar sempre com o Professor. Ao Luís Pessoa, muito obrigado não só por ter muitas vezes “iluminado” as dúvidas que persistiam, mas também por dar uma “luzes” acerca da componente mais científica do trabalho e por todo o apoio dado sempre que foi preciso arranjar algum tipo de material de laboratório, que nunca conseguia arranjar no departamento da faculdade.

De seguida, quero agradecer a toda a minha família, em especial aos meus avós, ao meu pai Alfredo, à minha mãe Florbela, e às minha duas irmãs, por ordem hierárquica, a Mariana e a Camila. Toda ela foi capaz de me dar força sempre que precisei, educação porque sempre precisei, motivação, inspiração, carinho,... basicamente um horror de coisas que nunca caberiam numa dissertação só. Agradeço só em especial a ambos os meus pais, por nunca duvidarem de mim, quando eu próprio o duvidei, e de me terem dado toda a liberdade para fazer tudo o que queria e quando queria, pois confiaram (e confiam) cegamente que farei tomarei sempre a escolha correta. É graças a eles que vivi tudo neste cinco anos. De resto, neste curto tempo para a dissertação, foram só boleias incontáveis até a faculdade a todas as horas, ir buscar a faculdade bem cedo (3h, 4h da manhã) para ainda poder dormir umas horitas, fazer diretas a ajudar a fazer testes num tanque de água na faculdade. Depois de cinco anos a viver ao máximo a vida académica, esta dissertação foi um passeio para eles... Às minhas irmãs, à Mariana quero agradecer por me ter mostrado o que é vida académica. Foste um exemplo e uma fasquia para mim, sendo a primeira a entrar na faculdade e a tentar viver tudo a que tinhas direito. Foi o teu amor ao teu curso e tudo que ele representa, que me fez quer ter aquilo que tu tinhas, e amar com tanta força como tu. À Camila obrigada por estares sempre presente quando precisava de descarregar o meu stress em alguém. A partir de agora, já sabes quem é que tens de superar. Boa sorte. Fico à espera dos meus agradecimentos. Ahhh... também deixo uma palavra à minha prima Catarina, por sempre ficar com aquele brilho nos olhos quando falava do primo que era Engenheiro.

À minha namorada Tina, também é outra pessoa que poderia dar numa dissertação. Desde de me ligar mais de 20 vezes de manhã para me acordar, a levar a casa quando a estrada estava complicada, a obrigar a descansar quando não queria mas precisava, . . . não sei como consegues, mas tens uma capacidade de me aturar que não acho normal. Não há ninguém como tu. . . Obrigado por toda a motivação, amor, carinho, paciência que me deste ao longo destes anos, e obrigado por nunca desistires de mim, mesmo quando nada funcionava. Mesmo NADA! Graças a ti que agora sou capaz de pensar em coisas de uma forma diferente, e de vivê-las de uma forma diferente. Por mais palavras que escreva, estas nunca farão jus a quem és nem ao que representas para mim. Deste-me um novo significado diferente ao número 13.

Estrategicamente, coloquei este último ponto nos agradecimentos. Deixo este último para todas as amizades que criei neste curtos cinco anos. Todas elas não fizeram parte da minha vida académica. Todas elas FORAM a minha vida académica. Não é possível escrever uma dissertação ou tese sobre elas, é preciso vivê-las para percebê-las. Foi só graças a elas, que consegui aprender tanto, num tão curto espaço de tempo. Com essas amizades, é que fui capaz de criar ainda mais amizades, e sentir como uma pessoa que já viveu mil e uma coisas e que conheceu tudo que havia para conhecer, para no momento a seguir, voltar a por numa situação totalmente nova e diferente. Foi a melhor experiência de vida, que alguma vez ambicionei ter. Não quero ser injusto para ninguém, mas deixo um abraço especial à F.A.N.F.A.R.R.A. de Electro, por me ter dado algo que nunca pedi, mas nunca irei esquecer, a pessoal mais velho que me moldou e fez pensar, pessoal mais novo com quem me diverti a gozar, e a pessoal do meu ano. A juntar a esta legião, aquele abraço especial ao Chuck, Corrector, Rodriguez, Locomotiva e Pintor. Ao Chuck por ser uma das pessoas que me ensinou mais, e um dos gajos mais filho da mãe que eu conheço. Ao Corrector por ser uma das pessoas que sempre acreditou em mim desde novo e com mais espírito, e um dos gajos mais filho da mãe que eu conheço. Ao Rodriguez por estar sempre aberto a falar comigo sempre que precisava de um ombro amigo, e um dos gajos mais filho da mãe que eu conheço. Qualquer um destes três senhores tem uma das características ditas. Ao Locomotiva não agradeço só eu, mas também esta dissertação, pois sempre que tive um problema no percurso académico, muito mais durante a realização desta dissertação, era sempre a ti que dirigia e tirava dúvidas. Este trabalho foi possível também graças a ti. E ao Pintor, por ter sido provavelmente quem sofreu mais comigo em cinco anos, mas que também quem pude sempre confiar para o que der, e vier. E também por ser um filho da mãe. Mereces tudo que ganhaste e conquistaste. Serão sempre estas grandes amizades que nunca esquecerei.

Dedico esta dissertação a todos vós.

Abraço,

Bernardo "Maquetista" Silva

*“Não chores porque acabou.  
Ri porque aconteceu.”*

Chuck Norris



# Contents

<b>Abstract</b>	<b>i</b>
<b>Acknowledgments</b>	<b>iii</b>
<b>Abbreviations</b>	<b>xiii</b>
<b>1 Introduction</b>	<b>1</b>
1.1 Context . . . . .	1
1.2 Motivation . . . . .	2
1.3 Objectives . . . . .	2
<b>2 State of the Art</b>	<b>3</b>
2.1 Underwater Communication Methods . . . . .	3
2.1.1 Acoustics . . . . .	3
2.1.2 Radio-Frequency . . . . .	4
2.1.3 Optical . . . . .	5
2.2 Underwater Optical Wireless Communication . . . . .	7
2.2.1 Optical Properties of Water . . . . .	7
2.2.2 Related Work . . . . .	12
2.3 Summary . . . . .	15
<b>3 Implementation</b>	<b>17</b>
3.1 System Design . . . . .	17
3.1.1 Design Constraints . . . . .	18
3.2 Optical Transmitter - Tx . . . . .	18
3.2.1 Light Source . . . . .	19
3.2.2 Light Source Driver . . . . .	20
3.2.3 Transmitter Tests . . . . .	21
3.3 Optical Receiver - Rx . . . . .	23
3.3.1 Photo-Receiver . . . . .	24
3.3.2 Acquisition and Processing of the Signal . . . . .	24
3.3.3 Receiver Tests . . . . .	29
3.4 Physical Casing . . . . .	39
3.5 Proposed Prototype . . . . .	40
3.5.1 LED Layer . . . . .	41
3.5.2 PD Layer . . . . .	43
3.5.3 Tx Layer . . . . .	44
3.5.4 Rx Layer . . . . .	46
3.5.5 Assemble and Connection . . . . .	50

3.6	Summary . . . . .	50
<b>4</b>	<b>Test Results</b>	<b>53</b>
4.1	Test Procedure . . . . .	53
4.1.1	Determining a Result and Related Problems . . . . .	55
4.2	Control Tests . . . . .	58
4.3	Workbench Tests . . . . .	63
4.4	Laboratory Pool Tests . . . . .	68
4.5	Summary . . . . .	71
<b>5</b>	<b>Conclusions and Future Work</b>	<b>73</b>
5.1	Summary of the performed work . . . . .	73
5.2	Concluded Objectives . . . . .	73
5.3	Future work . . . . .	74
<b>A</b>	<b>PCB Footprints and Schematics</b>	<b>77</b>
A.1	Initial Version . . . . .	79
A.1.1	Tx Layer . . . . .	79
A.1.2	Rx Layer . . . . .	82
A.2	Final Version . . . . .	85
A.2.1	Tx Layer . . . . .	85
A.2.2	Rx Layer . . . . .	88
	<b>References</b>	<b>91</b>



# List of Figures

2.1	RF propagation speeds in different types of water. . . . .	6
2.2	Different underwater optical wireless link configuration [1]. . . . .	7
2.3	Scheme representing the light propagation [2]. . . . .	8
2.4	Absorption of the EM spectrum in water. . . . .	9
2.5	Petzold VSF for various water types [2]. . . . .	10
2.6	Illustration showing how the multiple scattering in water affects the temporal dispersion of an impulse of light propagating through the water [2]. . . . .	12
3.1	Primary system design overview. . . . .	17
3.2	Detailed system design. . . . .	18
3.3	Simple Tx system design. . . . .	19
3.4	A MCPCB with green LUXEON Rebel LEDs. . . . .	19
3.5	Primary driver design. . . . .	20
3.6	The test setup for the MOSFET testing. . . . .	21
3.7	P30NF10 response time test: $F = 1\text{MHz}$ , $T = 250\text{ns}$ . . . . .	22
3.8	BS170 response time test: $F = 1\text{MHz}$ , $T = 250\text{ns}$ . . . . .	22
3.9	Setup scheme for Tx with MOSFET driver. . . . .	23
3.10	Simple Rx system design. . . . .	23
3.11	The BPW34 photo-diode. . . . .	24
3.12	Example of a TIA. . . . .	25
3.13	BPF configuration. . . . .	26
3.14	Frequency response of the BPF . . . . .	28
3.15	Comparator layout. . . . .	28
3.16	Initial Rx test setup. . . . .	29
3.17	The final test setup for the TIA testing. . . . .	30
3.18	Feedback resistor comparison: $F = 100\text{kHz}$ , without $C_p F$ . . . . .	30
3.19	Time response of the TIA with high gain: $F = 1\text{MHz}$ , $R_f = 100\text{k}\Omega$ . . . . .	31
3.20	Output signal of TIA: $F = 1\text{MHz}$ , $R_f = 10\text{k}\Omega$ , without $C_f$ . . . . .	31
3.21	Time response of the TIA: $F = 100\text{kHz}$ , $R_f = 10\text{k}\Omega$ . . . . .	32
3.22	Output signal of TIA: $F = 500\text{kHz}$ , $R_f = 10\text{k}\Omega$ , without $C_f$ . . . . .	32
3.23	Time response of the TIA: $F = 500\text{kHz}$ , $R_f = 10\text{k}\Omega$ . . . . .	33
3.24	Time response of the TIA: $F = 1\text{MHz}$ , $R_f = 10\text{k}\Omega$ . . . . .	34
3.25	Test setup for the BPF testing. . . . .	35
3.26	BPF output at $1\text{MHz}$ . . . . .	36
3.27	BPF at $1\text{MHz}$ with inverted output. . . . .	36
3.28	BPF inverted output at $5\text{MHz}$ . . . . .	37
3.29	BPF inverted output at $10\text{MHz}$ . . . . .	37
3.30	BPF inverted output at $10\text{kHz}$ . . . . .	38

3.31	BPF inverted output at $1.6kHz$ . . . . .	38
3.32	Test setup for the comparator testing. . . . .	39
3.33	Time response of the comparator at $1MHz$ . . . . .	39
3.34	Initial waterproof casing prototype. . . . .	40
3.35	Communication module prototype scheme and its layers. . . . .	40
3.36	Prototype light source components. . . . .	41
3.37	Final assembled light source. . . . .	42
3.38	Final assembly of the PD detection ring. . . . .	43
3.39	First prototype of the Tx layer. . . . .	44
3.40	The improvised capacitor in the primary prototype. . . . .	45
3.41	The primary Tx prototype on the left and the final Tx PCB on the right. . . . .	46
3.42	First assembly of the Rx layer. . . . .	47
3.43	Visible improvised modification in the first version of the Rx layer. . . . .	48
3.44	The change from the initial prototype to the final. . . . .	49
3.45	Preview of the order of the layers. . . . .	50
3.46	The nucleus of the communication module, assembled all together. . . . .	51
4.1	The two tested casings. On the left, the long one, and on the right, the short one. . . . .	54
4.2	The blue Tx, the module holder and green Tx. . . . .	54
4.3	The derivation circuit board. . . . .	55
4.4	The initial classification according to the Rx output (CH1:Tx, CH2:Rx). . . . .	56
4.5	The assumed classification according to the Rx output (CH1:Tx, CH2:Rx). . . . .	57
4.6	Results of the green and blue transmission with no casing nor optical lens. . . . .	58
4.7	Results of the green and blue transmissions, now with the optical lens. . . . .	59
4.8	Test results of the transmission at different levels of light interference. . . . .	60
4.9	Test results using different transmission frequencies of $100kHz$ and $1MHz$ . . . . .	62
4.10	Workbench test setup. . . . .	63
4.11	Results of the green and blue transmissions, using the two casing types. . . . .	64
4.12	Results of the interference of different levels of ambient light. . . . .	65
4.13	Results of the different module deviations. . . . .	66
4.14	Test results using different transmission frequencies of $100kHz$ and $1MHz$ . . . . .	67
4.15	Laboratory pool test setup. . . . .	68
4.16	Results of the green and blue transmissions, using the two casing types. . . . .	68
4.17	Results of the interference of different levels of ambient light . . . . .	69
4.18	Results of the different module deviations. . . . .	70
4.19	Test results using different transmission frequencies of $100kHz$ and $1MHz$ . . . . .	71
A.1	Initial PCB Schematic - Tx layer. . . . .	79
A.2	Initial PCB Footprint - Tx layer (only top layer). . . . .	80
A.3	Initial PCB Schematic - Rx layer. . . . .	82
A.4	Initial PCB Footprint - Rx layer (only top layer). . . . .	83
A.5	Final PCB Schematic - Tx layer. . . . .	85
A.6	Final PCB Footprint - Tx layer (only top layer). . . . .	86
A.7	Final PCB Schematic - Rx layer. . . . .	88
A.8	Final PCB Footprint - Rx layer (Top) . . . . .	89
A.9	Final PCB Footprint - Rx layer (Bottom) . . . . .	90

# List of Tables

2.1	Comparison table of some conventional underwater acoustic solutions [6, 7, 8, 9, 10, 11]. . . . .	4
3.1	Electrical and spectral characteristics of the LUXEON Rebel LEDs. . . . .	20
3.2	TIA block specifications. . . . .	34
3.3	BPF block specifications. . . . .	38
3.4	Comparator block specifications. . . . .	39
3.5	Electrical and spectral characteristics of the Cree XLamp XP-E2 LEDs. . . . .	41



# Abbreviations

APD	Avalanche Photo-Diode
AUV	Autonomous Underwater Vehicle
BER	Bit Error Rate
BPF	Band-Pass Filter
bps	bits-per-second
BPSK	Binary Phase-Shift Keying
DEEC	Department of Electrical and Computer Engineering
EM	Electromagnetic
ESR	Equivalent Series Resistance
IC	Integrated Circuit
IR	Infrared
LED	Light Emitting Diode
LD	Laser Diode
LOS	Line of Sight
MCPCB	Metal-Core Printed Circuit Board
MOSFET	Metal–Oxide–Semiconductor Field-Effect Transistor
OP-AMP	Operational Amplifier
OTS	Optical Telemetry System
PC	Personal Computer
PCB	Printed Circuit Board
PD	Photo-Diode
PMT	Photomultiplier
PSK	Phase-Shift Keying
QAM	Quadrature Amplitude Modulation
QPSK	Quadrature Phase-Shift Keying
RF	Radio-Frequency
RGB	Red-Green-Blue
ROV	Remotely Operated Vehicle
Rx	Receiver
SMD	Surface-Mount Device
TIA	Transimpedance Amplifier
TTL	Transistor-Transistor Logic
Tx	Transmitter
VGA	Variable Gain Amplifier
VSF	Volume Scattering Phase Function



# Chapter 1

## Introduction

### 1.1 Context

Technology has reached a point where much importance has been given to the creation of remote and autonomous robots, in order to enhance the preservation and comfort of human life, to contribute to the investigation and evolution of technology, among others. With such recent developments, the tasks at hand have been increasing in complexity and precision. In these case scenarios, when it is too dangerous, risky or complicated for a human to perform a task, these are mainly entrusted to a machine. To instruct this machinery and robots, it is necessary to establish communication between the operator and the machine. This communication is also valuable since it can transmit information that has been extracted from sensors.

Besides establishing communication via a physical cable, which has some limitations since it is a wire communication, wireless radio waves have been one of the most commonly used solutions in the aerial and terrestrial environments. However, trying to implement communications in underwater conditions raises completely new problems, since radio and other electromagnetic (EM) waves are highly attenuated underwater. Since wireless communications are a big advantage for this kind of environments, alternatives such as the use of acoustic modules became the standard option to communicate underwater. The inherent problems of this solution, despite the low attenuation and long distance range, reveals limitations in bandwidth and presents a high latency and high power consumption.

These problems have been the main barrier that restrains the use of underwater robots in a large scale, making underwater explorations an even more challenging and difficult task. Due to such limitations, alternative methods that allow underwater robots (like autonomous underwater vehicles (AUVs) and remotely operated vehicles (ROVs)) to transmit information have been an emerging thematic in the past few years and still represents many challenges, in order to achieve a more reliable solution.

## 1.2 Motivation

The necessity of underwater wireless communications results from the mobility requirements of robotic-based activities [12]. This is the main reason why physical connectors are not a viable solution to establish communication underwater [13]. In submarine operations, where a robotic vehicle has to perform complex movements, being dependent on a physical connector could limit the range and the precision of its moves. Besides, it represents an additional risk if the cables, for some reason, end up entangled, which could result in loss of valuable equipment and subjects of study. Even though acoustical-based systems are the default choice and are capable of establishing wireless communications underwater at a long distance range, the slow data-rates and high latency does not allow a real-time control and data harvesting. For these reasons, maintenance and surveillance operations based on acoustics are very limited.

There are many areas where an improved performance of the underwater wireless communications may have a big impact, such as in oil, gas and mining explorations, under the sea constructions, the study on the impact of deep-sea raw material resources exploitation, and the measurement and monitoring of physical, biological and bio and geochemical parameters (e.g. climate change) [12, 14, 15, 16, 2].

In order to surpass many of the obstacles presented in the underwater wireless communication, an optical light emitting diode (LED) based solution is suggested, since it presents the potential to overcome many limitations shown by other methods.

## 1.3 Objectives

The proposed solution is to create a short range underwater optical wireless communication system based on LED technology, in order to increase the efficiency in underwater communications. Ideally, the solution has to be a viable option to be implemented in an operational platform, such as an AUV. The experiments carried out along the whole period of work will be tested in wide and varied test scenarios, such as in a controlled laboratory scenario, simulating communications inside a test pool, and in real life scenarios, trying to communicate in two distinguished environments: the ocean and the river. To reach this goal the following objectives will be considered:

- Assembly of a LED and photo-sensor based test system;
- Creation of an underwater wireless link that enables the transmission of information;
- Create a system that is able of test different transmission parameters;
- Create a real-life solution, that could be implemented in a robotic platform;
- Test of the system in the laboratory;
- Test of the system in the laboratory pool; and
- Test of the system in real life environments (Ocean and River).



## Chapter 2

# State of the Art

In this chapter, it is presented all the major scientific work developed about underwater communication. It starts by analyzing the many methods of underwater communication, considering all the pros and cons for each presented approach.

Subsequently, it will focus on developing the thematic of underwater optical wireless communication, taking in special consideration the optical properties of the various water types that are used as transmission channels, and it will be studied all the related works and solutions that have been developed until this moment, academic and commercial.

In the end, there will be a sum up about all the chapter.

### 2.1 Underwater Communication Methods

As analyzed by [12, 17], underwater communications are traditionally made with a physical connector, made by cables or fiber-optics. These represent some advantages, since they are capable of transport electrical power and offer a high speed and reliable communication. However, their use can limit the range and maneuverability of underwater operations, and the presence of a long and heavy cable and the associated hydrodynamic drag, increases the risks of an operation.

For these reasons, there is a high interest on the investigation of alternative ways to transmit information underwater, without being dependent on a cable connection. This is why it has been given a big importance to the wireless communication techniques. Next it is presented the most common methods of underwater wireless communication, referring their advantages but also the problems they face [16].

#### 2.1.1 Acoustics

Acoustics has for a long time been the standard solution for submarine missions because of the fact that sound propagates well underwater, it enables the transmission of the information without been dependent on an "umbilical" cable, which gives to the underwater vehicles the necessary mobility to perform complex movements freely. Adding to this, its relative low signal attenuation and long range allows the transmission of information in the order of the kilometers. Despite all these

advantages, this solution also carries some problems that begin when the speed of transmission is important[16].

As referenced by [18], this method has its disadvantages, because it presents a low propagation speed (high latency). Moreover, it has a low bandwidth with a maximum data-rate in the order of the tens of thousands bits-per-second (bps), making the acoustics communication a slow option for transmission. This method also presents other problems, such as its susceptibility to multipath propagation, dispersion, frequency fading and ambient noise (specially in shallow waters).

The next table 2.1 contain some available acoustical solutions and their main characteristics.

Table 2.1: Comparison table of some conventional underwater acoustic solutions [6, 7, 8, 9, 10, 11].

Model	Distance (m)	Data-Rate (kbps)	Power (W)	Weight in Air (kg)
HERMES	120	150	32	—
Sonardyne AvTrak6 Type 8220	3000	9.0	50	5.1
AquaSeNT - AM-OFDM-P1	4000	9.0	20	7.6
AquaSeNT - AM-OFDM-S1	4000	1.6	20	2.4
Benthos - ATM-916	6000	15.36	15.75	4.5
Benthos - ATM-926	6000	15.36	15.75	4.1
Benthos - ATM-966	6000	15.36	24.5	6.8
EvoLogics - S2CR 48/78	1000	31.2	60	6.5
EvoLogics - S2CR 18/34	3500	13.9	80	6.5
EvoLogics - S2CR 12/24	6000	9.2	40	7.78
EvoLogics - S2CR 7/17	8000	6.9	80	7.78
LinkQuest Inc. - UWM1000	350	19.2	2	4.2
LinkQuest Inc. - UWM2200	2000	38.4	6	3.0
LinkQuest Inc. - UWM3000	5000	5	12	4.1
LinkQuest Inc. - UWM4000	4000	9.6	7	7.6
LinkQuest Inc. - UWM10000	10000	5	40	21.0

### 2.1.2 Radio-Frequency

On the other hand, there are the EM waves such as radio, a very popular choice to transmit information via wireless in terrestrial communications. As stated by [15, 16], EM waves such as radio-frequency (RF) compared to acoustic waves, are much faster and have a higher bandwidth, in this terrestrial transmissions.

In addition, radio produces a high throughput compared to sound waves, with speed levels surrounding the hundreds of kbps up to ten meters, and achieving tens of Mbps at the range of one meter. Again, comparing both power consumptions, the radio reveals to be more energetically efficient than acoustic technology, needing less power.

Even with these characteristics, there are many limiting factors when using RF in water. The EM waves have different behavior in freshwater and seawater.

According to [16], freshwater is considered to the EM as a *low-loss medium*, and its propagation speed  $c$ , and the absorption coefficient  $\alpha$  can be represented as:

$$c \approx \frac{1}{\sqrt{\epsilon\mu}} \quad (2.1)$$

$$\alpha \approx \frac{\sigma}{2} \sqrt{\frac{\mu}{\epsilon}} \quad (2.2)$$

In the equations  $\epsilon$  is considered the dielectric permittivity,  $\mu$  is the magnetic permeability and  $\sigma$  is the electric conductivity. By observing this expressions, it can be concluded that the absorption for freshwater is independent of the frequency of the signal, and propagation speeds of EM are smaller than light, but still faster than sound [16]. The only inconvenient for this solution, in freshwater, is the antenna size that is required in order to obtain a large bandwidth.

To EM waves, the seawater is considerate as a *high-loss medium*, and its propagation speed  $c$ , and the absorption coefficient  $\alpha$  can be represented as:

$$c \approx \sqrt{\frac{4\pi f}{\mu\sigma}} \quad (2.3)$$

$$\alpha \approx \sqrt{\pi f \mu \sigma} \quad (2.4)$$

As it can be concluded by the equations 2.3 and 2.4 both are dependent of the frequency of the signal  $f$ , meaning that if a high frequency is used, a high speed is obtainable, but the absorption of EM waves is also high.

It is possible to conclude that communication through EM waves is limited in freshwater by the size of the antenna needed, and has a critical problem because of the high attenuation in seawater. In figure 2.1 it is shown the different RF waves in different types of water, comparing their performance with the light and sound waves.

Although it is known that RF is not the ideal method to communicate, there are some commercial possibilities. WFS Technologies Ltd commercializes a underwater wireless RF system for sub-sea exploration, the Seatooth® , a system series claimed to have a model capable of achieving 156 kbps over 7 meters [19]. Although there are some situations where this system could be used, it still requires a high power consumption, around 15 Watts, and an antenna with large dimensions (1 meter squarial antenna).

### 2.1.3 Optical

An optical solution is another transmission method still in development that shares some advantages of the RF, but not all of its disadvantages. The major advantage comparing to RF communications is the possibility of maintaining the same conditions underwater without considerable losses. As RF, this solution can obtain in a underwater environment, a high throughput in the

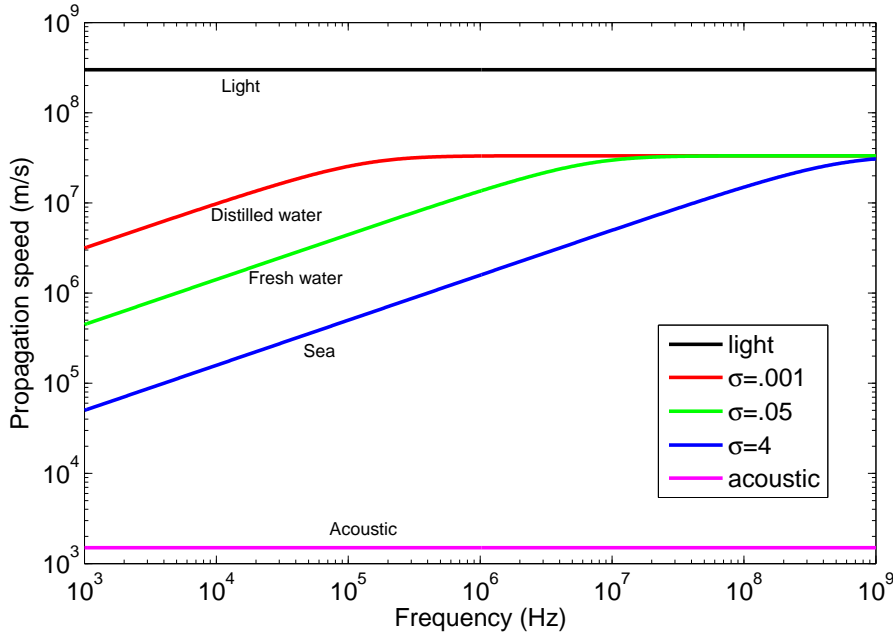


Figure 2.1: RF propagation speeds in different types of water.

order of several Mbps to Gbps, a high propagation speed (low latency) and achieve short and mid-range link distances in the order of 100-200m [14, 1, 17]. In [14] also referred that underwater optical communication can benefit meaningfully from the progress made in the terrestrial optical wireless communication, becoming an area in constant evolution.

Like any system, optical solutions have some inherent problems. Although optical signal have a low attenuation, it becomes relevant in long distances [14]. For that reason, acoustic vastly outperform the optical channel when comes up to distance range. Other relevant disadvantages, in addition to the absorption, optical scattering is significant and the ambient light can also interfere with communications [16].

Another complex problem associated to this method is the dependence on a clear way for the light to travel, a line of sight (LOS) [14]. In the beginning, without a clear LOS it was impossible to establish communication, since the light cannot reach the destination. For that reason, some alternative methods were created to prevent the loss of the LOS, and to create optical links. Figure 2.2 shows some of these methods.

With these variant high bandwidth links options, it is possible to create sophisticated and collaborative paths for planning and observation [14, 1].

In figures 2.2a and 2.2b is represented a communication channel based on a clear and simple LOS, where communication exists by emitting light in a narrow beam (similar to laser) and in a diffuse beam, respectively. Figure 2.2c shows a retro-reflector link type, used when limited dual communication is necessary, and the receiver is awfully low powered to perform as a full transceiver (such as underwater sensor nodes). In this configuration the light of the transmitter is

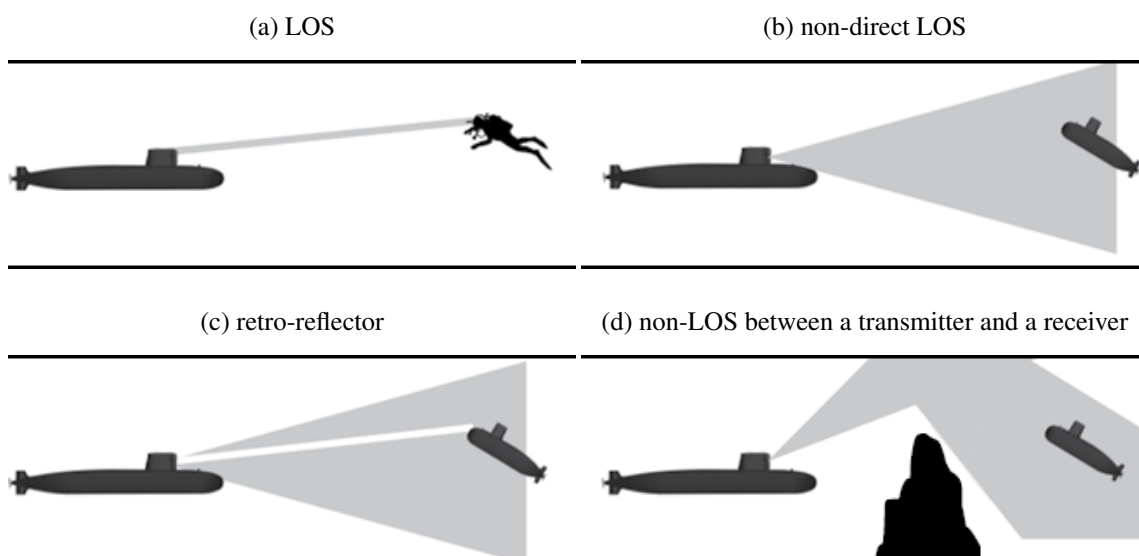


Figure 2.2: Different underwater optical wireless link configuration [1].

reflected back from a modulated retro-reflector on the receiver that, in the meantime, is encoded with information. Another link represented in 2.2d is a non-LOS transmission where the transmitter and the receiver position themselves diagonally upwards to transmit and receive the light reflected in the surface of the water.

## 2.2 Underwater Optical Wireless Communication

Seeing the potential of the optic channel in the underwater environment, the attention of this work is focused on study, with some detail, the optical communications. It starts by analyzing the optical properties of the water channel to obtain a detailed overview of the behavior of light in water, and will end in reviewing some major achievements in the field of knowledge.

### 2.2.1 Optical Properties of Water

As concluded by [2], the behavior of light in water is a very complex issue. There are extensive works regarding this thematic, since it has many interests in many fields of science. Since this work is mostly focused in the conception and implementation of a practical solution, this thematic will be briefly referenced, taking into account the work done by [2].

Assuming a differential portion of water (represented by a volume with three dimensions), with a width of  $\Delta r$  and with an small height and length, it is assumed that the amount of light entering the volume equals the amount of light leaving it, less any loss that occurred on the volume in the form of absorption and/or scattering. This phenomenon is represented in figure 2.3.

The incident power is represented by  $\Phi_i$ , the absorbed power by  $\Phi_a$ , the scattered power by  $\Phi_s$  and the transmitted power is represented by  $\Phi_t$ . These values are dependent of the wavelength  $\lambda$ .

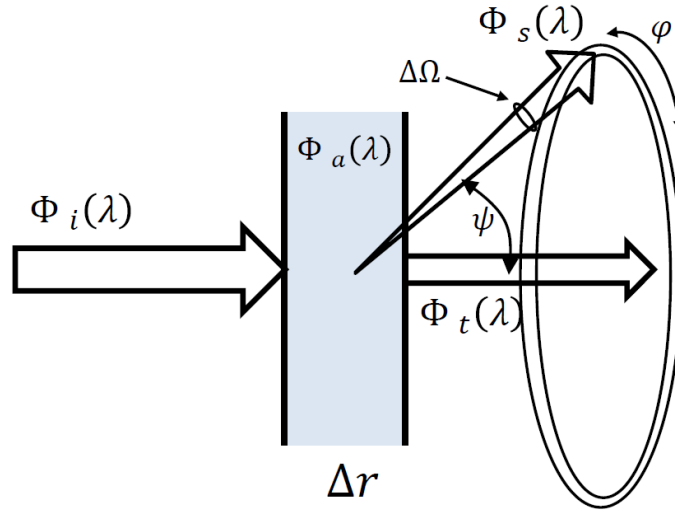


Figure 2.3: Scheme representing the light propagation [2].

The incident power  $\Phi_i$  is measured as:

$$\Phi_i(\lambda) = \frac{hc}{\lambda} \frac{N}{\Delta\lambda}, \text{ (W/nm)} \quad (2.5)$$

By relating the incident power with the resulting power transfers, it is obtained the absorptance defined by  $A(\lambda)$ , the transmittance  $T(\lambda)$  and the ratio of scattered power  $B(\lambda)$ . They are equal to:

$$A(\lambda) = \frac{\Phi_a}{\Phi_i} \quad (2.6)$$

$$T(\lambda) = \frac{\Phi_t}{\Phi_i} \quad (2.7)$$

$$B(\lambda) = \frac{\Phi_s}{\Phi_i} \quad (2.8)$$

Dividing the previous result by the distance  $\Delta r$ , as it approaches zero, the values are reduced to coefficients which measure the losses per unit of distance. So the absorption coefficient  $a(\lambda)$  and the scattering coefficient  $b(\lambda)$  equal to:

$$a(\lambda) = \frac{dA(\lambda)}{dr}, \text{ (m}^{-1}\text{)} \quad (2.9)$$

$$b(\lambda) = \frac{dB(\lambda)}{dr}, \text{ (m}^{-1}\text{)} \quad (2.10)$$

With this, the total loss is expressed by the attenuation coefficient  $c(\lambda)$  and equals to:

$$c(\lambda) = a(\lambda) + b(\lambda), \text{ (m}^{-1}\text{)} \quad (2.11)$$

Another value that can be used is the single scattering albedo which defines the ratio of scattering loss to total losses that is represented by  $\omega_0$ , and as the value:

$$\omega_0 = \frac{b}{c} \quad (2.12)$$

In a closer overview on the energy losses, the power absorption occurs when the photon energy is lost due to interaction with the water molecules or other particles. This energy is lost in the form of heat, leading to an attenuation of the light signal.



Figure 2.4: Absorption of the EM spectrum in water.

As it can be observed in figure 2.4, the EM spectrum reveals a small gap in the visible light, where the absorption is reasonably low, making the visible light a good transmitter in those values of wavelength. This assumed value can vary depending on the type of water and its characteristics, such as the suspended materials in it, the chlorophyll concentration, among others. In [1] it is assumed that absorption seems to be lower in sea water between the 400nm and 505 nm, which translates in the visible spectrum from the dark purple to the cyan light, but also stated further in the same document that typical communication links are usually between 430 and 530 nm. But in [17] it is announced that the spectral range goes from 450 and 550 nm, from deep blue to green light, respectively. Again, these assumptions may vary depending on the characteristics of the water.

The scattering happens when the photon's path is changed due to the interaction with particles. This results in a widening of the beam, in terms of space and time, making the light signal more diffuse. This effect is strongly dependent of the turbidity of the water.

Also as shown by figure 2.3, the beam loss from scattering  $\Phi_s$  is dependent on the angle  $\psi$  of deviation from the incident beam direction. As the scattering particles in ocean water are randomly distributed, the radial angle of scattering is symmetric. With this, the angular distribution of scattering, called the volume scattering phase function (VSF), is defined as:

$$\beta(\psi; \lambda) = \lim_{\Delta r \rightarrow 0} \lim_{\Delta \Omega \rightarrow 0} \frac{\Phi_s(\psi; \lambda)}{\Phi_i(\lambda) \Delta r \Delta \Omega}, \quad (m^{-1} sr^{-1}) \quad (2.13)$$

If  $\beta$  is integrated over all angles, a  $b(\lambda)$  can be expressed as:

$$b(\lambda) = \int_{4\pi} \beta(\psi; \lambda) d\Omega = 2\pi \int_0^\pi \beta(\psi; \lambda) \sin(\psi) d\psi \quad (2.14)$$

In figure 2.5, it is possible to see the VSF as a probability distribution of scattering versus angle.

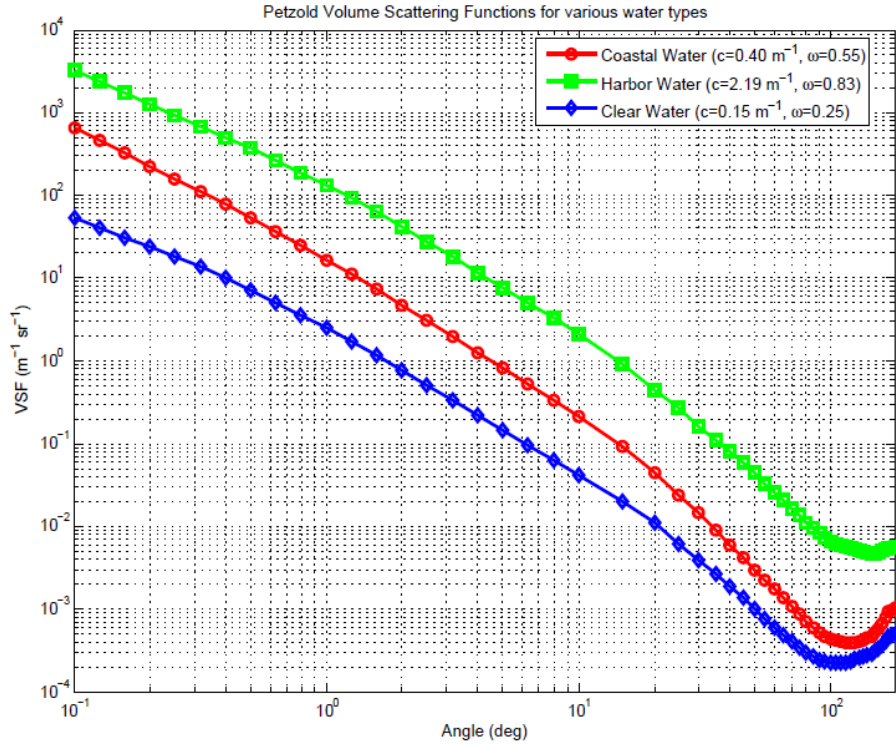


Figure 2.5: Petzold VSF for various water types [2].

By analyzing the image, it is possible to note that VSF peaks at small angles, suggesting the tendency of light to scatter at small angles as it propagates.

After analyzing the output optical power, it is given a view from the receiver. The received optical power entering the receiver can be expressed as:

$$P_{receiver} = P_{transmitter} \tau_{optics} \tau_{channel} \tau_{pointing} \tau_{geometric} \quad (2.15)$$



Where  $\tau_{optics}$  is the loss from the receiver and transmitter optics, the  $\tau_{channel}$  is the loss absorption and scattering, the  $\tau_{pointing}$  is the loss from angular and spatial misalignment between transmitter and receiver and  $\tau_{geometric}$  is the geometric loss from the beam spreading.

Being the incident power described by  $I$ , over a path length  $r$ , the attenuation coefficient can be used to describe the total loss. That said, the differential path loss is:

$$\frac{dI}{dr} = -cI \quad (2.16)$$

Integrating this expression it is obtained:

$$\int_{I_0}^I \frac{1}{I} dI = -c \int_0^r dr \Rightarrow \ln(I) - \ln(I_0) = -cr \quad (2.17)$$

When simplified, becomes the common expression for Beer's Law-type loss:

$$I = I_0 \exp(-cr) \quad (2.18)$$

This equation assumes that all scattered light is lost from the beam and that no multiplied scattered light returns to the beam. In addition, the radiative transfer equation expresses the conservation of energy of an underwater beam of light. It takes into account losses and gains into the central received beam. This equation takes the form of:

$$\cos(\theta) \frac{dL}{dz} = -cL + \int_{4\pi} \beta L d\Omega \quad (2.19)$$

Where:

$$L(z, \theta, \phi) = \frac{\Phi(z, \theta, \phi)}{\Delta A \Delta \Omega} \quad (2.20)$$

This  $L$  represents the radiance at depth  $z$  in the direction defined by the angles  $\theta, \phi$ .

The geometric losses can be calculated as the ratio of receiver area to transmitter beam spot area at the receiver. The surface area of a diffuse point source light field at the measurement distance is calculated by:

$$A_{rx} = \pi R^2 \tan^2(\theta/2) \Rightarrow A_{rx} = \frac{\pi}{4} (R\theta)^2 \quad (2.21)$$

The geometric loss can be expressed as:

$$\tau_{geometric} = \frac{P_{rx}}{P_{tx}} = \frac{D_{rx}^2}{(R\theta)^2} \quad (2.22)$$

Lastly, the temporal dispersion can be problematic, since multiple scattering affects the temporal dispersion of an impulse of light propagating through the water. This effect is illustrated in figure 2.6. A common method to analyze this temporal response is to estimate it in the frequency domain.

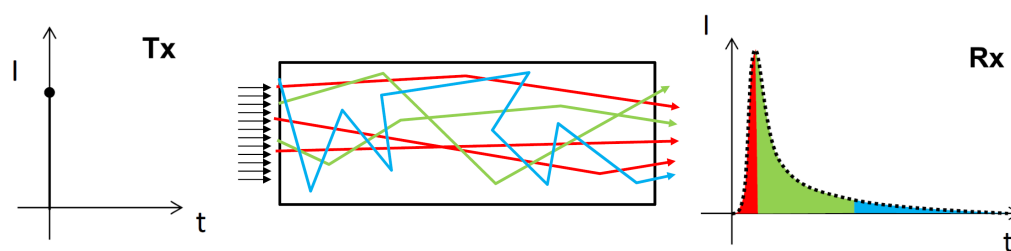


Figure 2.6: Illustration showing how the multiple scattering in water affects the temporal dispersion of an impulse of light propagating through the water [2].

After this overall look on the physical behavior of light, the research is continued by reviewing other works in the area.

### 2.2.2 Related Work

The pretended approach to this work is to develop and implement an LED-based underwater communication module. Many works and ideas have been done in this area of research and some have the pretended characteristics. This section reviews the systems that are the most relevant to this dissertation. This review will be mainly focused on experimental works, and the prototypes created ever since. It is hoped that, in the end of this section of this review, a solid idea of the system and their many components is reached. It starts by analyzing [21], where the author, using LEDs as a laser, with wavelengths of 660 nm and 450 nm and off-the-shelf components, achieves, in clear, dark waters, a communication rate of 10 Mbps over ranges of 20 meters.

In [22], it is used an amplifier to drive a 1-W LED with a 10BaseT Ethernet signal and a PD as a receiver also with a 10BaseT. It was tested in a tank with 4.6 meters of distance, with successful results. It is extrapolated that the system is possible to reach up to 16 meters.

In both [23, 24] the author tried to calculate the power required to maintain a bit error rate (BER) of  $10^{-6}$  for many distances and speeds. His model used the Beer's Law to combine the losses of absorption and scattering. He was able to compute a required transmit power of 300 mW a data rate of 10 Mbps over 100 meters. It was also admitted that effects such as multipath and signal spreading was irrelevant to speed down to 10 Mbps. Their structure used six LEDs transmitting in a wide angle of  $2\pi$ .

A small optical communications transceiver was designed by [12] with the idea of using this to control a swarm of submersible robots. To do this, a physical (PHY) layer based on the MCP2120 IrDA encoder/decoder chip was used. The receiver was a PD with a MAX3120 for amplification and filtering. It used LEDs with wavelengths of 460, 490 and 520 nm. With a UART transmitting at 57.6 kbps, the tests made in air achieved 1.71, 2.02 and 1.49 meters, to each wavelength respectively, and in water all of them achieved 1.7 meters of range.

In both [26, 27], a commercial solution to establish communication, the Ambalux modem [28] (a more detailed description will be given further in this document) is presented. The tests were performed in a lake in Canada and in a pool, obtaining a 9.69 Mbps at 11 meters and 8.2 Mbps at

21 meters, respectively. It was also presented a prototype of a spherical transmitter and receiver, projected to obtain transmitting data-rates of 20 Mbps over 11 meters, although it only achieved the 115kbps over 15 meters. After some improvements in software, it was able of reach 1.5 Mbps.

In [14], it is used a 405-nm laser for transmission and the miniature Hamamatsu R7400U photomultiplier (PMT) in conjunction with a variable gain amplifier (VGA) on the receiving side. The system is tested using a water tank with reliable communication at 500 kbps in distance of 3.66 meters width.

It was demonstrated in [29] that a laser-based system was capable of error-free data rates of 1 Gbps over a 2 meters path in a water-filled pipe. The system uses a 7 mW, to generate a 532 nm laser. It was use an avalanche photo-diode (APD) as a receiver.

In [30], it was built a glass sphere to improve the field of view of the receiver, which also housed a PMT, and used an external power source to feed the output signal to an external digitizer. The system was able to communicate at rates up to 5 Mbps and distances up to 200 meters in deep clear waters in Bermuda, and in shallow murky waters achieved 2.5 Mbps over 40 meters at Woods Hole dock, in Woods Hole, Massachusetts, USA.

The [31] created 3 distinguish models, a long range modem, a short range modem and a hybrid one, where only the components complexity differs between them. It was able to achieve an error-free communication at 4 Mbps over 2.2 meters and 2.4 meters, with a wavelength of 470 nm and 532 nm, respectively. In the short range and hybrid the receptor used a PD, and in the long range was used an APD.

In [32] it was proposed a two-transmitter two-receiver spatial diversity system that used a 200 mW, 405 nm laser together with a beam splitter to generate two parallel optical beams. The lenses are used to focus the light for two amplified photo detectors. It was transmitted through a water tank where it was previously injected bubbles to generate interruptions of the optical beam. It is shown that the setup, using a data rate of 500 kbps, reduces fading-induced errors by a factor of 10, when compared to a single 200 mW transmitter, single-detector system.

The system projected in [15], implements a unidirectional communication system using a light engine that consumes 4.8 W, has 465 nm of wavelength and uses a PD as a receptor. It uses a MOSFET as a driver for the LEDs. The communication is made with OOK modulation and achieves a 1 Mbps communications over 13 meters of distance, with no errors.

In [33] it transmits data through a water tank using a 3-W LED at 470 and 525 nm. It is used two setups: in one, they transmit over a length of 3 meters through turbid water, and in the other they transmit over a length of 7.7 meters through less turbid water (one to two attenuation lengths). A PMT is used to receive the first signal and a PD to receive the second signal. Their system achieves 5 Mbps throughput.

Another reference is [34] who presents an improvement of [31] by making a bidirectional version, called AquaOptical II, which uses 18 LEDs and the same APD as the previous version. The LEDs transmit at a wavelength of 470 nm with a total transmit power of 20W. An FPGA is used for PHY processing, and an ARM7TDMI processor handles the MAC and provides an

external 10 Mbps Ethernet interface. The communication has a data rate of 4Mbps at a distance of up to 50 m in a pool. In a laboratory setting transmitting through air it is 32 Mbps.

In both [35, 36] is described an optical telemetry system (OTS) with which it downloaded 20 MB of data over a 5 Mbps link at a range of 80 meters. It reports communications at a data rate of 10 Mpps at a distance of 108 meters, 5 Mbps at distances of up to 128 meters, and 1 Mbps at distances of up to 138 meters.

In [37] the author tries a different approach by designing a more efficient transmitter and receiver. With an array of 7 LEDs to the transmitter, and 7 PD for the receiver, displayed in the form of a truncated hexagonal pyramid structure with a special lens, the transmitted light gets more focused and the received light can be captured more efficiently, obtaining a quasi-omnidirectional transmitter and receiver.

Document [38] gives a continuation work on the AquaOptical project [31, 34], which uses the developed hardware, and its upgrades resulting in the AquaOptical II. Also in this paper, by using the AquaOptical II, a base signal strength model to end-to-end communications is projected. It is a great literature that reviews all the recent works done in the area.

In [39], using a laboratory set-up, it was investigated the impact of background noise on the receiver in shallow waters. It was used a 2.5 meters test pool to study the effect. The two transmitters used LEDs, but the receiver was constituted by an APD and a PD. For this experiment it was obtained, using Manchester Coding 6.25 Mbps, 12.5 Mbps using NRZ 8b/10b code and 58 Mbps with DMT. It was estimated that maximum distance was around the 60 meters in clear water and 10 meters in murky.

Now, it will be shown some of the commercial solution available, for underwater optical wireless communication.

As referred before, the Ambalux Corporation [28] manufactures modems that establish communication point-to-point, capable of achieving 10 Mbps and up to 40 meters range. The interface is 10BaseT Ethernet compatible allowing TCP/IP and UDP connections. The transmitter consumes up to 36 W and the receiver 7.2 W.

As a product from the investigation in [26, 27], the devices created by the author were posteriorly commercialized by the company Penguin Automated Systems, Inc. [40]. Same characteristics of the developed device are considerate.

Another commercialized product is the Neptune, produced by SA Photonics [41], that is claimed that it can achieve 250 Mbps over 200 meters, with a power consumption larger than 5 W.

From the work of [30], the company Sonardyne International Ltd. adopted the system along with an LED-based model for near-surface communications. The product is the BlueComm [42] and it claims that is capable to achieve up to 20 Mbps of data rate and up to 200 meters of range.

## 2.3 Summary

This chapter presented the research work that has been done in underwater communications, beginning with a reference on the underwater optical wireless communications. It was possible to conclude that, in all the underwater communication methods, wireless communications are a must-use solution and the optical communications are a new and promising method to make communication links underwater. After all, this is an area that is still in investigation, for its incredible benefits, but also its complex problems.

When studying the optical properties of water, it was clear that different environments, where water visibility is not the ideal, will obviously limit the propagation of light, not only affecting the speed of the connection, but also influencing the wavelength needed for the attenuation to remain low.

In the review of other works, some knowledge was obtained about the architecture of the system, their main components and what are the best materials to obtain the best, expected results, and common errors and difficulties found in this area of work. With this acquired information, a solid and studied design system can now be done.



## Chapter 3

# Implementation

In this chapter it is presented the implementation and development of the underwater communication module prototype.

Initially, it is shown the proposed methodology for the implementation of the system, showing the design and its constraints, the different layers that form the proposed module, specifying the component selection, dimensioning and its design, ending with the display of the produced prototype.

### 3.1 System Design

In the primary system design, shown in figure 3.1, it was intended that a pack of data would be present in a computer and, by modulating this data into a light signal, it would be sent by a transmitter (Tx), then this light signal would be captured by the receiver (Rx), and the end terminal would demodulate and show the data.

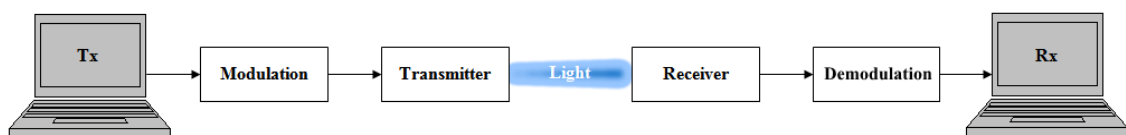


Figure 3.1: Primary system design overview.

After some development, the more detailed redesign solution in figure 3.2 was achieved. It is similar to the initial one, where a computer terminal tries to communicate with a peer, using the optical channel, but it is intended that the computer communicates with a micro-controller that connects to the computer (PC) and the Tx/Rx via serial communication. Also, after some considerations, the design would be physically able of establish bidirectional communications with two distinct colors.

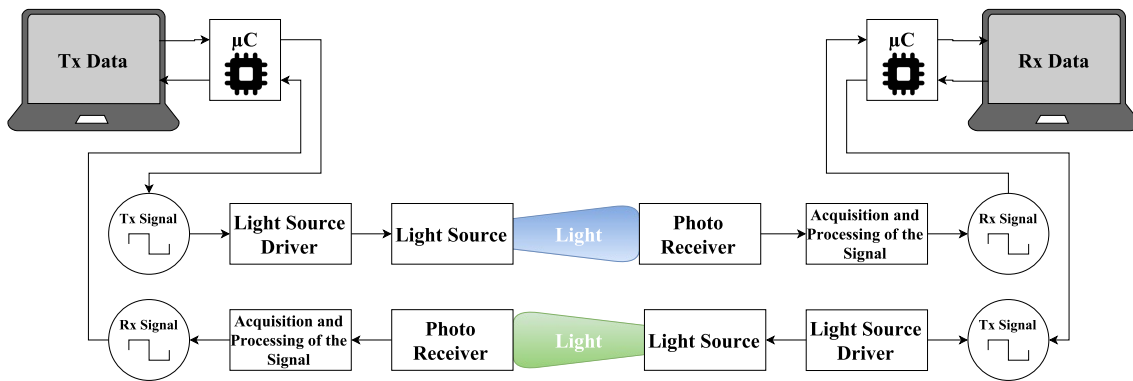


Figure 3.2: Detailed system design.

### 3.1.1 Design Constraints

The reviews that were made show that underwater optical wireless communication is a viable solution to be implemented in an operational platform, such as an AUV, for communication purposes. So, if it is pretended to implement a module in an AUV, some standard necessities must be taken into account. Because an AUV is an autonomous vehicle that operates in an underwater environment, the device that will be attached to it, in addition to the full protection of the electronics from water, which has to be assured, must be as efficient as possible, mainly in terms of energy, and also have a small physical size. For that reason, these initial simple requirements are noted:

1. Maximum range - up to 5 meters;
2. High data-rate - at 1Mbps;
3. Low power - below the 5W;
4. Small size - relatively smaller than 15 centimeter long;
5. Low weight - made with light materials; and
6. Low complexity - simple and modular.

There are other requirements, such as a low-cost solution, that could be considered, but for the purpose of this dissertation, these will be somewhat overlooked, making the choice based on common sense.

## 3.2 Optical Transmitter - Tx

With the optical transmitter, it is pretended to design a circuit that is capable to output as much light as possible. This operation will be done through a driver that feeds the chosen light source to obtain the maximum performance of it, to be able to achieve a wide range. The data rate will also be limited by the time response of the components that the transmitter is made of, so a studied



selection for the module components is advised. Figure 3.3 gives a simple view of the optimal solution.

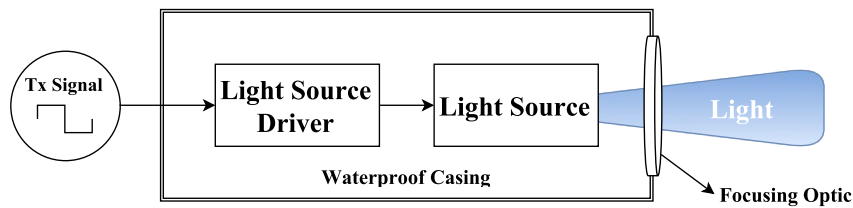


Figure 3.3: Simple Tx system design.

In the following subsections, a study and some functional tests will be performed to better choose the best light source and adequate driver for it.

### 3.2.1 Light Source

Since one of the objectives of this dissertation was the creation of a LED-based system, primarily it was necessary to decide a light source for the transmitter. Two possibilities for a general LED-based light engine were considered: a diffuse light source, available as a LED or a concentrated beam, as a laser, in this case a laser diode (LD).

Between the two choices, the diffuse LED light source was considered as a more appealing solution. Although using a LD would be efficient since it has a narrower EM spectrum, higher light intensity at long distances and faster switching speed, the LD presents a complex problem of misalignment at long distances, and a diffuse light engine is able to adjust its light beam using an optic, making it a much more versatile solution. Other issues regarding the LD were also taken into account, such as a higher power consumption and a much greater cost.

The light source for the Tx ended up to be high-power LEDs, where characteristics such as small size, high-brightness, narrow EM spectrum and other optical features were desirable. Also, the existence of the three colors (blue at 470 nm, cyan at 505 nm and green at 530 nm) originally pretended would be an advantage.

For these reasons, for the initial testing and understanding of the system, it was only used LUXEON Rebel green LEDs, shown in figure 3.4, since it was available an example of these LEDs (provided by INESC TEC) and these met up the principal necessities described before.

Table 3.1 shows some of the most relevant information about the LUXEON Rebel LEDs, distributed according to their light color. Since the seven LEDs are connected in series, to obtain the maximum output of light, but still respecting the typical data-sheet values, it is necessary to supply about 20.3V at 700mA. But since one of the objectives is to be implemented in an operational



Figure 3.4: A MCPCB with green LUXEON Rebel LEDs.

base or an AUV, the LEDs supply will be set to more typical values of 24V at 700mA (which corresponds to two batteries of 12V), with the remaining voltage been dissipated by a dimensioned resistor, indicated for this operation.

Because the system is supposed to be controlled by a micro-controller, the switching signal respects the transistor-transistor logic (TTL) levels. So it was necessary to dimension a LED driver that was able to switch the LEDs at the necessary frequencies and, at the same time, supplying the necessary current and voltage they require.

Table 3.1: Electrical and spectral characteristics of the LUXEON Rebel LEDs.

Component	Typical Voltage (V)	Typical Drive Current (mA)	Typical Wavelength (nm)
Green: LXML - PM01	2.9	700	530
Cyan: LXML - PE01	2.9	700	505
Blue: LXML - PB01	2.95	700	470

As referred, although with the sample there was no optical lens available for testing, for the final prototype it is intended to use some optical device to increase and optimize the light output of the 7 LEDs.

### 3.2.2 Light Source Driver

As explained previously, it is expected that the signal respects the TTL, meaning that it will vary between 0V and 5V (depending if the bit value is '0' or '1', respectively).

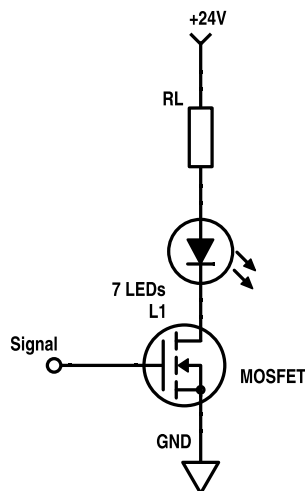


Figure 3.5: Primary driver design.

There are some driver solutions available in the market that can drive these kind of high-brightness LEDs, just like the previously used, but for this application in this dissertation, the LEDs must be switched in the highest frequency rate as possible, maintaining a maximum throughput power at the same time. Although commercially there are some solutions to drive this sort of LEDs with high power outputs pretended or with relative high frequency switches, finding a solution that can perform both operations at the same time is another issue. The solutions presented in the market are too complex, large in size or inefficient. For those reasons, it was considered more beneficial to design an appropriate LED driver for this application, which is capable of meeting the requisites, while maintaining a simple complexity.

One of the initial ideas was to control the high current supply of the LEDs through a transistor. There are many types of transistors that could perform the pretended function (BJT, JFET, IGBT and more), but for this kind of application, precisely because of the high current and relatively high voltage to control, a MOSFET was considered a more logical choice, not only because of its low cost, with a small size and a fast response time but also because a micro-controller, by default,

is not able to produce a high current, and a MOSFET is able to operate using a signal with low current, needing just to be controlled mainly by the voltage applied to the gate.

The idea is that a command signal is applied to the gate of the MOSFET. If the signal is at +5V, the LEDs turn on and when the signal is at 0V the LEDs turn off. The proposed LED driver, as shown in the circuit 3.5, is consisted of a MOSFET, where the drive signal is applied to the gate, the 24V and the LEDs are connected to the drain and the ground to the source.

After some primary considerations, an additional resistor was placed between the 24V and the LEDs to protect the LEDs and to dissipate the residual power that typically remain from the LEDs. The value of the LEDs load resistance  $R_L$  is obtained:

$$V_L = R_L I_f \Leftrightarrow R_L = \frac{V_L}{I_f} \Leftrightarrow R_L = \frac{V_{supply} - V_f}{I_f} \Rightarrow R_L = \frac{24 - (2.9 \times 7)}{700 \times 10^{-3}} \approx 5.3\Omega \quad (3.1)$$

And  $R_L$  must be able to dissipate a power of:

$$P_L = I_f^2 R_L \Rightarrow P_L = (700 \times 10^{-3})^2 \times 5.3 \approx 2.6W \quad (3.2)$$

The value of the current  $I_f$ , used in the previous calculation, was established by the datasheet in order to ensure that the device could sustain the worst case scenario: a continuous transmission at full power.

### 3.2.3 Transmitter Tests

For these first tests, to analyze the behavior of the LEDs and check if the concept would work, it was used some power and switch MOSFETs available in the DEEC.

For this first stage tests, the input signal is created by a function generator that outputs a square wave that operates between the +5V and 0V. The objective was to see the delays generated by the transistors and to study their behavior at different signal frequencies. To achieve this goal, a test setup, as shown in figure 3.6, was assembled.

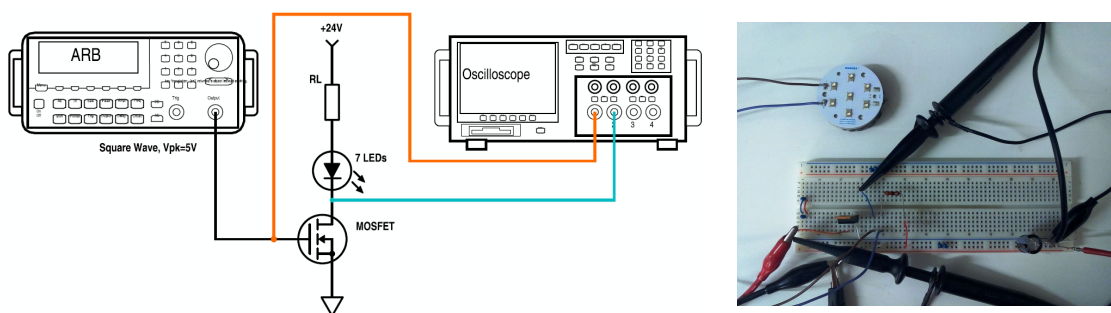


Figure 3.6: The test setup for the MOSFET testing.

Initially, it was assumed that MOSFETs for power applications, although able to switch greater power loads, they would only be capable of producing slower response times.

By using a sample founded in the laboratory, in this case the P30NF10, it is visible in the print 3.7, the influence of the slow response time in a transmission.

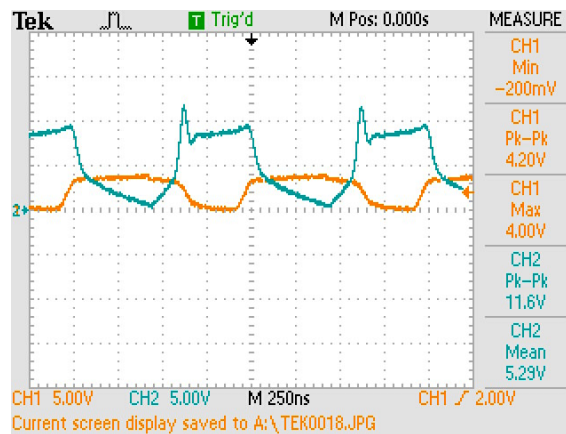


Figure 3.7: P30NF10 response time test:  $F = 1\text{MHz}$ ,  $T = 250\text{ns}$ .

So, since the pretended operation frequencies demand a fast switching speed, a more appropriate MOSFET for these operations is needed. The challenge behind this type of switching MOSFET, is to find a sample that can bear the supply voltage and drive current.

In order to test the concept the BS170, which is a more appropriate MOSFET for this application, was used. However in the future, a more considered choice will be made, since this MOSFET is not capable of supporting the necessary 24V of voltage supply and 1A of drive current.

In figure 3.8, it is possible to see that the BS170 is capable of following the transmission signal, with a considerable small delay along the broadcast.

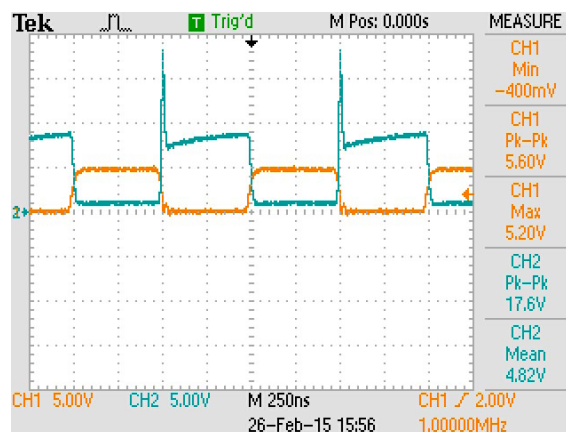


Figure 3.8: BS170 response time test:  $F = 1\text{MHz}$ ,  $T = 250\text{ns}$ .

Based in the work done by [15], it was also the possibility of using a MOSFET driver was also explored, in order to increase the current of the transmission signal inserted in the MOSFET's gate. This is a desirable amplification because if a higher current is injected in the MOSFET's gate, the intrinsic capacities of the MOSFET would be saturated, which could decrease the commutation delay produced by it.

In figure 3.9, it is shown a possible circuit, that would work based on a MOSFET driver. The complexity of this layout is higher, comparing with the previous scheme, but still relatively simple.

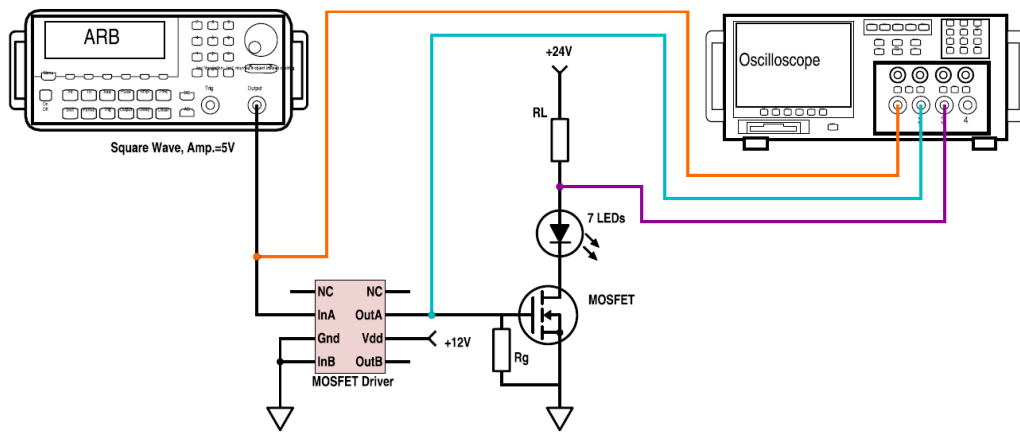


Figure 3.9: Setup scheme for Tx with MOSFET driver.

Despite of its advantages this option was overlooked, since the delay produced by this driver, in the output, was superior in comparison to time gain by charging the MOSFET capacitance.

### 3.3 Optical Receiver - Rx

Just like the optical transmitter, it is also necessary to design another important component of the system, the optical receiver. Basically, as shown in 3.10, this part has to be capable of capturing the emitted light signal, transmitted by the Tx, through a photo-receiver. Then the light signal sent, passes through some processing to be able to retrieve the original message. This block is one of the most complex and important parts of the system, because not only the response time of the layer is important, again, not to limit the data rate, but also the receiver must be able to receive the light of the signal ignoring the ambience light that adds noise to the transmitted signal.

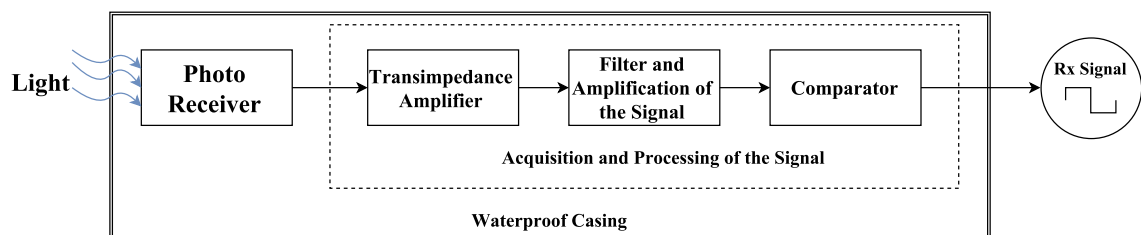


Figure 3.10: Simple Rx system design.

In this section it will be described the selection of the photo-receiver, the many stages of the acquisition and processing of the received signal, and testing each element of it, finalizing with a test to the all receiver layer.

### 3.3.1 Photo-Receiver

For this part choice, it can end up to be a simple photo-resistor, a PD, a photo-transistor, a PMT or even an APD. In other reviewed works, the detectors that generally are chosen the most are the PD, APD and the PMT because of their optical sensibility and their fast response time, so the choice will rely on these three possibilities.

In a first approach, the PMT loses its utility and interest for this work, since it has highest power consumption of all the detectors mentioned, a considerable large size, has a very high cost and applying it in scenarios with some ambient light it would be hard to filter the signal from the noise, since it is a very sensitive sensor.

In the last years, there have been some developments in the PD and the APD, and the recent blue/green enhanced PD/APD seems to be a promising option because it is specially designed to be more sensitive detector to the blue and green light, which is the range of wavelengths that it is on the interests of this work.



Figure 3.11: The BPW34 photo-diode.

Despite the similarities between the PD and the APD regarding their small size and fast response time, the APD internal gain makes it more vulnerable to the interference of ambience light, while the gain of the PD can be obtained through amplification and filtering of the received signal, making it a more configurable choice.

Since the decision ended up to be PD, once more, for the initial study and understanding of the system, and because of the availability of the components (also provided by INESC TEC), it was used the PD BPW34 (figure 3.11). Although it does not have the blue/green enhancement characteristic (its sensibility is higher in the infrared (IR) region), its high speed photo detection was considered an important feature to be studied. For the final prototype that enhancement characteristic will be searched.

For the high speed application pretended, the PD must be supplied with a reverse bias. The datasheet of the component shows that at 12V the response time is very acceptable, since the diode capacitance is lower, and the reverse light current is close to maximum.

### 3.3.2 Acquisition and Processing of the Signal

In this block the main function is to receive the analog signal provided by the photo-receiver and to try to restore the original message sent. As represented in the scheme 3.10, it is composed by three main functions, the first is responsible for converting the current produced by the PD to voltage, then it filters the signal and amplifies it, and finally tries to convert the analog signal into a digital one, through a comparator.

### 3.3.2.1 Transimpedance Amplifier

The first step of the processing of the signal is to convert the current generated by the PD to a voltage signal. For this step it is necessary to look up for a solution that receives the signal and makes the conversion with the smallest delay possible, in order to not damage the response time of the system. For this reason it was searched solutions for an active current-to-voltage converter, proper for high speed detection.

For these reasons it was implemented a transimpedance amplifier (TIA), that is basically a feedback resistor crosswise an operational amplifier (OP-AMP). Since the importance of this block is to execute its operation as fast possible, it requires a very fast OP-AMP, and also a weighted feedback resistor, because if this component is too high it gives a higher gain to the circuit but a slower response. Any additional components inserted in the active circuitry, like capacitors to cleanse the signal, will also delay the response time.

As it can be deduced by the figure 3.12, the output voltage  $V_{TIA}$  can be calculated by:

$$V_{TIA} = R_f I_{PD} \quad (3.3)$$

With it is possible to assume that the TIA gain is equal to the value  $R_f$ . If there is any value of  $C_f$  the output voltage will not change, it will only interfere by inducing delay to the signal and reduces the  $V_{TIA}$  overshoot, as previously explained.

For this block it is necessary to have an OP-AMP with a relatively high slew rate and wide supply range. It was founded a sample of the THS4631 that covered these major parameters, so it was used for the initial tests. Additionally in the datasheet of the THS4631, it was found a table that contained some recommended values for the  $R_f$  and  $C_f$ , and their limitations according their values.

In order to obtain the best performance in terms of response time, it was determined to use a  $R_f = 10k\Omega$ , so that, according to the information on the refereed table, in the worst case scenario the system is able to transmit at a bandwidth of 5.5MHz. The values of  $C_f$  would be tested experimentally by using three different capacitor values described in the datasheet of 2pF, 2.2pF and 3pF.

### 3.3.2.2 Filter and Amplification of the Signal

After the input current signal is converted into voltage, it requires an amplification for the small signal that outputs of the TIA. This is an asset as with this gain, even transmitted signal that are attenuated by the elements and the distance between the Tx and Rx might be received and acknowledge, resulting in an increase of the range of transmission. The configuration of this

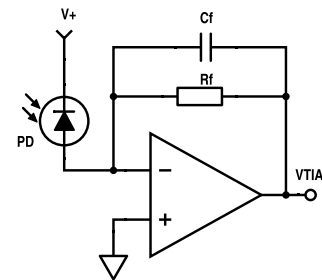


Figure 3.12: Example of a TIA.

amplifier will be inverting, in order to invert the received signal from the TIA, retrieving the original message as sent.

Additionally, in order to clear the analog signal from interferences, and other effects like ambient light, it will be implemented an active bandpass filter (BPF) that is capable of filtering the signal in some determined frequencies. It was preferred to use a bandpass because some of the ambient light goes either in the region of high frequencies but also to the low ones.

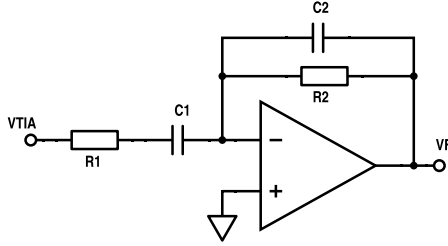


Figure 3.13: BPF configuration.

The configuration of the amplifier is shown in scheme 3.13. As it can be seen, a gain  $A_F$  is generated, and in the first part the pair  $R_1$  and  $C_1$  are responsible for the high-pass of the filter, and the pair  $R_2$ ,  $C_2$  is responsible for the low-pass of the frequencies, meaning any frequency of transmission lower than  $f_{c1}$ , or higher than  $f_{c2}$ , will be cut-off. The values of the elements can be calculated by:

For this amplification and filtering of the signal, once again a fast amplifier is required that is able of make the operation without delaying the response time. By searching he available AMP-OPs for testing, the AD8041 seem to be a suitable choice due to its fast response time with a bandwidth up to 160MHz and a rail-to-rail topology for simplifying the supply, needing just 5V to thee circuitry.

$$A_F = \frac{V_F}{V_{TIA}} = -\frac{R_2}{R_1} \quad (3.4)$$

$$\begin{cases} f_{c1} = \frac{1}{2\pi R_1 C_1} \\ f_{c2} = \frac{1}{2\pi R_2 C_2} \\ f_{c1} < f_{c2} \end{cases} \quad (3.5)$$

The passive components value were obtained through calculation. It is started to characterize the current created by the PD. According to the information extracted from the datasheet the reverse light current  $I_{PD}$  variates between the minimum  $40\mu A$  and can reach the  $75\mu A$ , also the reverse dark current  $I_{PD_{dark}}$ , that can be considered residual noise, in the worst case scenario reaches the  $30nA$ . After passing the  $R_f$  from the TIA the voltage of the signal reaches the  $400mV \leq V_{TIA} \leq 750mV$ , and  $V_{TIA_{dark}} = 0.3mV$ .

For the first step the amplification will be dealt with. Since the incoming signal even if is in its minimum power is in the interest of this work to be processed the gain will be adjust according to the estimated  $V_{TIA_{min}} = 400mV$  to achieve a reasonable value. So the gain was calculated so  $V_{TIA_{min}}$  after been amplified reaches the 5V (it was calculated the absolute values):

$$V_{F_{min}} = 5V = A_F V_{TIA_{min}} \Leftrightarrow A_F = \frac{5}{400m} = 12.5 \quad (3.6)$$

With this gain the voltage output of the BPF is  $5V \leq V_F \leq 9.375V$ , and the noise can reach



the  $V_{F_{dark}} = 3.75mV$ , which is an acceptable difference between them. Now that the gain value is determined the BPF resistor can be assigned. To simplify the calculations it was assumed that the  $R_2$  was  $1k\Omega$ , so the value of  $R_1$  is calculated:

$$A_F = \frac{R_2}{R_1} = 12.5 \Leftrightarrow R_1 = \frac{1k}{12.5} = 80\Omega \quad (3.7)$$

With the resistors already dimensioned it is necessary to dimension the capacitors, and for that the cut-off frequencies must be established. This values will determine the interval were the signal is not attenuated by the filter, so the frequencies stipulated are  $1.6kHz$ , to eliminate low frequency light noise, and  $10MHz$  since it eliminates the higher frequency light noise, although it will also limit the system to that frequency, for this work purpose it was assumed to be an acceptable data-rate limit. Finally the values of  $C_1$  and  $C_2$  can be calculated:

$$\begin{cases} f_{c1} = 1.6kHz = \frac{1}{2\pi R_1 C_1} \\ f_{c2} = 10MHz = \frac{1}{2\pi R_2 C_2} \end{cases} \Leftrightarrow \begin{cases} C_1 = \frac{1}{2\pi \cdot 80 \cdot 1.6k} \approx 1.2\mu F \\ C_2 = \frac{1}{2\pi \cdot 1k \cdot 10M} \approx 16pF \end{cases} \quad (3.8)$$

With this circuit configuration, the transfer function of the filter resumes to:

$$H(s) = -\frac{\frac{R_2 \cdot \frac{1}{sC_2}}{R_2 + \frac{1}{sC_2}}}{R_1 + \frac{1}{sC_1}} \quad (3.9)$$

By making the calculation with the help of MATLAB, substituting the components of the transfer function by their values and by plotting the resulted equation, it is possible to simulate and analyze the behavior of the filter along the frequency domain. In figure 3.14 it is possible to see the tracing of the frequency response of the filter with a Bode plot.

As it can be seen, between the two cut-off frequencies, in the active bandwidth area of the filter, the signal should not be attenuated, have an insignificant phase shift, and it should transmit at its full power. When the frequencies get near to the cut-off region, the signal begins to suffer from attenuation and phase shifting, depending if it is a low or high frequency. If the frequency gets close to the low region of  $f_{c1}$ , the signal is ahead of its time, and if the frequency is near the high region of  $f_{c2}$  the signal starts suffering from delay. For the testing, it should be tested the behavior of the filter inside the active zone, near the cut-off frequencies, and out of the active area.

### 3.3.2.3 Comparator

Finally this final block is responsible for the reconstruction of the initial signal. Since the original transmitted signal was a square wave that respects the TTL, which mean that has an amplitude of 0V or 5V, the objective is that in the end this block shows exactly the same signal but with some delay originated by the system components.

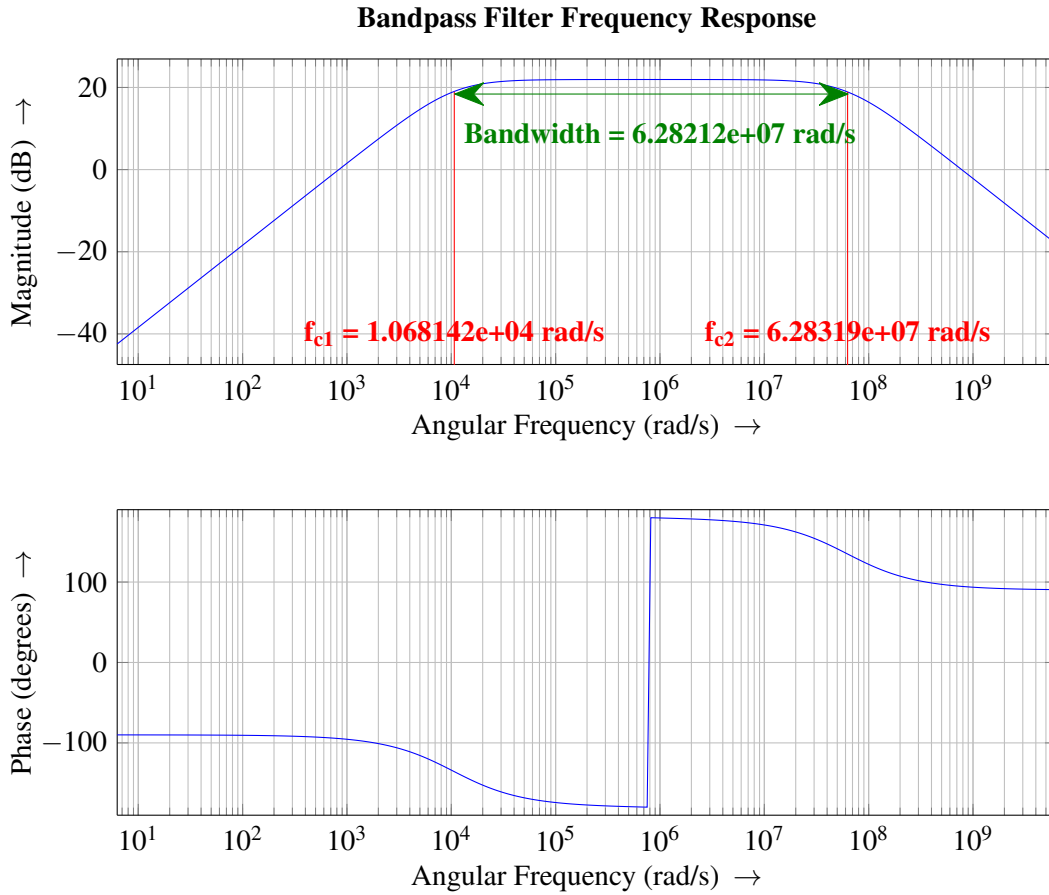


Figure 3.14: Frequency response of the BPF

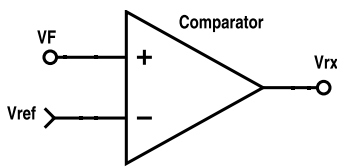


Figure 3.15: Comparator layout.

For this operation a simple comparator was chosen. The basic function of this element is when it receives the signal generated by the previous blocks  $V_F$  it compares to a voltage reference value  $V_{ref}$ . If value of  $V_F$  is superior than the reference, the output value of the comparator is a logical '1' which corresponds to a voltage value of the positive supply of the comparator, if in the other case  $V_F$  is inferior comparing with the  $V_{ref}$ , its logical output becomes a '0', corresponding to a negative supply output.

For the selection of this component, some important features must be taken into account. The main attributes to consider are the response time of the comparator that, as the other selected components, must be as fast as possible, and a single power supply of 5V is also important for the output be limited for the pretended values. An AMP-OP could be used to perform the comparators function, but because of the reasons described before, and the ease of accessibility, it was chosen to utilize the comparator AD8561 since is the proper device for this application and meets the pretended requirements.

The  $V_{ref}$  will be obtained through a voltage divider, that can be regulated with a potentiometer

or with resistors. The only requirement for this voltage divider is that must be able of achieve an output voltage value lower of the estimated  $V_{T_{min}}$ . Although there are risks associated to the choice of  $V_{ref}$ , if the threshold is too close to the  $V_{T_{min}}$  there can be flaws in the output signal, but if the threshold is to low the ambience light associate to the dark current noise can affect the output. So a weighted  $V_{ref}$  must be chosen, and adjusted if necessary.

### 3.3.3 Receiver Tests

#### 3.3.3.1 Initial Setup and Problematics

The receiver tests were divided by its block functions and tested each part separately. The first part to test in the receiver is to test the TIA, and for that purpose, it was intended to use a simple rail structure, where would be a light source assembled in one end and connected to the already tested Tx circuit, and in the other end would have the chosen PD that would be connected to the TIA. This test setup is exhibited in figure 3.16, outputting a blue light.

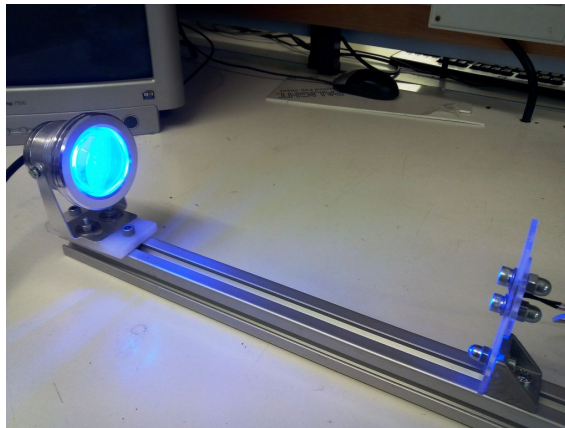


Figure 3.16: Initial Rx test setup.

This light source, that was intended to be used, is an underwater light, that had an RGB LED in the interior, that is controlled by a remote control to variate its color output. The reasons to choose this light source as a transmitter was to study and observe the behavior of the PD and the output of the TIA, with different light spectrum transmissions. The problem of this approach is the light source intended to use initially for the testing, seems that it could not keep up with the transmission speed intended to use.

Another problem occurred, when through the measurements made on the oscilloscope, a very high interference was produced by the function generator in the Tx part, which was an unpredictable result since there were no common connections between the Tx and Rx. They were working like independent parts. It was observed that this interference was created by the rail itself, probably because of the physical connection between the light source and the rail, and the high power commutation of the Tx, it created a kind of an antenna, which was responsible for the noisy interference. Also the long thin cable that was connected to the PD also contributed for the noisy transmission.

### 3.3.3.2 Transimpedance Amplifier

So a more simple and direct setup was created to be able to acquire the transmission as shown in figure 3.17, by using the already tested Tx. Although this setup is more limited, since it cannot test the range with precision, it permits to better testing the TIA time response.

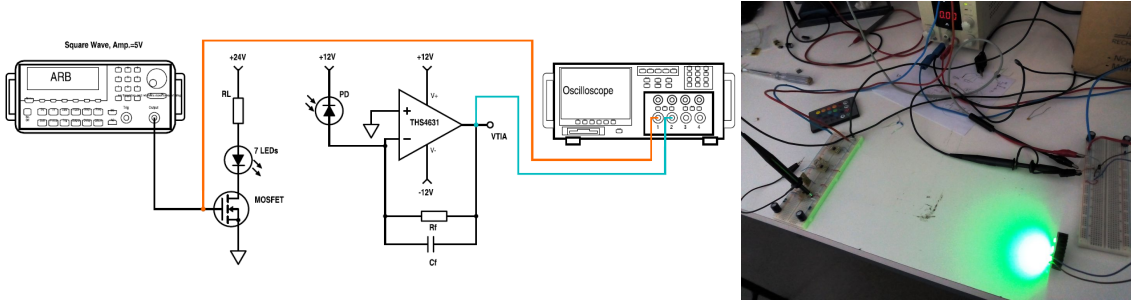


Figure 3.17: The final test setup for the TIA testing.

This simple test is performed by placing the Tx and the "Rx" in a fixed position, where a plausible transmission might occur, and test the output of the TIA with some advisable values for the resistors and capacitors, at different transmission frequencies of  $100kHz$ ,  $500kHz$  and  $1MHz$ . The values of the resistors used were  $10k\Omega$  and  $100k\Omega$ , and the capacitors values were  $1.8pF$ ,  $2.2pF$ ,  $2.7pF$  and  $3.3pF$ .

In a first approach, the output gain was studied by testing the TIA using only the feedback resistor. As it can be seen in the prints 3.18, the gain of the TIA, is ten times greater with the  $100k\Omega$  resistor, as it could be predicted.

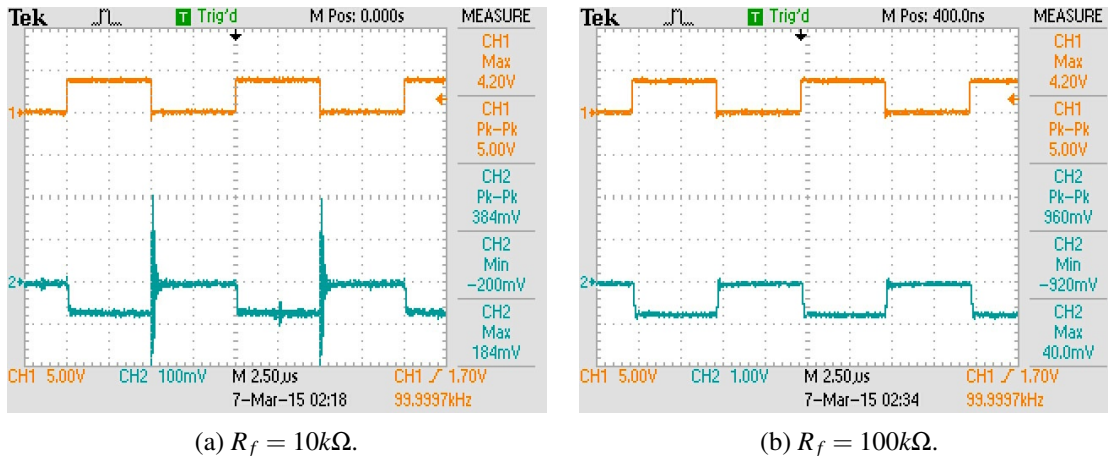


Figure 3.18: Feedback resistor comparison:  $F = 100kHz$ , without  $C_pF$ .

Although a higher gain can be seen as an asset, with a bigger feedback resistor, the greater is the delay generated by it, since the RC time constant  $\tau$  (expressed in seconds) is related to the resistance of a circuit:

$$\tau = RC \quad (3.10)$$

In addition, as it can be seen in the prints 3.19a, at a frequency of  $1\text{MHz}$ , the output signal, even without a capacitor that could extend the delay, the signal is highly affected. Although that at a first sight at 3.18b, seems that it does not need to be filtered, if a capacitor is placed, as figure 3.19b shows, the signal becomes almost impossible to be reconstructed, making it impracticable.

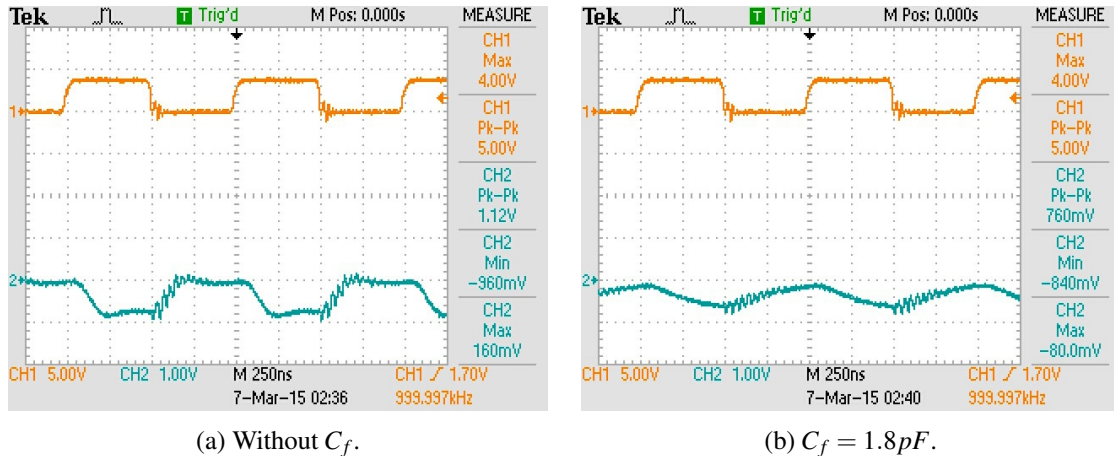


Figure 3.19: Time response of the TIA with high gain:  $F = 1\text{MHz}$ ,  $R_f = 100\text{k}\Omega$ .

Because of this visible delay, it was assumed that using a feedback resistor of  $10\text{k}\Omega$  would end up being the best option. Even though, the output signal of the TIA at  $1\text{MHz}$  requires some filtering, as it can be concluded with figure 3.20.

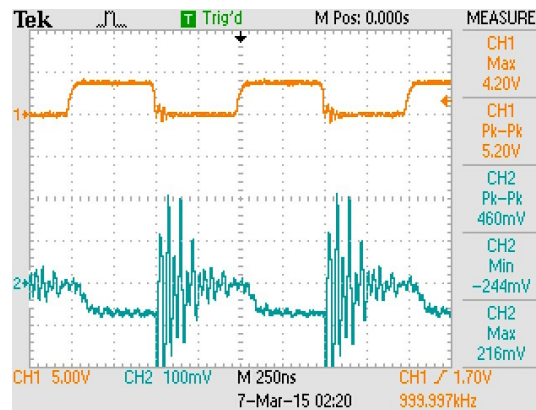


Figure 3.20: Output signal of TIA:  $F = 1\text{MHz}$ ,  $R_f = 10\text{k}\Omega$ , without  $C_f$ .

The next step for the TIA testing only the feedback resistor of value  $10\text{k}\Omega$  was used, varying only the values of the feedback capacitors. Never forgetting that the TIA delay is always dependent of equation 3.10, which means the larger the capacitor, the higher the delay. In the lower frequencies tested, the delay generated by the capacitors is not entirely perceptible, the only significant difference is in the output noise of the signal. The larger the capacitance, the less noise remains in the output signal, as it can be assumed by the prints 3.21.

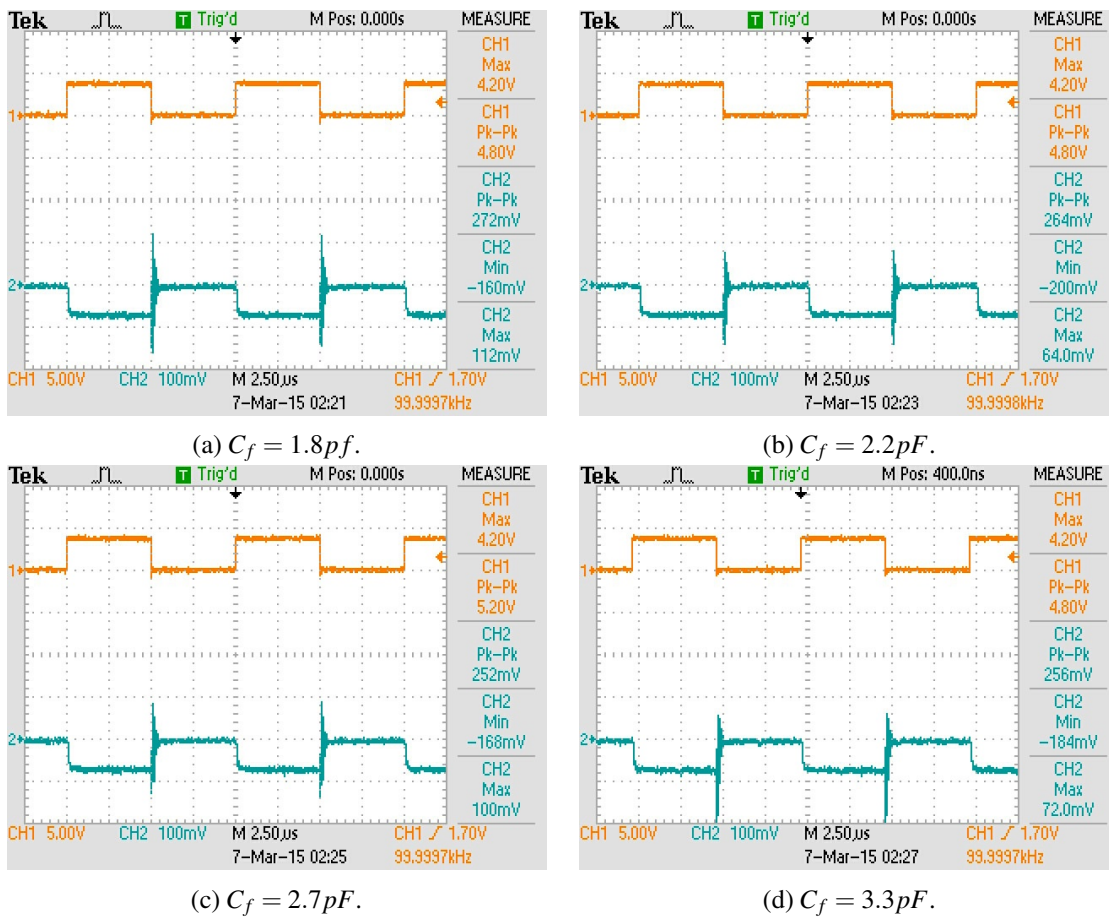


Figure 3.21: Time response of the TIA:  $F = 100\text{ kHz}$ ,  $R_f = 10\text{ k}\Omega$ .

By critically analyze and compare with 3.18a, the results in 3.21, at  $100\text{ kHz}$ , it was considered the best result were the  $2.2\text{ pF}$  and  $2.7\text{ pF}$  capacitances, the figures 3.21b and 3.21c respectively.

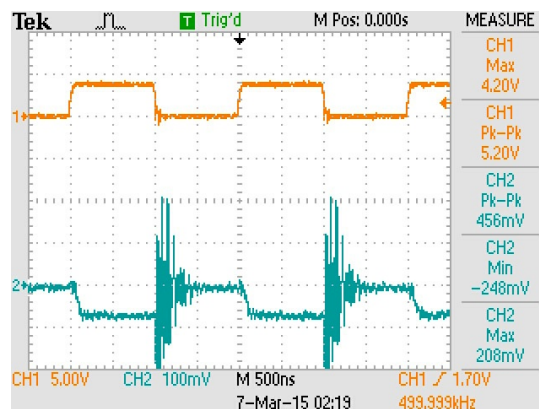


Figure 3.22: Output signal of TIA:  $F = 500\text{ kHz}$ ,  $R_f = 10\text{ k}\Omega$ , without  $C_f$ .

At the transmission frequency of  $500\text{ kHz}$  in figure 3.22, it is noticeable the signal slowing down and the noise still remaining, and with the capacitors the delay begins to increase, although



there are not very significant variations between capacitances, being the noise remove factor more preponderant, as shown in figure 3.23.

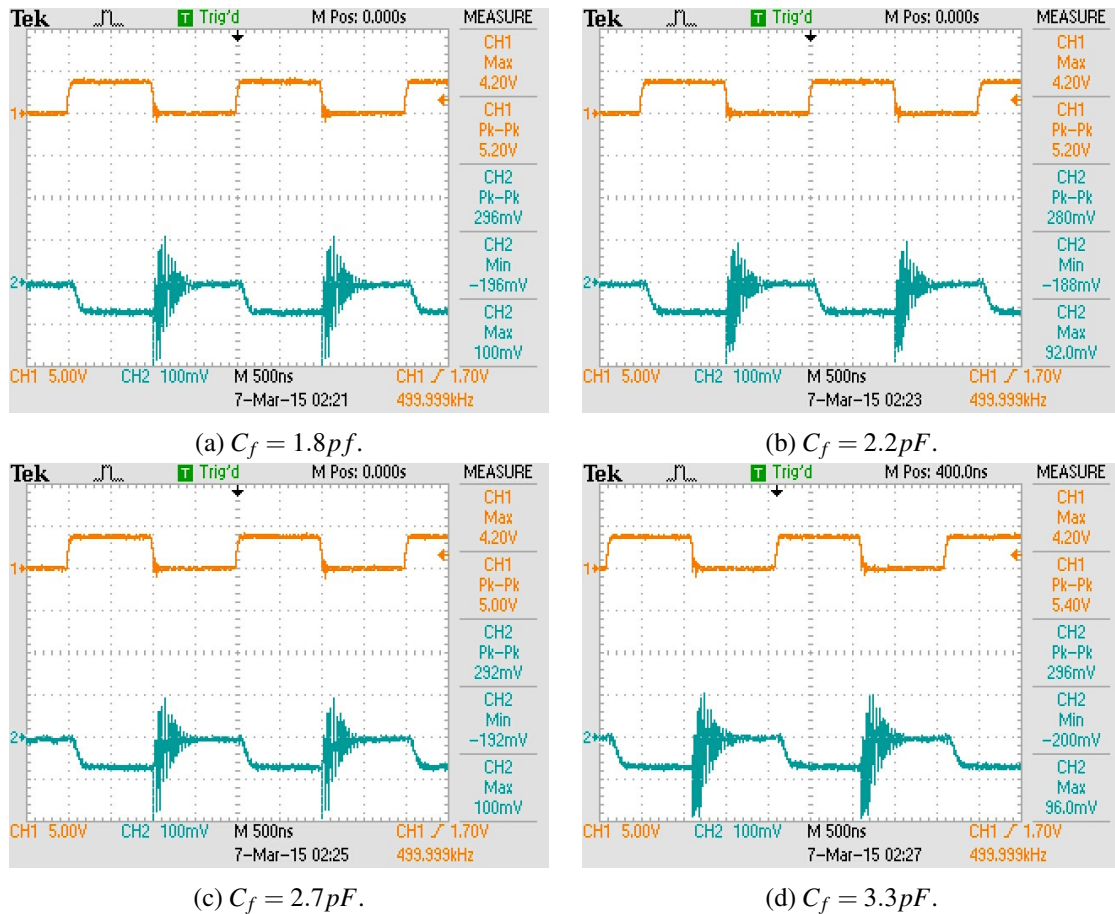


Figure 3.23: Time response of the TIA:  $F = 500\text{kHz}$ ,  $R_f = 10\text{k}\Omega$ .

Again by analyzing the figure 3.23, the responses of 3.23b and 3.23c seem to be the better results.

Finally, the TIA is tested at  $1\text{MHz}$ , where an improvement must be done to the output signal represented in figure 3.20. In the prints presented in 3.24 are displayed the results from the various capacitors.

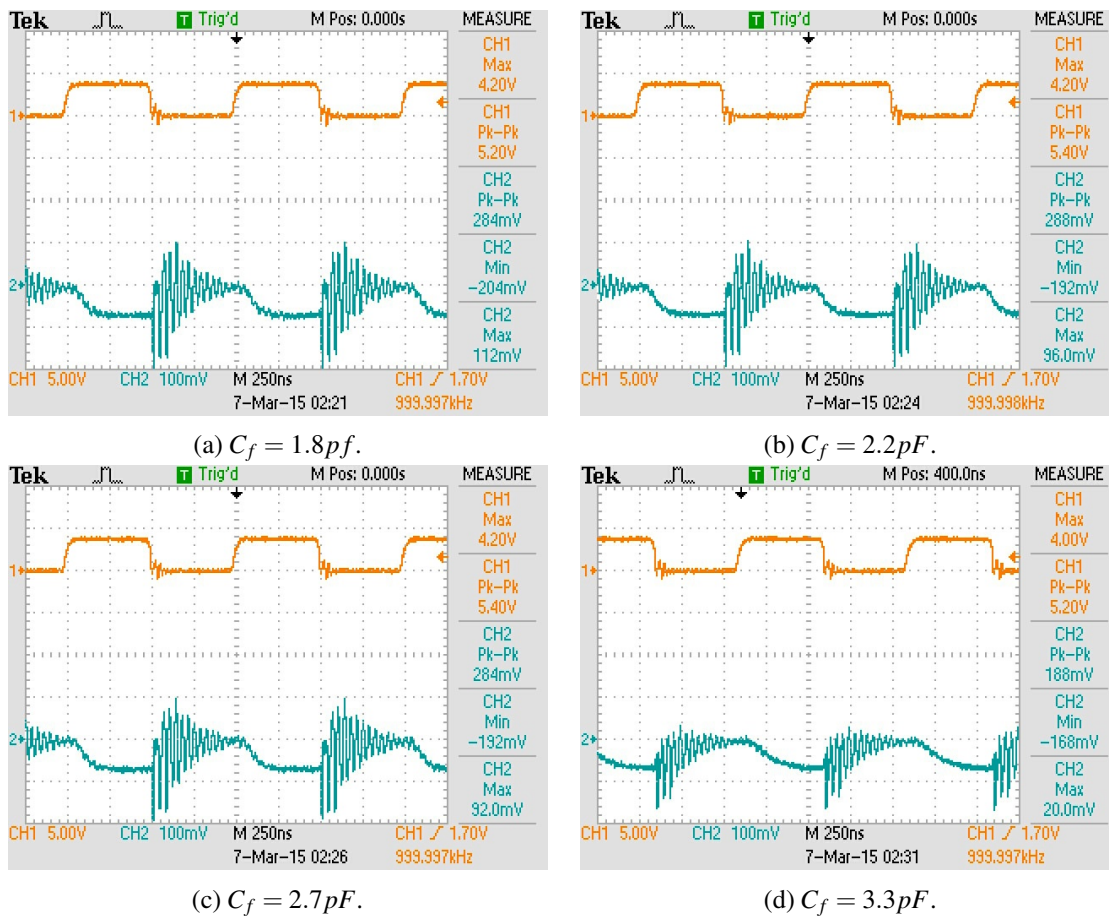


Figure 3.24: Time response of the TIA:  $F = 1 \text{ MHz}$ ,  $R_f = 10 \text{ k}\Omega$ .

At this frequency, the response times are at their lowest obtaining the highest delay. In the print 3.24d, although it might show a more filtered output, the delay displayed in the fall time is too high to be considerate a viable choice. Taking into account all the previous tests and this last one, it seems that the print 3.24b, with a capacitor value of  $2.2 \text{ pF}$  is the most viable choice for the feedback capacitor of the TIA. With these tests, it is possible now to present the recommended features for the TIA, as shown in table 3.2.

Table 3.2: TIA block specifications.

<i>Transimpedance Amplifier</i>	
<b>Component</b>	THS4631
<b>Power Supply (<math>V_{S+}</math>, <math>V_{S-}</math>)</b>	+12V, -12V
<b>Feedback Resistor (<math>R_f</math>)</b>	$10 \text{ k}\Omega$
<b>Feedback Capacitor (<math>C_f</math>)</b>	$2.2 \text{ pF}$

### 3.3.3.3 Bandpass Filter

The next block of the processing is the BPF, and as explained previously the objective of this test is to analyze the behavior of the output signal by changing the frequency of the input transmission



and detect functional results, as when the magnitude of the signal declines and if the phase shifts.

Just as argued in the past subsection 3.3.2.2, it was believed that using a single supplied amplifier for the filter, would be more beneficial, since it simplifies the supply necessities and limit the output for the desired levels, but in very first tests, the output signal was not remotely the expected, since the single supply distorted the filtered output, where an input sinusoidal wave did not have the desired magnitude output, and phase shifts were not visible. Luckily, the chosen amplifier was able to withstand single a dual supplies of +5V and -5V, which would allow to obtain the desire output.

For that reason, a setup similar to the figure 3.25 was arranged.

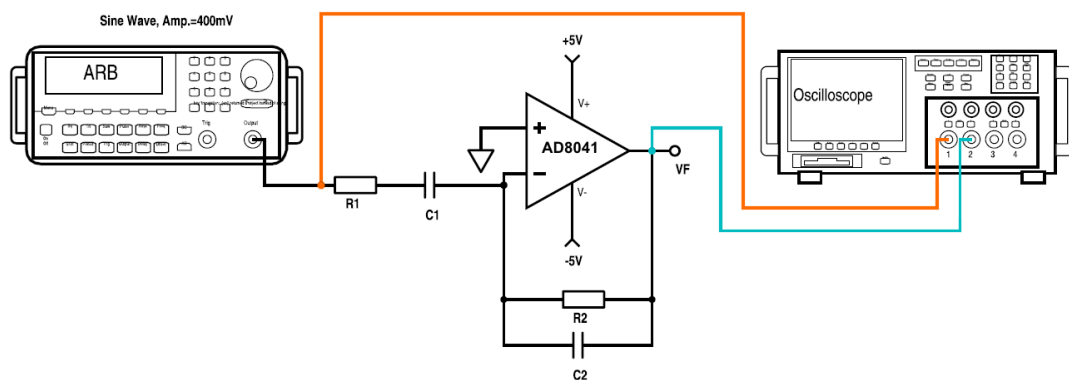


Figure 3.25: Test setup for the BPF testing.

Due to the absence of components with the proposed value to obtain the precise cutoff frequencies, for these tests it was used components with similar value to approximate as close as possible of the ideal values. The values of the components for these tests and respective cutoff frequencies are:

$$\begin{cases} R_1 = 100\Omega \\ R_2 = 1k\Omega \\ C_1 = 1\mu F \\ C_2 = 18pF \end{cases} \Rightarrow \begin{cases} f_{c1} \approx 1.6kHz \\ f_{c2} \approx 8.8MHz \end{cases} \quad (3.11)$$

The first frequency tested was at  $1MHz$ , because it is one of the pretended transmission frequency rates and also has been used as a base test frequency all along the work. The resulting output wave is shown in figure 3.26

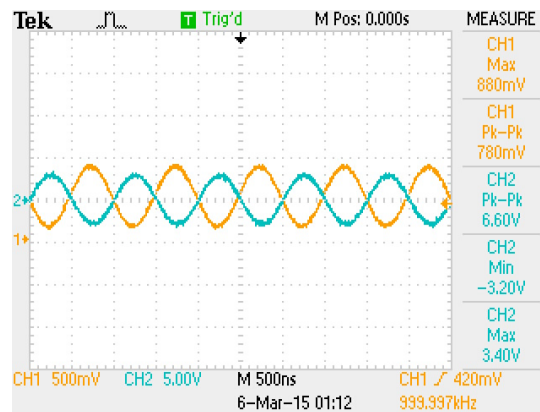


Figure 3.26: BPF output at 1MHz

As it may be assumed, at a first sight the output signal has the pretended magnitude and right phase, since it is an inverting filter, but is difficult to see the delay caused by it. Because of that problem, the prints of the oscilloscope were inverted to enable a better time response perception.

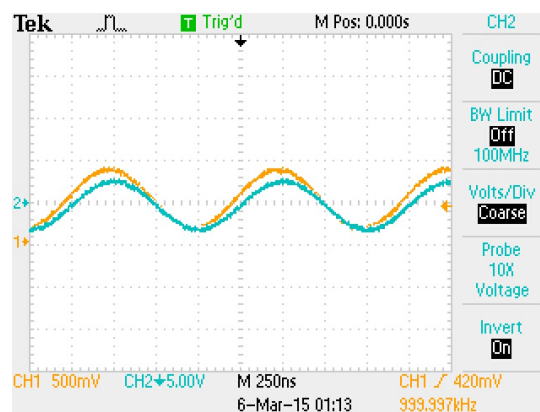


Figure 3.27: BPF at 1MHz with inverted output.

Now in figure 3.27 it is possible to clearly see that the output is suffering from a natural delay, since this frequency is closer to the region of high cutoff frequency. It is confirmed that the closer it gets from this region the greater the delay from the filter, as shown in figure 3.28, where the input is a 5MHz signal. As also can be seen the magnitude of the signal is affected as well.

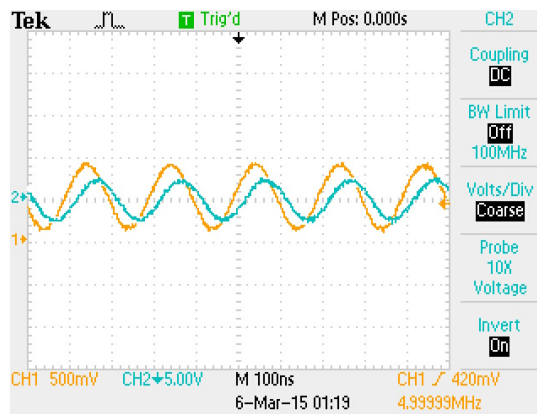


Figure 3.28: BPF inverted output at 5MHz

But eventually, if the signal reaches or surpasses the cutoff limit region, the magnitude of the signal is highly attenuated and the phase is completely shifted, as it is possible to see in figure 3.29, where the input signal is filtered.

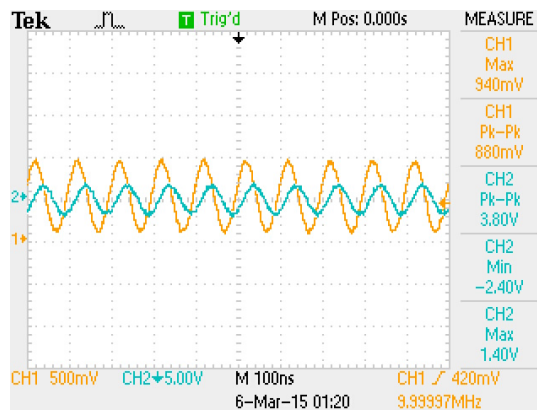
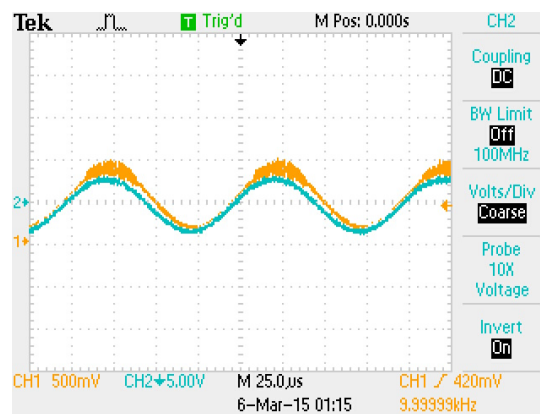
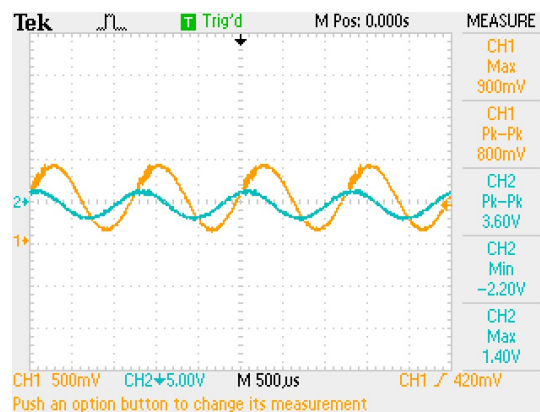


Figure 3.29: BPF inverted output at 10MHz

Then, if a signal approximates the high frequency cutoff region suffers from a delay, contrary, if a signal dislocates to the low frequency cutoff region the output is in advanced. The figure 3.30 shows exactly this phenomenon, where the output trace is ahead of the input trace.

Figure 3.30: BPF inverted output at  $10kHz$ 

And just as at the high frequency cutoff region, at  $1.6kHz$  the output signal suffers from high attenuation in the magnitude, and gets in advance of the input signal, as can be concluded in figure 3.31.

Figure 3.31: BPF inverted output at  $1.6kHz$ 

With these tests it was possible to confirm that it works like it should and it was able to analyze and predict the behavior of the filter in the range of frequencies. The possible specifications of the BPF are shown in table 3.3.

Table 3.3: BPF block specifications.

<i>Bandpass Filter</i>	
<b>Component</b>	AD8041
<b>Power Supply (<math>V_{S+}, V_{S-}</math>)</b>	+5V, -5V
<b>High Pass Components (<math>R_1, C_1</math>)</b>	$100\Omega, 1.2\mu F$
<b>Low Pass Components (<math>R_2, C_2</math>)</b>	$1k\Omega, 2.2pF$

### 3.3.3.4 Comparator

For this final block, to test the comparator, a very simple setup, as shown in figure 3.32, was assembled to test its response.

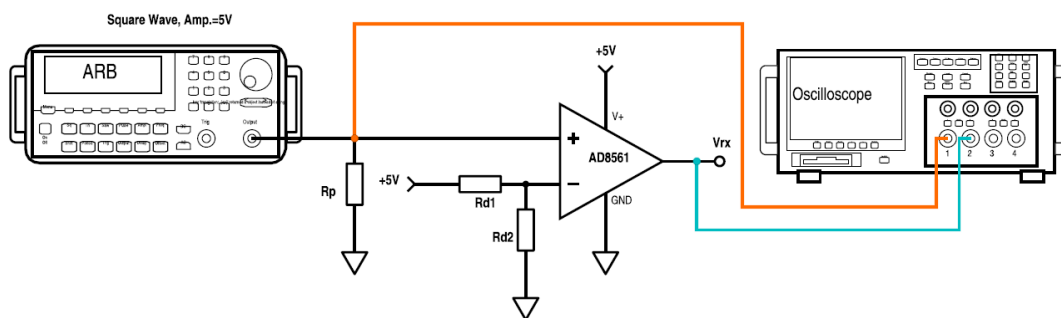
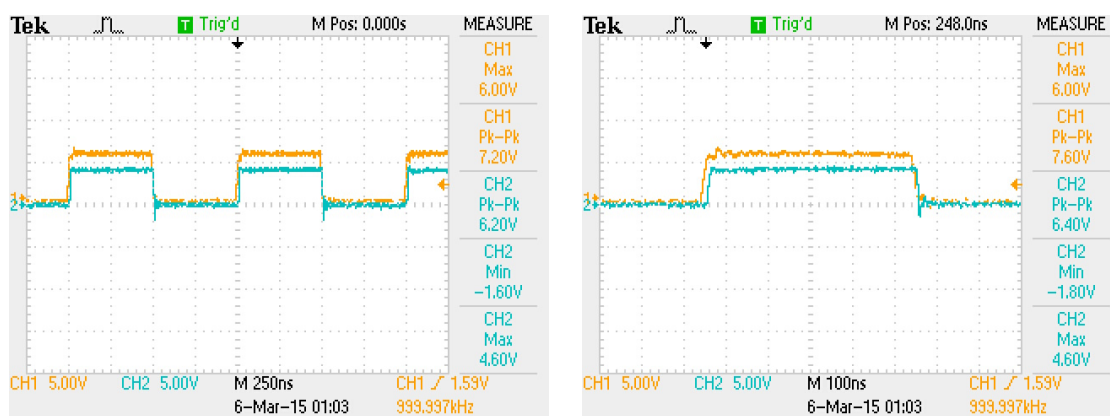


Figure 3.32: Test setup for the comparator testing.

Because the threshold was fixed as half of the supplied voltage, the resistors  $R_{d1}$  and  $R_{d2}$  must be equal. Also the resistor  $R_p$  works as a pull-down resistor that is responsible to speed up the comparator time response.

(a)  $T = 250\text{ns}$ .(b)  $T = 100\text{ns}$ .Figure 3.33: Time response of the comparator at  $1\text{MHz}$ .

As shown in the images of 3.33, the time response of the comparator is more than satisfactory, the only detail to tune in the prototype is the threshold.

Table 3.4: Comparator block specifications.

<i>Comparator</i>	
<b>Component</b>	AD8561
<b>Power Supply (<math>V_{S+}, V_{S-}</math>)</b>	+5V, 0V
<b>Pull-Down Resistor (<math>R_p</math>)</b>	$10k\Omega$
<b>Voltage Divider (<math>R_{d1}, R_{d2}</math>)</b>	$1k\Omega, 1k\Omega$

### 3.4 Physical Casing

As referred in the beginning of this dissertation, the main goal is to create a communication module that is able to communicate in an underwater environment. In order to achieve this it was necessary to create a waterproof casing to place all the electronic components inside. Additionally, it must

satisfy the design constraints mentioned previously, by being a small and light casing structure, but still robust enough to endure the water environment.

In figure 3.34 it is shown the initial idea for the casing prototype. This concept consists of two parts that join by screwing them together, and with a spacing ring, an acrylic lens and a rubber O-ring.

When tied up tightly it isolates its interior from water. The objective is to fit in the circuit parts inside the casing, according to the specifications of it, and fix them to the structure somehow, while supplying the operative voltage (namely the  $+24V$  and the  $GND$ ), the Tx signal and to extract the Rx through a cable that exits from the rear end of the casing.



Figure 3.34: Initial waterproof casing prototype.

The physical casing is internally restricted by a diameter of 40 millimeters and in order to properly isolate the interior of the casing with the acrylic and the O-ring, has a limit for the length of the internal stack of about 40 millimeters.

### 3.5 Proposed Prototype

For the final proposed prototype, the objective was to implement all the solutions studied and mentioned previously, and create a circuitry layout suitable for the physical casing design that would satisfy the main objectives and constraints of the module design.

For these reasons the prototype interior was divided by layers to make the Tx and Rx in the same module embedded, and making a bidirectional communication module. In the scheme 3.35 it is shown how the components of the optical transmitter and receiver are supposed to be connected, each block represents a different layer of the circuitry module and their connection.

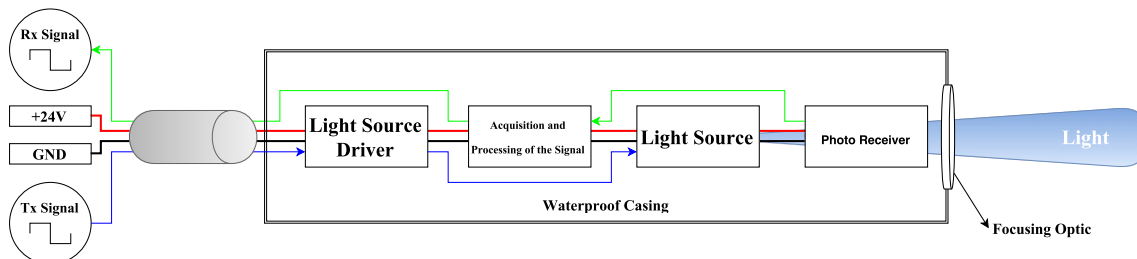


Figure 3.35: Communication module prototype scheme and its layers.

During the conception of these layers, in order to improve the system overall performance, a few changes were made in some layers, resulting in more than one version of the PCBs.

The following subsections describe the development of each layer, modifications made in the components after the preliminary tests, the steps in the development of the printed circuit boards (PCBs), ending with the assemble and connections of each of the layers.

### 3.5.1 LED Layer

Because it was intended to have two transmitters with distinct spectral output (different light color), it was necessary to order some LEDs that matched the pretended requirements. Although it was thought that the LUXEON Rebel LEDs, that were used as a light source in the earlier Tx tests, would be the best choice for the light source of the prototype, after an extended market search the choice of light source was reconsidered, choosing for the final prototype the Cree XLamp XP-E2 LEDs (figure 3.36b), a recent upgrade to the Cree XP-E LEDs series, these being a more radiant type of LED, while maintaining the typical forward voltage and current values.

To maintain the choice of light colors, it was chosen the green and blue light, since the cyan was not an available option by Cree. The characteristics of the chosen LEDs are shown in table 3.5.

Table 3.5: Electrical and spectral characteristics of the Cree XLamp XP-E2 LEDs.

Component	Typical Voltage (V)	Typical Drive Current (mA)	Typical Wavelength (nm)
Green: XPEBGR-L1-0000-00E01	3.5	700	520
Blue: XPEBBL-L1-0000-00201	3.25	700	465



(a) The 282 MCPCB for 7 cell optic (b) Cree XLamp XP-E2 LED (c) Cluster Concentrator Optic

Figure 3.36: Prototype light source components.

After the choice of the LEDs, it was necessary to find a circuit board proper for this type of LEDs, that could handle their current, contribute for the heat dissipation and that would assemble the LEDs in series. After some search it was found a company called Polymer Optics Ltd. that offered some interesting choices, being one of them a metal-core printed circuit board (MCPCB) proper for the Cree XP-E series, shown in figure 3.36a. But the most interesting feature provided



by this company, is their offer of optical lenses appropriate to focus the light of each LED, and that could properly fit into to their MCPCB. The chosen lens was a cluster concentrator optic, shown in 3.36c, that should focus the wide output ray of light of the LEDs, into to concentrated beam of light.

The only thing left to do with the light source, was to solder the LEDs to the MCPCB. At first it was thought that the soldering of these components would not be such a complex task, but because of the high heat dissipation of the MCPCB, and the location of the pads of the LEDs, a traditional soldering was not possible to do since the solder never adhered to the cooper pads, making it impossible to reach every part of the pads and to solder properly. For this reason, it was necessary to find a way to solder the LEDs through a special process called reflow soldering, a technique normally used in the industrial process for soldering surface-mount devices (SMDs).

Being this an industrial process, the faculty facilities could not provide the necessary tools for the process, therefore some companies were contacted to see if it was possible to order the soldering of the components. Unfortunately none of the companies contacted replied or gave a reasonable offer, so some alternative methods to solder the LEDs were investigated. One of the approaches was to use a heat-gun to heat up the MCPCB so that some solder paste could melt into the pads with the LEDs, trying to create the reflow. But this method proved to be very ineffective as the heat from the heat-gun was majorly dissipated in the air making it unable to heat the board to the necessary temperature.

So in order to enhance the direct temperature of the aluminum MCPCB, it was used a hot plate with temperature control, from the chemistry department, proper to heat up chemical solutions. By using the plate and the solder paste, it was possible to create the pretended reflow that permitted to solder the LEDs to the PCB.

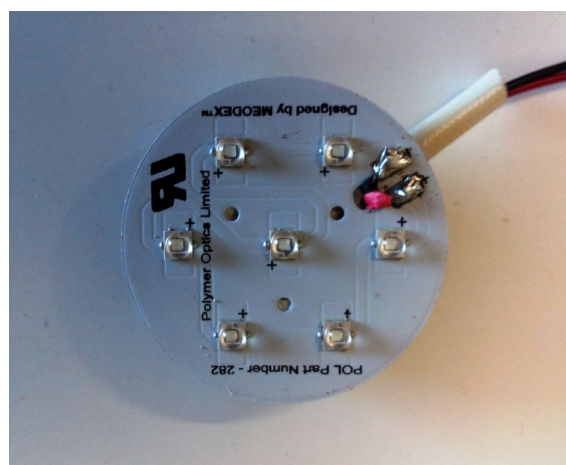


Figure 3.37: Final assembled light source.

In the end the final result can be shown in figure 3.37, being obtained the intended result.



### 3.5.2 PD Layer

The PD layer is the one responsible for receiving the light signal emitted by the transmitter, so is one of the layers that must be as close as possible to the acrylic layer of the casing in order to capture the maximum amount of light. As had already been said, one of the objectives was to use the newly blue/green enhanced PD for this application, but the PDs tested earlier were optimized to capture signal at the IR region of the spectrum. So a new market search was necessary to find a solution that would offer the desired blue/green enhancement characteristic while retaining a high speed response, such like the BPW34 earlier tested.

After some search, an ideal solution was found that had the two pretended requirements, the BPW34-B. Been this component from the same series of the BPW34, this new model had an enhanced blue sensitivity and an even faster response time than the previous one, making it a preferable solution.

Because the PD layer needs to be as close as possible to the acrylic layer, in order to optimize the light capture, a new problem was raised. With such a tight space, and this being occupied majorly by the LED layer and its lens, making space for the PDs became a challenge. In order to surpass this difficulty, it was design an idea of a detection ring composed of PDs all around it that could fit in the hexagonal gaps of the cluster optic, enabling the reception without cutting totally the receiver's sight.

In figure 3.38 it is shown the final detection ring composed of six PDs. The PDs are connected in parallel in order to sum all the currents generated by them.

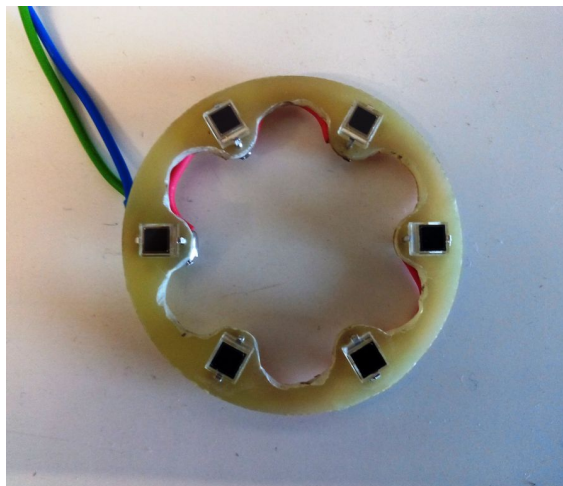


Figure 3.38: Final assembly of the PD detection ring.

The signal captured by the ring is sent by a pair of cables, blue and green, as it can be seen in the picture, to be connected to the other layers.

Although the PDs model used is the proposed, the optimal solution would be to use these PDs but in its SMD packaging. Unfortunately, they were not available to be acquired in the pretended period of time for this work.

### 3.5.3 Tx Layer

The design of these Tx and Rx PCBs resemble the MCPCB's size and shape, in order to produce a better fit in the designed casing.

Also the Tx layer, like as been discussed, receives the input signal to be transmitted and drives it to the LEDs, and since it has less components than the Rx layer it has more spare space.

First the components to be used here, after a market survey, for the MOSFET it will be used PMF87EN since it can handle voltages up to 30V, currents up to 1A and is specially designed for switching at high-speed applications.

Since the LEDs to be used are different, their forward voltage and current are also distinct, so a new load resistor must be dimensioned. Attending to the values given by the datasheets of the Cree XLamp XP-E2 LEDs forward voltage and current, the load resistors can be dimensioned:

$$\begin{cases} V_{L_{blue}} = R_{L_{blue}} I_f \Leftrightarrow R_{L_{blue}} = \frac{V_{L_{blue}}}{I_f} \Leftrightarrow R_{L_{blue}} = \frac{V_{supply} - V_{f_{blue}}}{I_f} \Rightarrow R_{L_{blue}} = \frac{24 - (3.25 \times 7)}{700 \times 10^{-3}} \approx 1.8 \Omega \\ V_{L_{green}} = R_{L_{green}} I_f \Leftrightarrow R_{L_{green}} = \frac{V_{L_{green}}}{I_f} \Leftrightarrow R_{L_{green}} = \frac{V_{supply} - V_{f_{green}}}{I_f} \Rightarrow R_{L_{green}} = \frac{24 - (3.5 \times 7)}{700 \times 10^{-3}} = 0 \Omega \end{cases} \quad (3.12)$$

As it can be deduced, the green light does not require any load resistor, and the  $R_{L_{blue}}$  must be able to dissipate a power of:

$$P_{L_{blue}} = I_f^2 R_{L_{blue}} \Rightarrow P_{L_{blue}} = (700 \times 10^{-3})^2 \times 1.8 \approx 0.9W \quad (3.13)$$

Additionally, to protect the LEDs from induction charges and linearize the drain voltage, a flyback diode was placed with the LEDs. The diode used was the Schottky diode PMEG4010ETR, which can handle 40V and up to 1A. As mentioned, because of the spare space in this PCB there were placed voltage regulators to generate the voltages needed in the Rx layer of 5V and 12V. The first PCB of the Tx is displayed in figure 3.39.

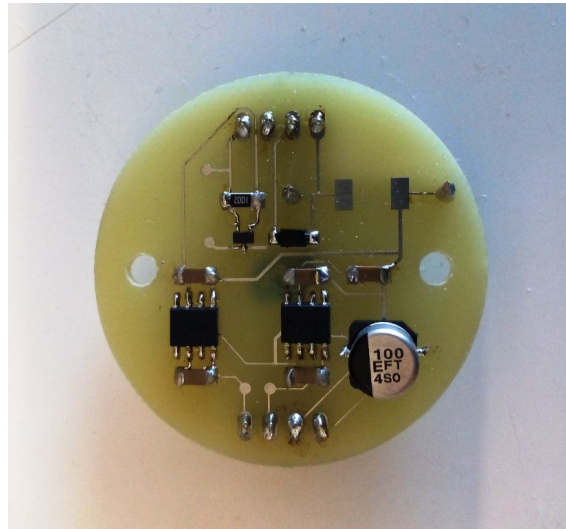


Figure 3.39: First prototype of the Tx layer.

One of the biggest problems was encountered right from the beginning, due to a printing error at the workshop, was the fact that the PCB was printed in mirror, which forced to solder the polarized and pin oriented components upside down. Fortunately, the pin-outs that connected the Tx layer and the Rx layer maintained their initial logic and it was still usable.

But before this printing problem, the initial idea was to face all the components of the PCB to the top, meaning that they would be faced against the bottom of the casing, in order to protect the circuitry and to obtain a more solid assemble. However, due to this mirror defect, this ideal construction was not possible. Adding to this, was the fact that the electrolytic capacitor presented in the PCB could not fit in the casing, because it bumped against the bottom. To surpass this difficulty an improvised through-hole capacitor was attached to the circuit, as shown in figure 3.40.



Figure 3.40: The improvised capacitor in the primary prototype.

Although the tested Tx PCB seemed to work like it should, in the way that it was able to switch the LEDs at the pretended frequencies, the high power commutation of the MOSFET induced an undesirable noise effect to the ground, affecting not only the output voltage of the regulators, but also affecting the Rx layer, where the noise in the ground would interfere with the signal acquisition. In addition to that, it was mentioned by the electronics workshop technician, that the traces of the PCB in this first version were too thin and its design inefficient, making it harder to work with and more susceptible to noise.

For all those reasons above it was decided to redesign a new Tx layer. In this new version, it was tried to enhance the circuit's behavior regarding the noise and, logically this time, a correct printing of the PCB was desirable.

In this redesign a ground plane was included, since its usage is recommended for high speed applications and being the intended frequency 1MHz it may attenuate the noise action in the ground.

Also some additional decoupling capacitor were included in all the integrated circuits (ICs), such as in the regulators, according to their datasheet, in order to reduce their noise. For each it was used a pair of ceramic and tantalum capacitors with a lower equivalent series resistance (ESR) than the typical electrolytic capacitor, to boost the decoupling performance, and to ease the overall PCB layout.

Finally the last change made to the circuitry was to include a MOSFET driver. Despite previously this was a discarded option, it was thought that with this driver a better isolation of the ground from the MOSFET, and a smaller distortion of the Tx signal was possible. With a new market search it was found the UCC27517 that looked like a viable option, since it is suitable for the use with micro-controllers and is compatible with the TTL, working with a logic level signal of 3.3V or 5V, and as a fast response time (rounding about the 20ns) that does not induce a significant delay to the transmitted signal. All the values of the gate resistor (represented by  $R_{gate}$ ) where the recommended from the datasheet.

In figure 3.41 it is shown the evolution and the differences of the first prototype and the final version.

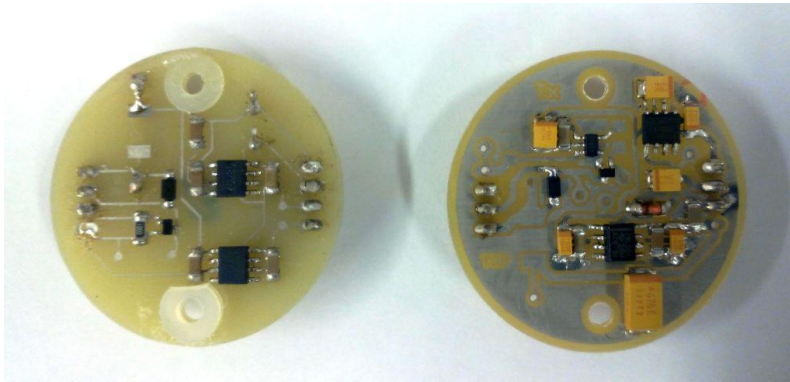


Figure 3.41: The primary Tx prototype on the left and the final Tx PCB on the right.

As it will be refereed later on this work, it was possible to achieve the possibility of have only the circuitry working with a supply of -5V and +5V, which resulted in removing the +12V regulator from the Tx layer, improving the system efficiency and simplicity. The negative voltage converter was relocated to the Tx layer.

In the appendix A it is possible to examine more precisely the PCB schematic and its layout.

### 3.5.4 Rx Layer

Finally, in the Rx layer is where the most complex operation of receiving the light message, is processed. Because of that, this layer has more components in it, to be able to perform the necessary operations.

Just like the Tx layer, the Tx required more than one version to achieve an acceptable prototype result. In the first approach, beginning with the TIA, the choice of components was maintained the same (the THS4631 with the  $R_f = 10k\Omega$  and the  $C_f = 2.2pF$ ) as the previous tests, taking into

account this same tests. In the BPF the amplifier used was changed, in order to avoid the necessity of having an additional regulator producing -5V that would only be used by this component. So the LM7171 was chosen to perform the filtration, since is more than able to handle the frequencies needed and as a similar voltage supply like the TIA, the rest of the components stayed the same as tested. For the comparator, the only change is the threshold value  $V_{ref}$  will be regulated with a potentiometer. Also because of the necessity, a voltage regulator was placed in the PCB to output the necessary -12V for the components.

The only problem in the assembly of this first version was only the fact that the pretended electrolytic capacitors to be used in the negative converter were not delivered until the end of June, making it impossible to be used according to the initial planning, so some default ceramic capacitors were used. Figure 3.42 shows the final product of the first version of the Rx PCB.

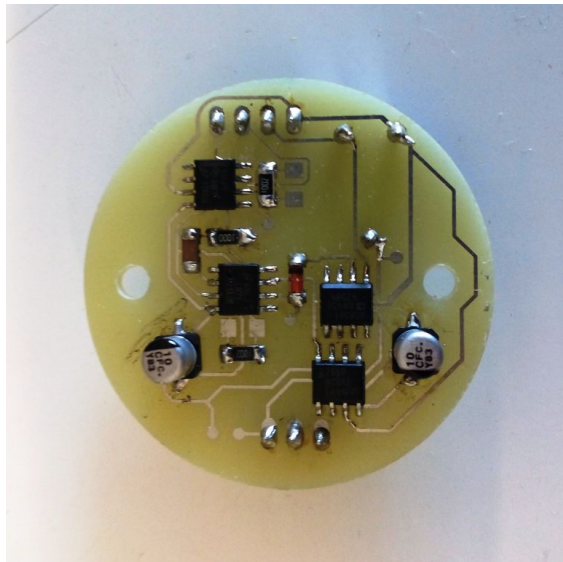


Figure 3.42: First assembly of the Rx layer.

Still short after the first tests on the PCB, some defects were found in the design. In addition to the inability of acquiring the signal while transmitting due the noise generated by the MOSFET, the normal acquisition was not possible by motives unknown. As well an audible sound noise was generated by the PCB from this Rx layer. It was presumed that a component was damaged or malfunctioning.

The first debug test was to cut and separate the function blocks from each other and analyze were the problem was. Meanwhile, it was identified the necessity of a buffer between the TIA and the BPF in order to separate the operations in current of the TIA, and the voltage amplification operation of the BPF, making it a good practice in this circuit.

In one of the Rx layers there was also an issue regarding the negative voltage converter, because one of them was working and the other was not. Later this complication was identified due to an unpredictable problem with this device, where in one of them a latch occurred because of residual charges in the capacitors. This problem can be fixed by following the datasheet steps, and use a default diode (LS4148) for this random issue, that can occur.



It was checked that the TIA was working properly, but after cutting the blocks connections, it was diagnosed a problem in the BPF where no signal was being filtered.

So a narrower debug test was applied to the BPF, by firstly using only the resistors as a simple Inverting Operational Amplifier and then adding the capacitors to check if the output is the expected. By redoing and testing step-by-step the BPF, it was possible to make it work like it was initially pretended. Subsequently an improvised buffer was included between the TIA and the BPF (using a BUF634, acquired in INESC TEC) and it was possible to see the receive signal with the correct filtration and amplification.

But even with this corrections when attempting to connect the BPF output to the comparator the audible noisy sound reappeared, so it was assumed that the problem resided in the comparator or even in its connection. Initially between the BPF and the comparator it was placed a default diode (again the LS4148) in order to avoid a negative input in the comparator, making it basically a safety measure and nothing more. But it was presumed that this diode could represent a complication, and that the potentiometer that control the threshold  $V_{ref}$  of the comparator was improper for this precision application necessity.

So even more changes were made to this first version of the PCB, by eliminating the connection diode, connecting a proper trimmer, to get a more precise  $V_{ref}$  and replacing the comparator to exclude any error regarding damaged material or other possible causes. After applying all this changes, for the first time, a successful output signal was possible to be extracted.

In the end of the preliminary testing of the PCB, in figure 3.43, shows the necessary modifications made.

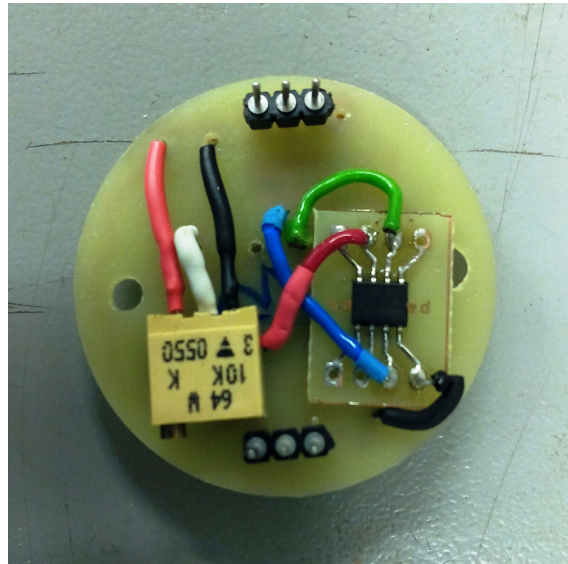


Figure 3.43: Visible improvised modification in the first version of the Rx layer.

On account of the same problem with the PCB traces such as the Tx initial layer, and all the other mistake mentioned above and some more considerations, it was deliberated that an enhanced version of this PCB would be an advantage.

So for new final version between the TIA and the BPF a Buffer was included, the only aspect to watch for is if this buffer is able to operate in the required frequencies and that would delay the signal as less as possible, and the previously used buffer BUF634 was more than able to operate in the required frequencies without delaying the signal significantly. Its simple connections and circuit layout were also attractive traits for its choice.

Like was mentioned earlier the trimmer was also an important change, so for this version a SMD  $10k\Omega$  trimmer was used to control the threshold with more precision, in order to make transmissions more effective.

Since it was given a new opportunity to create a new version of the Rx, a new hypothesis was explored to be able to operate the Rx layer without resorting to the +12V and -12V. To make this hypothesis to be true, it was searched an AMP-OP that would manage the pretended frequencies of operation, with a low noise input voltage and that can work at only +/-5V supply. After an extend market search, it was found an good option, the LMH6624, which has a remarkable performance at a low supply voltage of +5V and -5V, with a low noise input voltage and is able to operate in the intended frequencies.

With this modification, a new improvement was made to all the circuitry, making unnecessary the existence of the +12V regulator, simplifying the circuit. With this, as mentioned previously the negative voltage converter was placed in the Tx layer, changing slightly the module pin-out.

The remaining modification were similar to the Tx layer, by creating a recommended ground-plane in the PCBs and reinforcing the decoupling capacitor in each function block of the layer. For this layer, due to the complex layout it was additionally necessary to make this layer a dual plane layer. This made actually easier to test sequentially the layer blocks one-by-one.

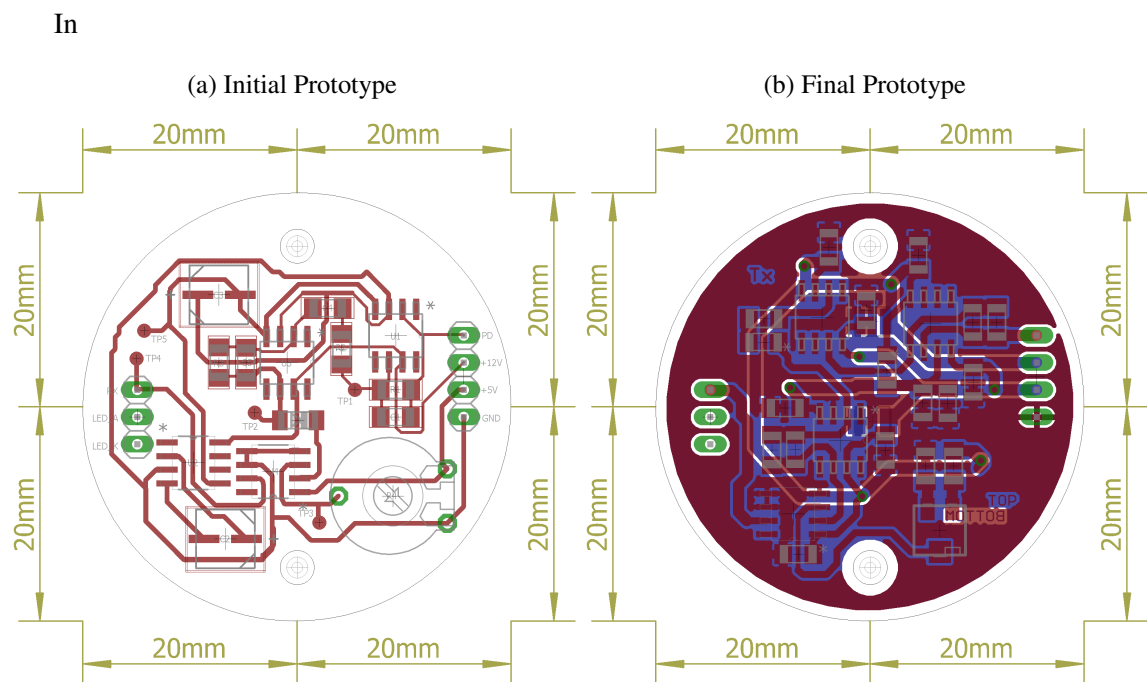


Figure 3.44: The change from the initial prototype to the final.

To finalize this layer, in figure 3.44 it is shown the evident changes of the initial model and the end prototype.

### 3.5.5 Assemble and Connection

To assemble all the electronic components of the Tx and Rx it was necessary to create different PCBs for each layer. To be able to do such a thing, each PCB would have to match up the dimension requirements of the physical casing, which means that the ideal solution is to create round PCBs for each layer with a maximum diameter of 40mm.

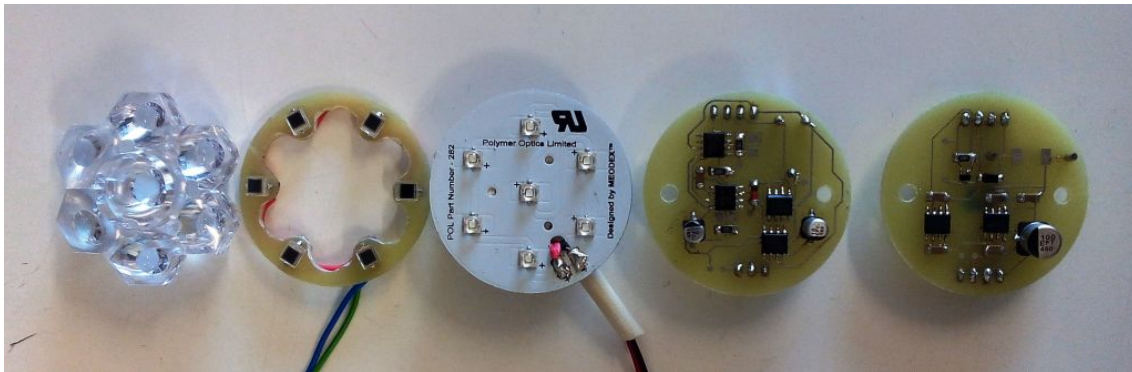


Figure 3.45: Preview of the order of the layers.

The module as shown in figure 3.35 begins with a physical cable where the necessary 24V and ground are supplied alongside with the transmitter and receiver cables. They connect to the first PCB, the Tx driver, by soldering the cables directly to the PCB. This one is fixed by screws to the casing, and then this layer connects to the Rx PCB through pin head (resembling the connection between an Arduino and a shield). Some of this pin heads are just some supply voltages for the Rx PCB, but also as some pin heads that have to connect to the LED PCB and other output pin heads to connect to the PD PCB.

Finally, by placing the PD layer in ring shape between the optical lens and the LED layer and attach the lens to the LED PCB, the module is complete. The optical lens focus each LED of the PCB and the PDs have some clear space to detect light through the hole present in the lens.

The figure 3.46 shows the final aspect of the module, showing the connections between all the layers of the system that are inside the casing.

## 3.6 Summary

In this chapter it was presented all the main components of the communication system separately, showing the preliminary tests made to validate the concept and to take some prior conclusions on how it will perform in different test conditions.

It was obvious that this real implementation of the prototype was way more elaborated than the expected, and a substantial amount of time was invested in it, in order to achieve a working



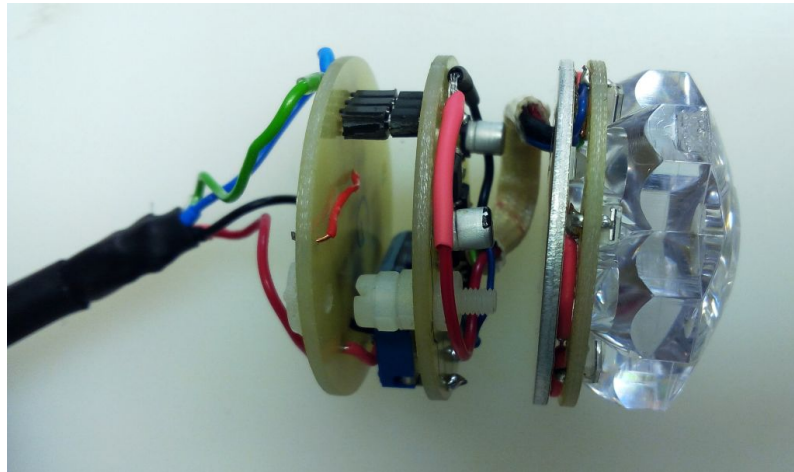


Figure 3.46: The nucleus of the communication module, assembled all together.

and testable prototype. With all this work is accurate to say that the physical conception of this prototype, is the solid core of all this work.

It goes without saying that a lot of improvements can be done to all the prototype, some which will have reference in the chapter of conclusions and future work.

Now that the implementation of the prototype is concluded some tests on bench and underwater must be done to validate the concept, and to see if there are any adjusts to be made to the system.



# Chapter 4

## Test Results

In this chapter, it is presented all the tests that have been done to validate the implemented solution.

The test methodology started with the simplest tests in a workbench with different physical factors and when the prototype is all tested in air-borne, its transmission is subjected underwater in the laboratory pool presented in the department.

First the test procedure is presented, explaining what important data is collected, how the test is done and how a result is registered. Then it is presented the results of the tests performed in different environments.

### 4.1 Test Procedure

For every test initially, the parameters which are recorded and varied, in each different test, are the following:

- **Date** and **Hour** of the test;
- The type of **Test Scenario**;
- Type of **Casing** to be tested;
- The **Light Color** of the transmission;
- Which **Frequency** is transmitting;
- The **Deviation** of the modules between each other;
- The ambience **Light Level**;
- The **Time** of transmission;
- And the value of the comparator **Threshold**;

There are two test scenarios, firstly testing the prototype out of water in the workbench and in the test pool. In the casing parameter it is possible to see the prototype performing without

casing nor the optical lens, only with the focusing crystal and with no casing, or with two different types of casing. One with a long end, able to better reject the influence of the ambience light, but obviously more sensitive to deviations, and a short end without the deviation problem but more affected by ambience light. The testing end parts of the casing can be seen in figure 4.1.



Figure 4.1: The two tested casings. On the left, the long one, and on the right, the short one.

Also, the two studied high brightness LEDs light colors were the green (figure 4.2c) and blue (figure 4.2a), testing at two different frequencies of 1MHz and the 100kHz. In terms of the deviation, the holder had some marks marking the deviations of 0, 15, 30 and 45 degrees, being this deviations subject of testing (figure 4.2b).

Since the tests were performed in a laboratory, the ambience light level was also somewhat controllable, so three cases were studied, with medium lights, maximum ambience light and with no light at all. The remaining parameters were only monitoring variables, so no tests were performed by varying them.

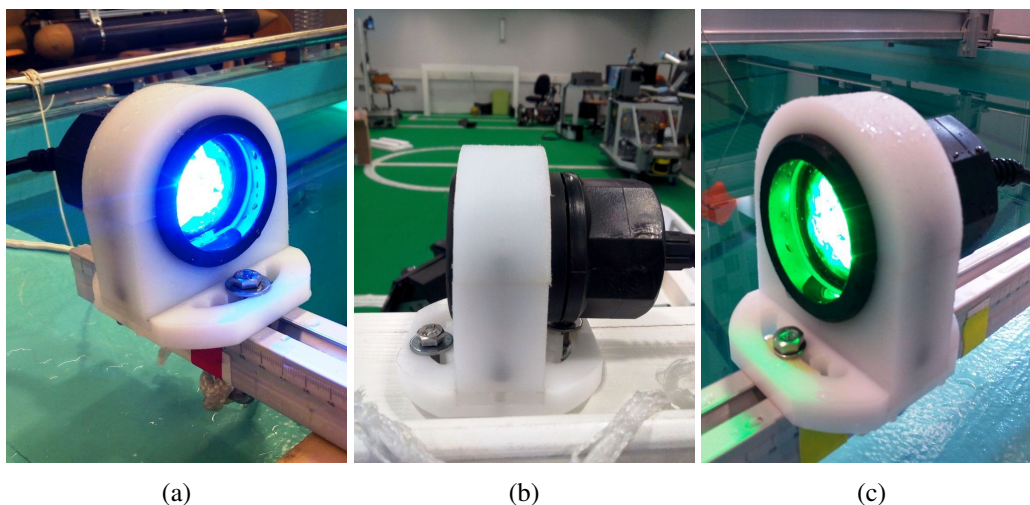


Figure 4.2: The blue Tx, the module holder and green Tx.

In addition, to connect the terminal of the modules cables to the respective source or output, it was necessary to implement a "derivation" board, in order to perform this task. So a very simple circuit board was created to fulfill this necessity. It features a connector to each cable of the module, some test points, a command switch and a fuse in order to protect the battery from a short-circuit if needed. The board is shown in figure 4.3.

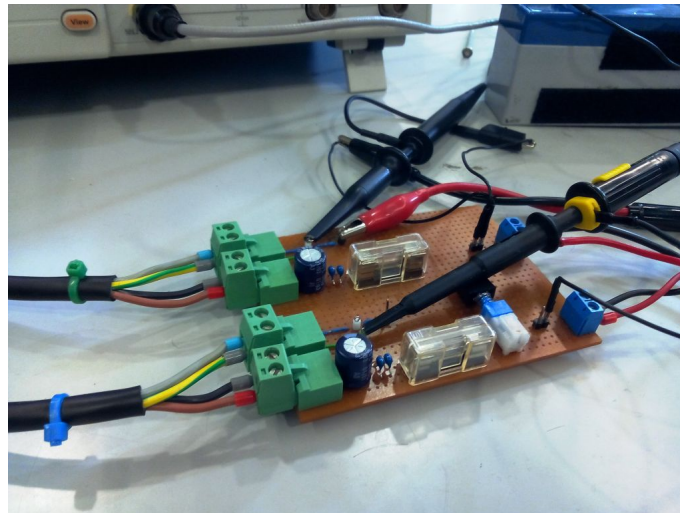


Figure 4.3: The derivation circuit board.

In every test it is followed a certain procedure, that can be interpreted like a protocol, that is roughly the same in each test scenario.

The pair Tx and Rx are placed in a certain range to be tested, fixed and then they are both supplied with their voltage suppliers. At this time, both of the modules are in active Rx mode, which means that both are able of receiving a light signal.

Then a signal, generated by a function generator or a microcontroller, is placed in the pretended transmission cable and the Tx turns on. By now, the receivers of the Tx are ineffective because they get absolutely dazzled by the light of the Tx.

Then the voltage is regulated until a plausible communication is established. When a transmission is settled, the initial consumed current is written down and this operation is maintained during a predefined time period. When this period ends the final current is recorded.

The testing case ends when the maximum supply, around 24V, is reached. At this point, if the device does not transmit at a certain range, this distance is known as its range limit.

#### 4.1.1 Determining a Result and Related Problems

Right after the implementation started to show some promising performances, a question occurred in terms of testing and retrieving results: *How can a transmission be classified as successful or even plausible, and how to measure error rates or derivatives?*

This is quite a debatable question, since this work does not explore software solutions that can quantify or acquire information of a transmission. Every communication is performed at real-time, and the output visible through an oscilloscope.

At first, and still in the final implementation phase, while testing the prototype for final tune-ups, primarily it was assumed that a successful transmission, only could be classified as such if the output signal of the Rx was clear with no change or disruption. Resorting to the figures in 4.4, this initial classification is explained.

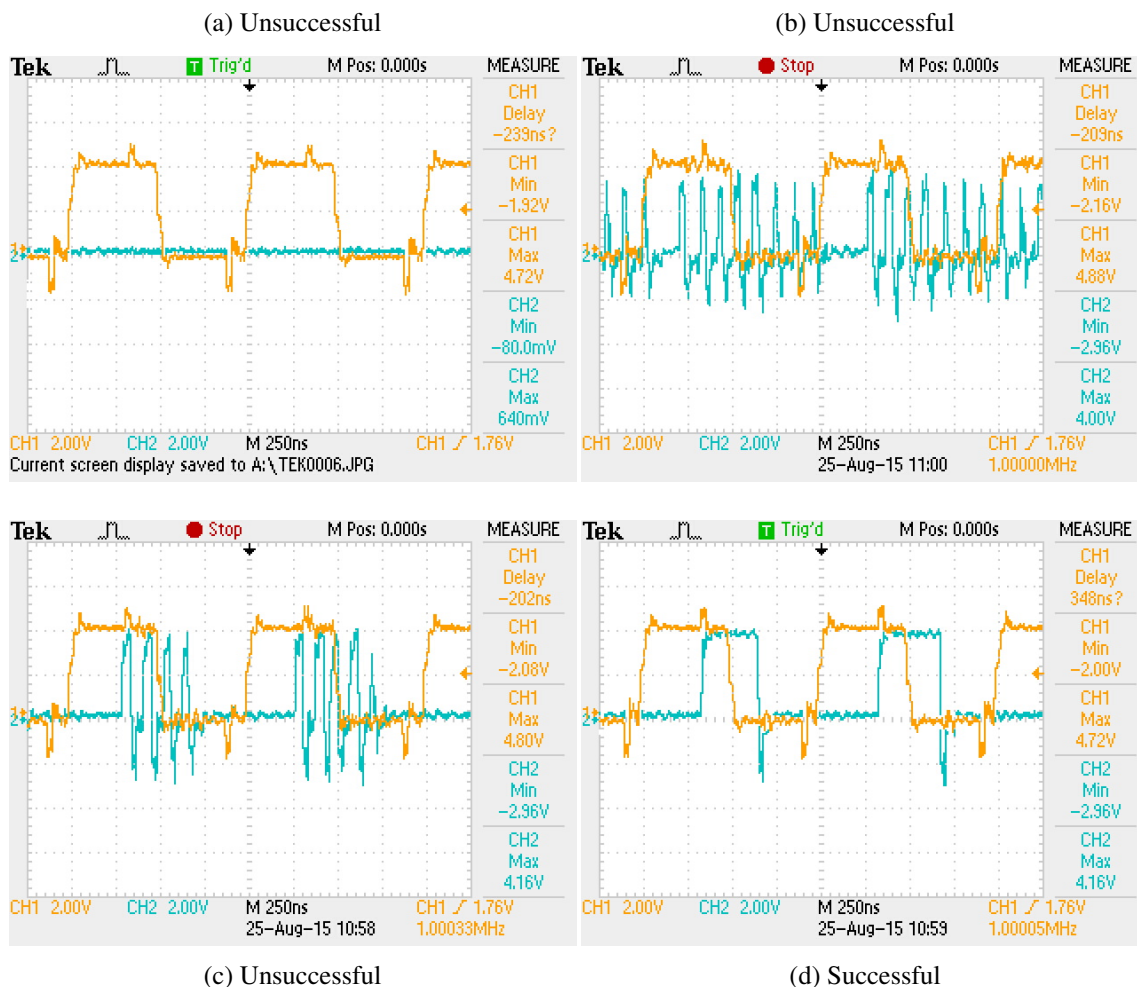


Figure 4.4: The initial classification according to the Rx output (CH1:Tx, CH2:Rx).

Initially, to determine the successful communication, only the clear outputs, like is shown in 4.4d, were labeled as success.

Even though it is globally acceptable to assume that in the print 4.4a, no communication is establish at all, other ambiguous outputs, such as 4.4b and 4.4c, not set in zero, were considered non-communication or noisy communication situations.

Assuming such criteria, and classifying the cases of 4.4b and 4.4c only as "noisy communication" is not entirely true and is rather restrictive since the output is not yet disputed.

When a clear successful transmission, like in 4.4d is detected, it means that the signal captured by the PD and processed by the TIA and the BPF, produce an output big enough to exceed the limit imposed by the  $V_{ref}$ .

The ambiguous situation occurs when this signal, when passing through the comparator, is too close to the value of  $V_{ref}$ . Because of the used comparator configuration, any peak of the signal that goes above the fixed threshold, the comparator outputs a '1' signal; anything below that, it produces a '0'. So in fact what figure 4.4c shows is the Rx is at its limit of communication.

By debating and consulting the co-supervisor Luís Pessoa, it was concluded that assuming only the clear signals such as 4.4d a successful transmission, would be a wrong assumption, since the ambiguous situations like 4.4c are also successful communication, but only with the comparator limitation. Furthermore in this work, some proposed solutions will be presented in the future works section, in order to enhance the comparators performance.

After this assumptions, the following classification shown in 4.5 were attribute to the possible transmission cases.

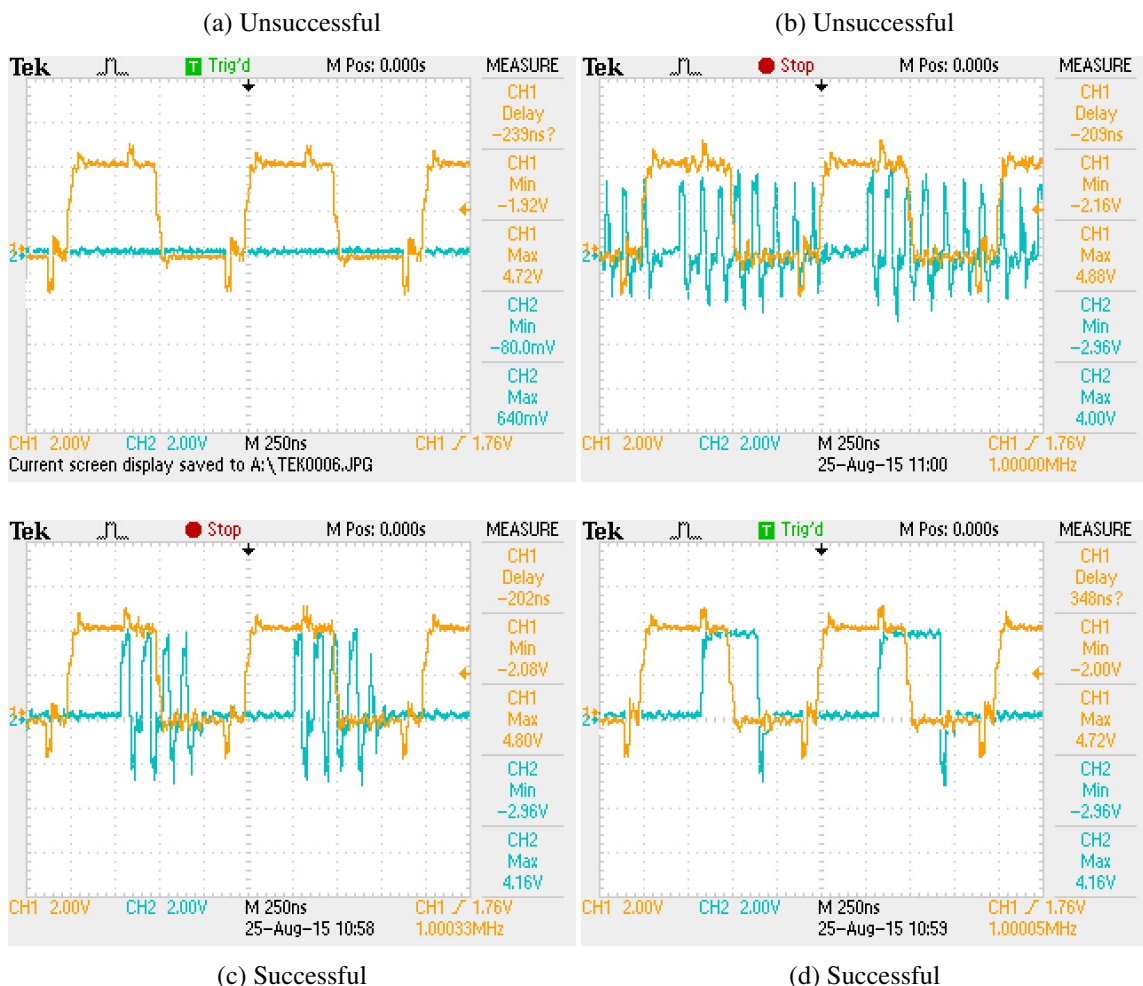


Figure 4.5: The assumed classification according to the Rx output (CH1:Tx, CH2:Rx).

Even though is a subjective presumption, likewise the initial assumption, in the 4.5a case no



communication is detected. On the other hand 4.5b is also considered an unsuccessful transmission because it is not possible to distinguish an output signal. In the tests, the cases like the 4.5c and 4.5d are assumed as a successful transmission.

For the fact that is work is mainly focused on the hardware conception, it was not possible to develop a software solution to extract an error estimation.

Now with the test setup, and the acquisition parameters outlined, the test results are presented.

## 4.2 Control Tests

Initially, these control tests were made with the pair Tx and Rx with no casing and, of course, out of the water.

Because this tests had no casing, it was not necessary to use the holder for this initial tests, placing the Tx and Rx in a marked position at a certain range.

For this first tests it was thought that it would be interesting to study the difference, if any, of the range of the green and the blue light. The communication frequency was set at 1MHz, the deviation, since there was no casing nor holder to orient the module was overlooked, and the ambience light level was in medium intensity.

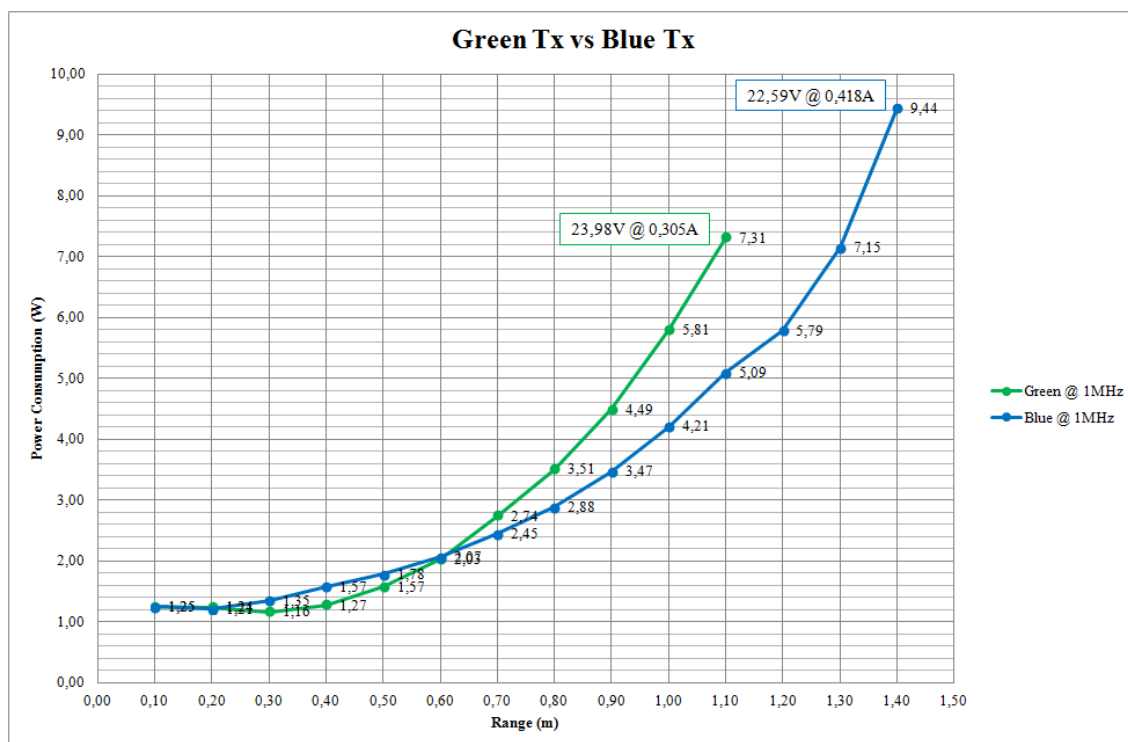


Figure 4.6: Results of the green and blue transmission with no casing nor optical lens.

It is possible to check in the graph 4.6, in this first approach, a better performance of the blue light in the communication. At first they start very similar, and between the 0.2 meters and



0.6 meters the green light performs slightly better than the blue, but at a higher range, the power consumption and range of the blue light outperforms by far the green light.

The green light in this test reached its limit at about 1.10 meters, while the blue light achieve an even greater result by transmitting up to 1.40 meters.

Next this results, named the control test, will be compared to the performance of the module using the ordered optical lens, naming the crystal subject, in order to see if an enhancement in the transmission. The test parameters maintained the same as the previous one, changing only the use of the lens.

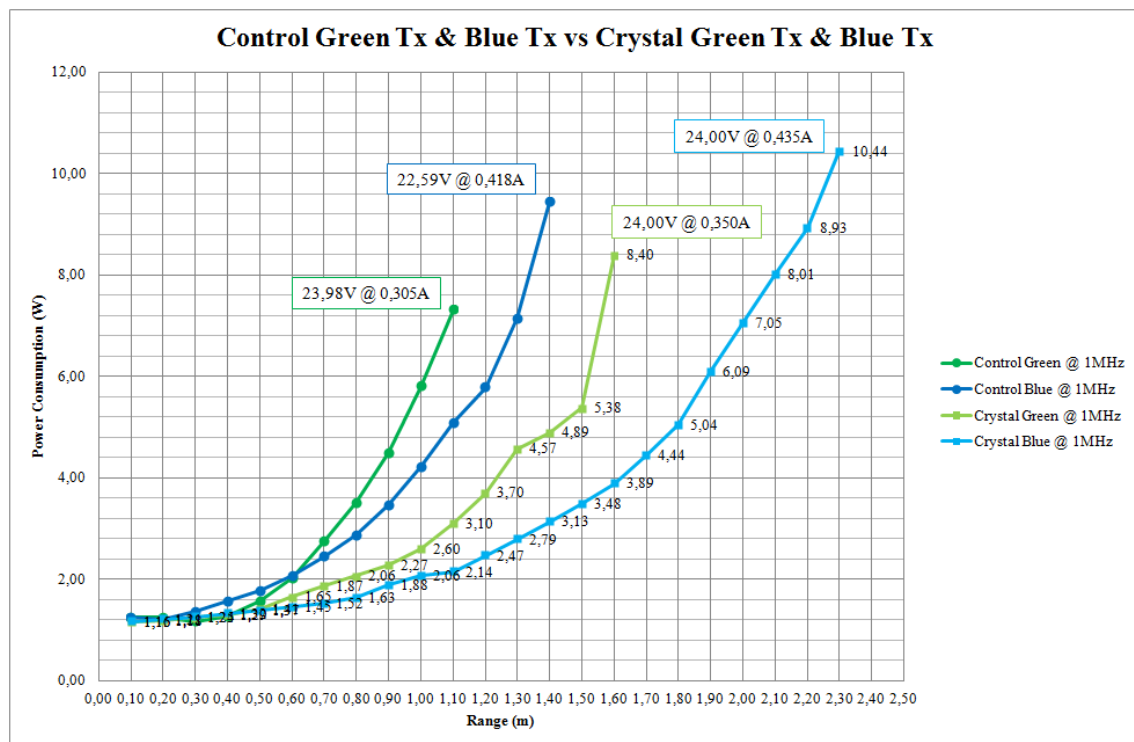


Figure 4.7: Results of the green and blue transmissions, now with the optical lens.

It is obvious, by analyzing the results in graph 4.7, that the optical lens did influence the light transmission in a positive side. The green light was able of enhancing its transmission by 0.5 meters, which is a significant improvement, and the blue light was able to achieve a remarkable range limit over 2 meters (2.30m, to be exact).

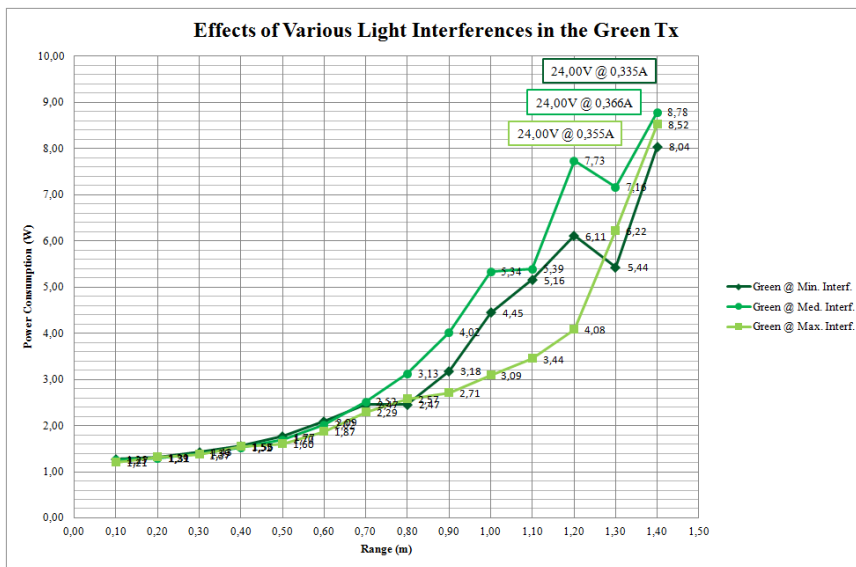
After these tests some conclusions could already be drawn. In an environment out of the test pool, the blue light was more effective in terms of range rather than the green light, and the acrylic focusing optical lens can significantly improve the performance of the light transmissions. So for the following experiments the crystal was attached to the LEDs in order to improve the transmission.

In the first test, too little attention was given to the sensitivity of the threshold of the comparator  $V_{ref}$ , which as a direct effect in the sensitivity of the Rx. After the first test,  $V_{ref}$  was measured in both green and blue Rx, and the values were of 720mV and 640mV, respectively. So in order

to obtain a more homogeneous and more informative data, both green and blue transmitter were calibrated to the same  $V_{ref}$  of 840mV, which seemed to be a comfortable value for a possible transmission.

The next step of the tests is to test the module at different ambience light interference. This tests are possible since the lights of the laboratory are adjustable, so for this experiments the transmission was tested with the light interference at its maximum, in a medium term that was the lowest output that those lights could produce, and with the ambience light completely shot down. The transmission frequency was maintained at 1MHz.

(a) Green Tx



(b) Blue Tx

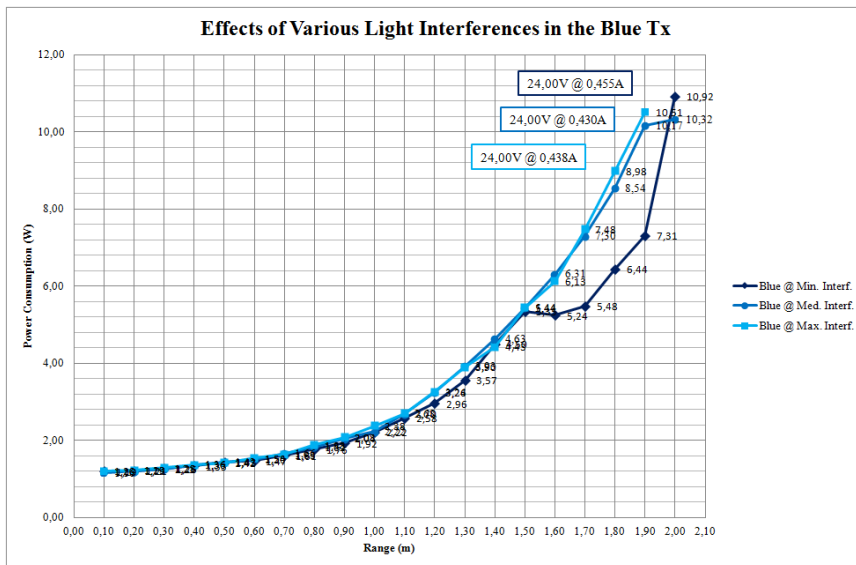


Figure 4.8: Test results of the transmission at different levels of light interference.

These tests, that are represented in the graphs in 4.8, proved to be the most challenging. It was possible to see, while experimenting, that as the range of the communication increased, the harder was to get a consistent subject of testing.

This happens, because the focusing optic had a dramatic effect on the output light, if the Tx suffered even the slightest deviation. Since this primary test did not use any casing nor any holder to better stipulate and control the deviation, it was hard to get consistent results. That is why some results of 4.8a after the 1 meter mark, and in 4.8b after the 1.50 meters mark, do not follow the expected exponential behavior that is shown in the first tests.

Due to this test results, it is arrogant to presume that this test values express truthfully the performance of the communication module. But by having a detailed view to the graphs, it is possible to see that the Rx with the medium and maximum interference are very similar (4.8b). Also in the end values of both 4.8a and 4.8b it is shown that, with less interference at a higher range, the lower is the power consumption, as it might be expected.

Despite this phenomenon and the these experiments did not have been as successful as expected, it is believed that once the modules are fixed and orientated by the test setup, this discrepancies will be attenuated.

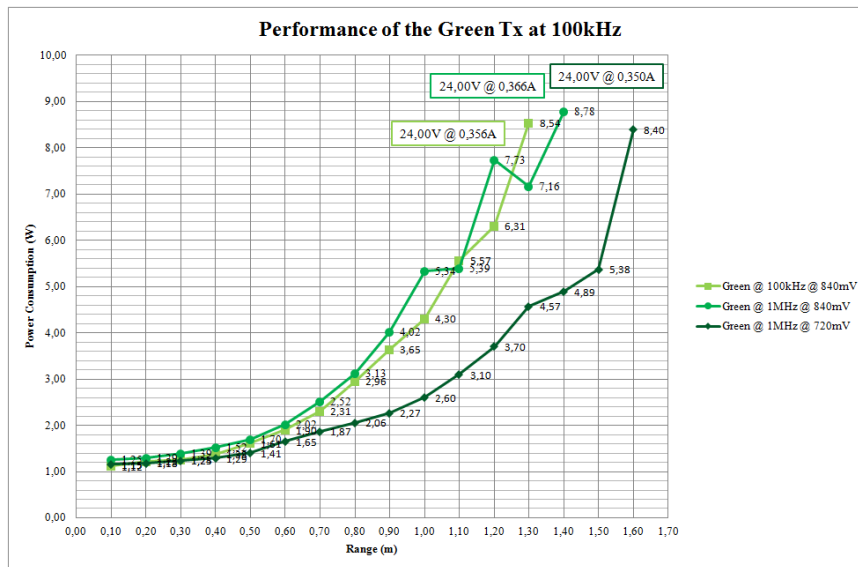
The final control experiment, will test the module capabilities when the transmission frequency instead of been the usual 1MHz, is decreased to 100kHz, a frequency range closer to the usual baud-rate of the serial communication protocol. This experiment will enable to imagine the behavior of the device if communicating using serial communication.

The 100kHz tests will be displayed with the 1MHz before and after the change of  $V_{ref}$ , so some conclusion regarding the manipulation of  $V_{ref}$  can be taken. The remaining parameters remained the same, using the medium light interference.

By analyzing the test result of the graphs in 4.9, it seems that the change in the transmission frequency did not influenced the Tx performance significantly. Although the graph 4.9a, due to the explained distortion event, a conclusion is hard to assume, the results of this 100kHz signal reception were way more consistent, and the differences, between this signal and the 1MHz, are not very meaningful. Resorting to this graph 4.9a, it is also possible to see the impact that the different  $V_{ref}$  had on the Rx output side.

Likewise, in the graph 4.9a all the results are coherent, describing the predictable characteristic exponential curve. Between the two signals at the same light interference levels and same  $V_{ref}$ , at different frequencies their behavior is very similar, only minor variations occur. Also, it is visible the high influence of the  $V_{ref}$  in the recorded test results.

(a) Green Tx



(b) Blue Tx

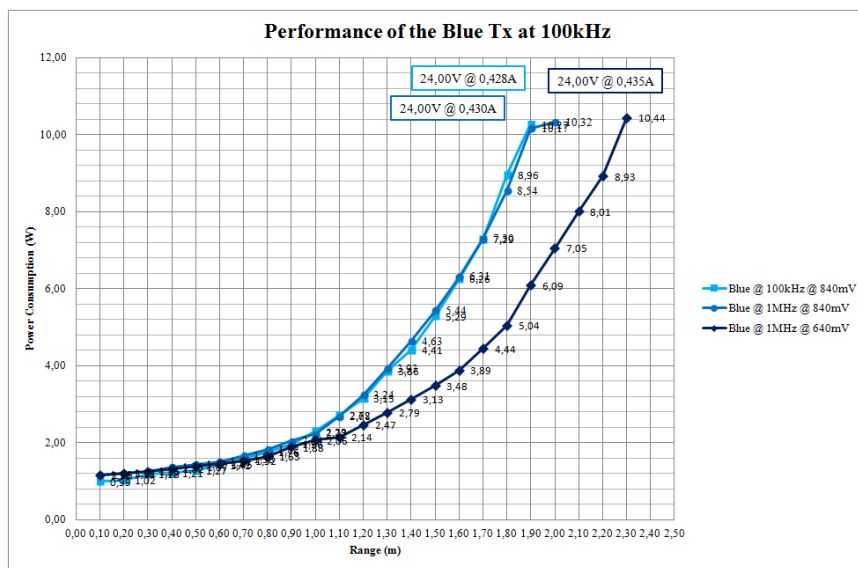


Figure 4.9: Test results using different transmission frequencies of 100kHz and 1MHz.

Summing up, it is concluded that in environment out of water, in terms of the wavelength of the emitting light, the relation of the PD and the blue transmission LEDs seems to be the strongest combination, rather than the green light, which seems to be way less bright than the blue Tx.

It was confirmed that the acrylic lens does enhance the device range significantly, by performing its function of focusing the output light of the Tx, and still enabling the reception of light by the Rx.

In the other experimental cases, the light level interference tests were pretty much inconclusive, since the high influence of the deviation due to the using of the acrylic lens, produced

inconsistent results that did not allow a more critical verdict.

Meanwhile, the impact of the threshold that controls the comparator output, seemed to be another preponderant factor to achieve a better transmission. Still this is a delicate matter since if a too low threshold is defined, higher the probability of error captions and erratic outputs due to the ambience light interference.

Finally, in the two different transmission frequencies, no major influence was detected, which means that in both frequencies the transmission is much alike.

### 4.3 Workbench Tests

Since the first tests are concluded, it is necessary to test the module with the waterproof casing, to check if it can transmit even with the closed casing. This casing capability test will be confirmed first out of water and after in the underwater environment.

Now that the casing is going to be tested, all the structure that will be used in the underwater tests will also be added. So for this simple setup, as it is shown in 4.10, the casings of the Tx and Rx were fixed to a holder with marked positions for the deviation angle to be tested. This holder is settled in a sort of runway with marks on it, in order to mark the various range positions.

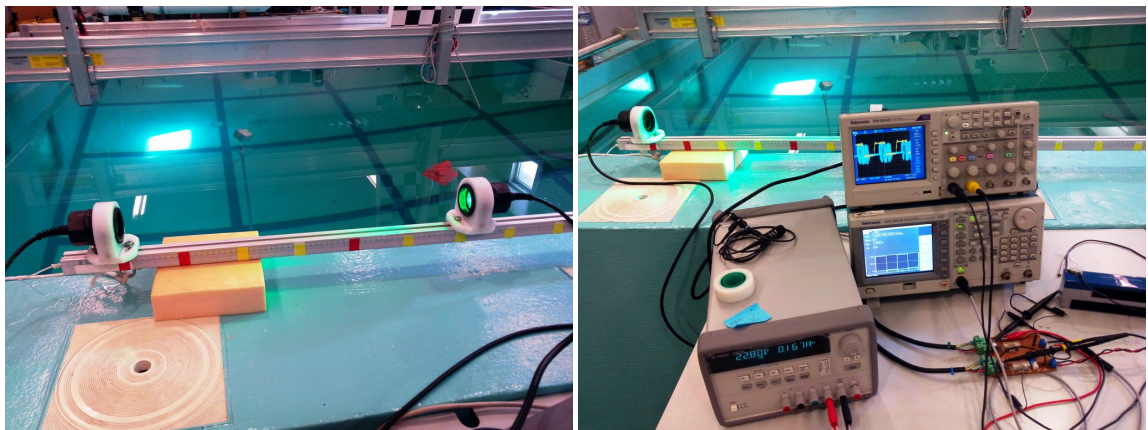


Figure 4.10: Workbench test setup.

The testing parameters are the same as the previous tests, but now the deviation angle is considered in four different positions: no deviation, 15 degrees, 30 degrees and 45 degrees. Also it was possible to test this casing with more than one end terminal, and with a long head and a short head.

In a more important note, since the control of the  $V_{ref}$  is not accessible with the casing closed, it was needed to calibrate the threshold in a fixed value. Since, for the Rx, a lower value would enhance its performance, but at the same time, makes it more susceptible to the noise, a pondered middle term needed to be reached. So both thresholds were calibrated to 740mV, in order to improve the communication, without inducing so much noise.

So for the first test, it will be tested the performance of the green and the blue light at 1MHz, by applying no deviation, and with an average interference of light.

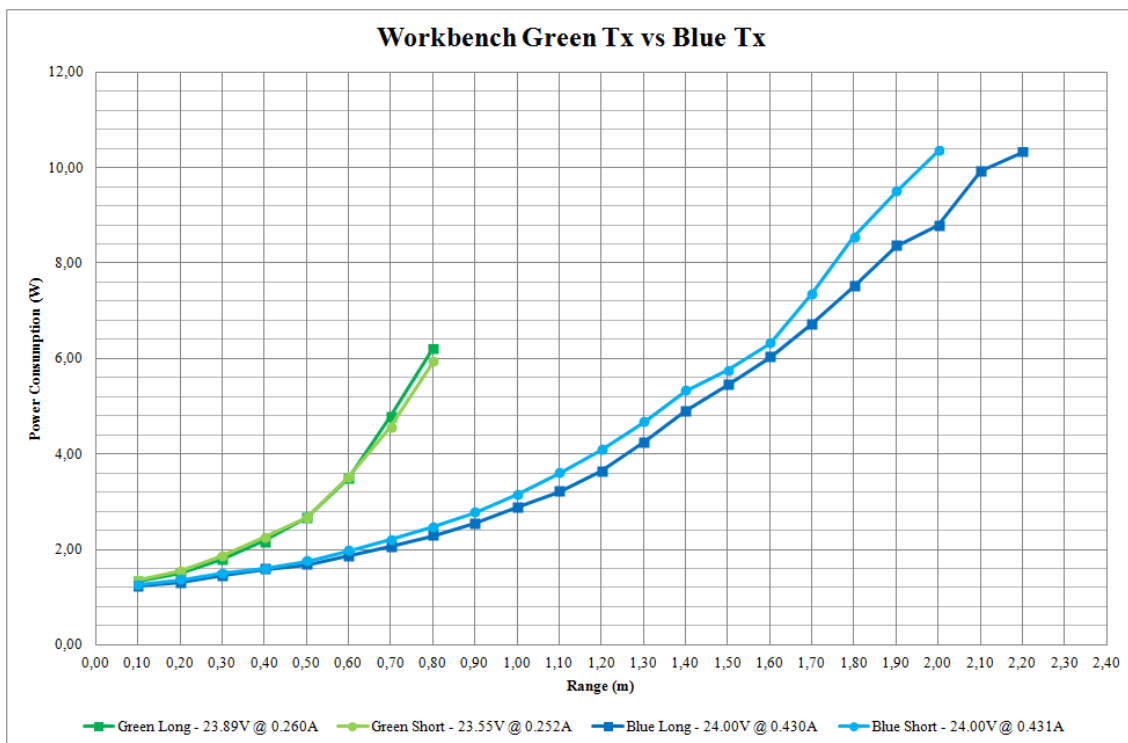


Figure 4.11: Results of the green and blue transmissions, using the two casing types.

As it is shown in the graph 4.11, the use of the casing, independently if it is the long or short type, the range of the transmission, visually comparing to the control subject, is more limited. This is probably because of the design of the casing and the positioning of the PD ring. Even though it is able of captioning the signal, at a satisfactory range, it always limits the capture of the signal.

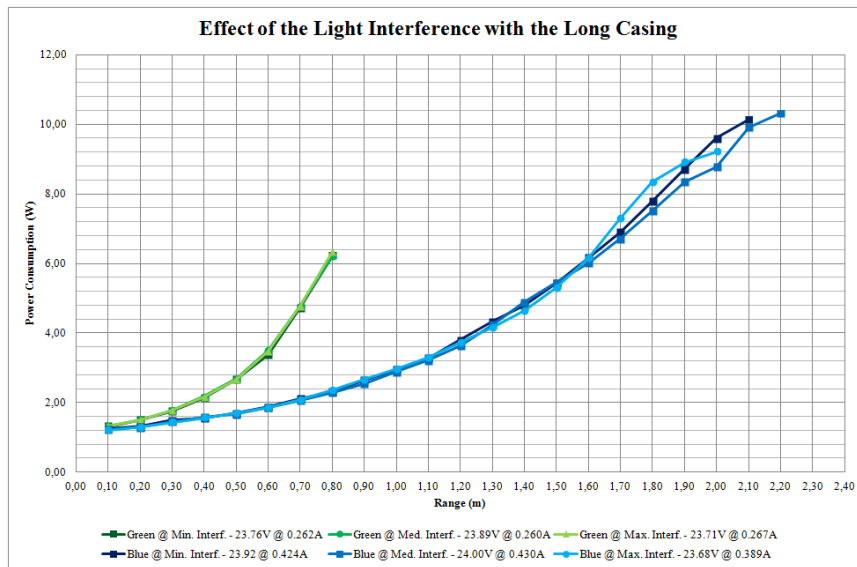
In terms of which casing in this test was the effective, their difference is almost irrelevant. In the green light performance, the traces of the long and short casing are almost coincident, so the different casings did not influence the transmission in terms of the range or the power consumed. Only in the blue light case, when no deviation is presented in the transmission, the long casing seems to perform a little better than the short one.

In a first impression, the long casing comparing to a short one, in a transmission, such as experimented in the test 4.11, indeed does not represent a very relevant difference, since the entry and exit point are supposedly well aligned.

The most relevant difference between this two casings might occur in two different scenarios: when the interference of the ambience light is higher, where in this situation, the long casing potentially has an advantage, since it properly isolates the Rx from this effect. And when a deviation between the two modules exist, where now in this situation the long casing might have a disadvantage comparing to the short, since it can limit the Tx light output.

So for the following experiments, firstly, the ambience light influence will be tested by applying the three different light intensities. Then after some conclusions are made, the deviation behavior will be tested, in order to confirm or not the presumed conclusions.

(a) Long Casing



(b) Short Casing

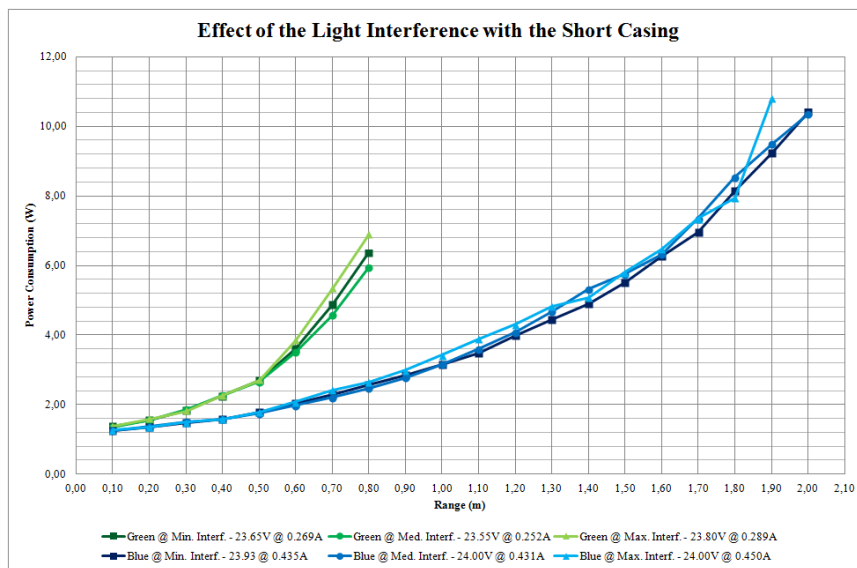


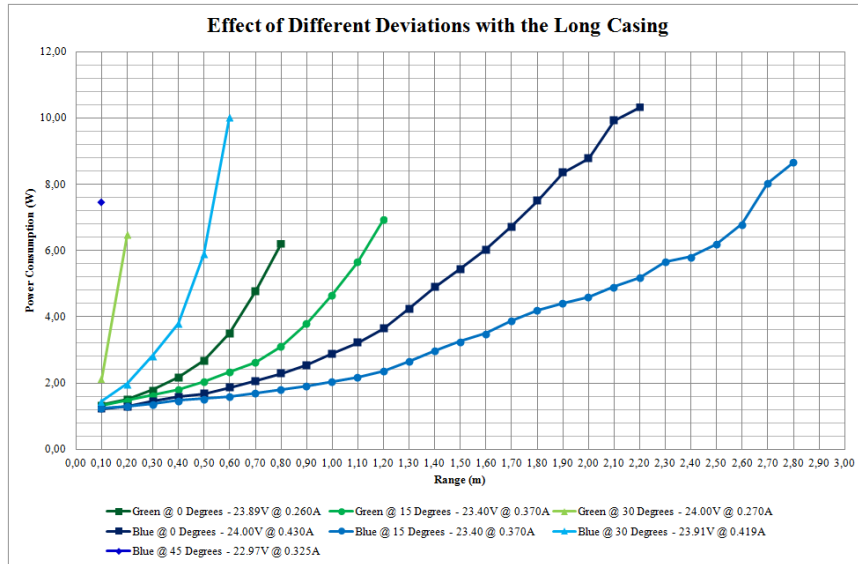
Figure 4.12: Results of the interference of different levels of ambient light.

The results displayed in the graphs 4.12, shows the predicted behavior. By analyzing the results on the green light, although it is a very small difference, in the long casing end, shown in graph 4.12a, the reception for the three different interference maintained practically the same, and in the short end, shown in 4.12b a small difference between the receptions can be detected. As for the blue light, it has thinner trace all along its domain, in the long end, meaning that has a smaller variation, and in the short end shows a more unstable output.

Despite all this conclusions, even with the different light interference all the outputs are satisfactory.

Since the impact of a deviation, on the previous control tests, was very visible, it is possible to assume, that by deviating the modules between each other, the output will respond to the stimulation. It is only necessary to analyze how big the casing will limit the reception and transmission.

(a) Long Casing



(b) Short Casing

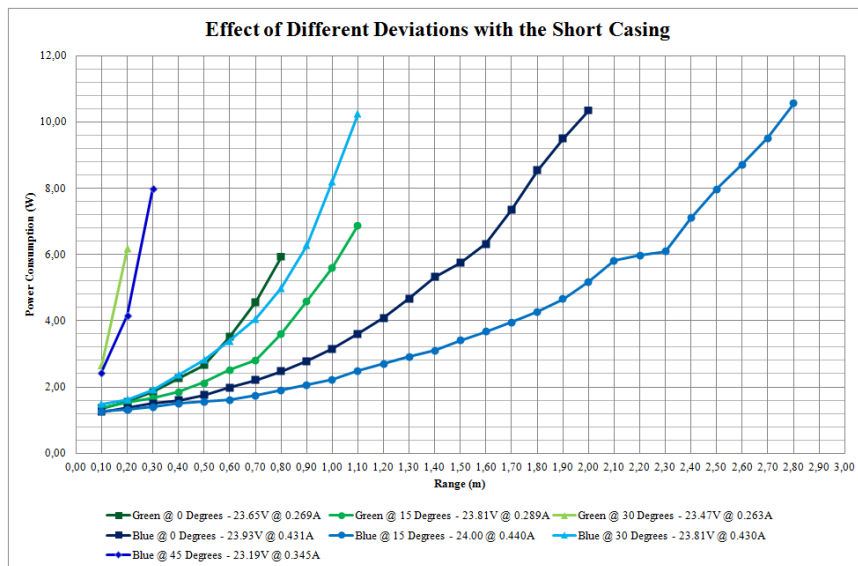


Figure 4.13: Results of the different module deviations.

As expected, in the graph 4.13 the deviation add a huge impact on the light output, both in the green and the blue Tx. The deviation that achieved the maximum range was the value of 15 degrees. The other deviation values greater than this had a worse performance than the average signal.



It is important to state that by comparing the long and short casing outputs, respectively graph 4.13a and 4.13b, is clearly visible the limited range of the Tx when the deviation is superior to 15 degrees, which means that the long casing limits the transmission of the signal to deviations superior to 15 degrees.

The only experiment that is left to do is the transmission at 100kHz, in order to stipulate the behavior of the module working at a lower frequency, capable of being serial communication supported. For this test, it was only performed using the long casing, since no advantage was predicted in testing in the short casing.



Figure 4.14: Test results using different transmission frequencies of 100kHz and 1MHz.

In this transmission at 4.14 the only particular occurrence, only applicable to the blue light, is the more limited range, which started to be insignificant but in the end it got considerably large. Also at 100kHz the power consumption is higher.

Now that the behavior out of water is known, the concept will be tested underwater.

## 4.4 Laboratory Pool Tests

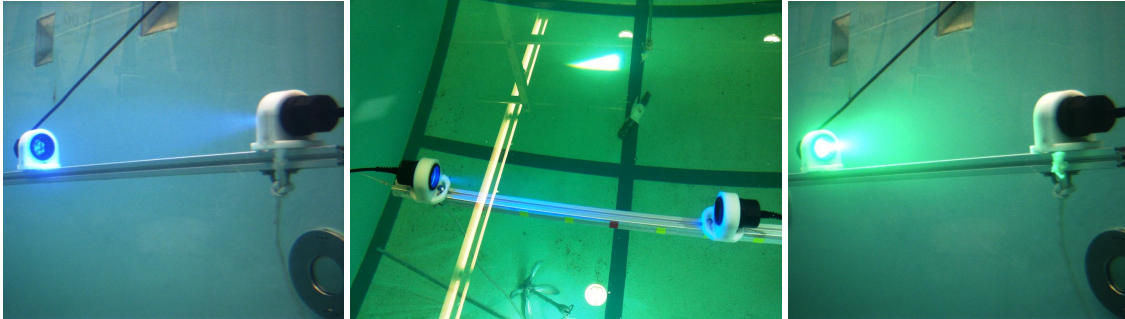


Figure 4.15: Laboratory pool test setup.

Before beginning the transmission underwater, some attention like avoiding the cables being wet were also necessary.

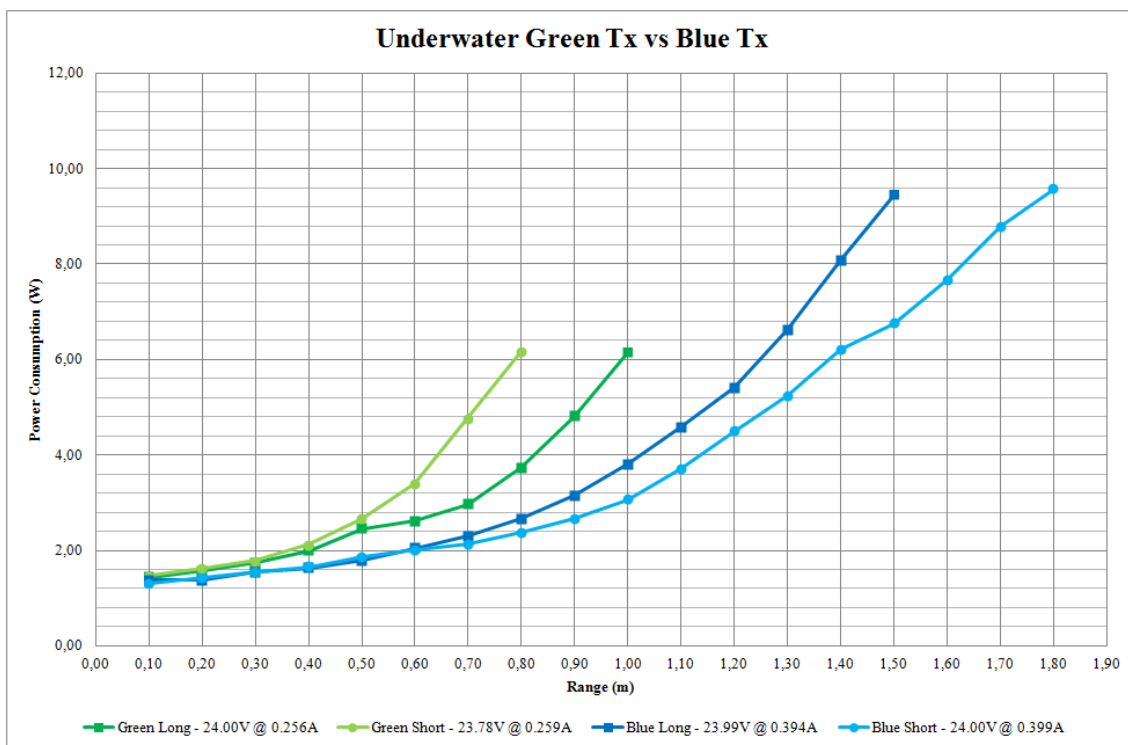


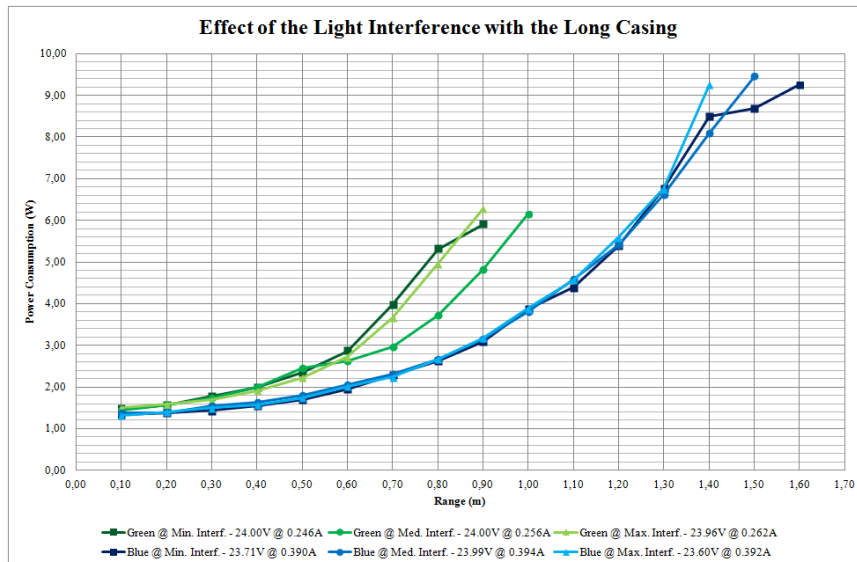
Figure 4.16: Results of the green and blue transmissions, using the two casing types.

The results of graph 4.16 show a result other than the predicted. Due the communication underwater, the signal output is slightly attenuated, being the maximum range of 1.80 meters, not as good as other cases.

The test of the green light with the long casing, was not very successful, inducing some error to the measurements.

Now the system will be tested for the different ambient light level interference. Since this happened in the previous test, some attenuation is predictable for this case.

(a) Long Casing



(b) Short Casing

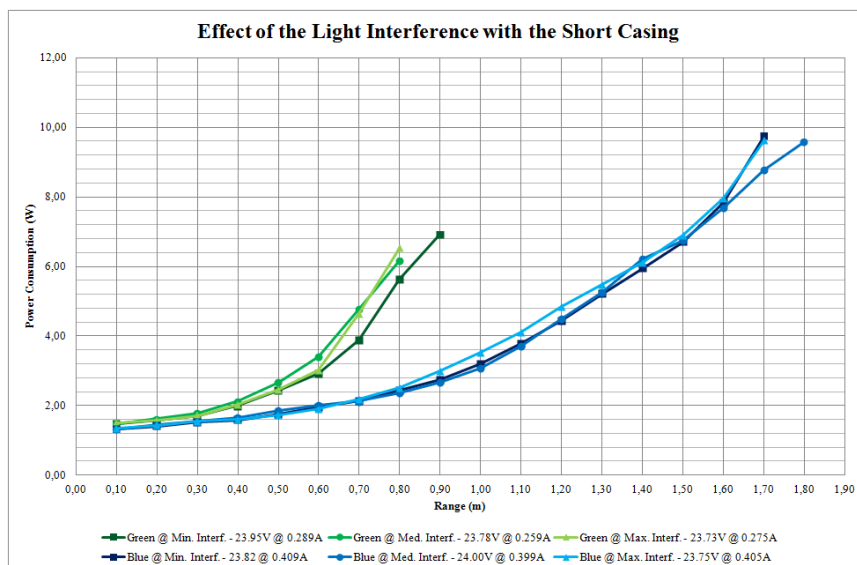


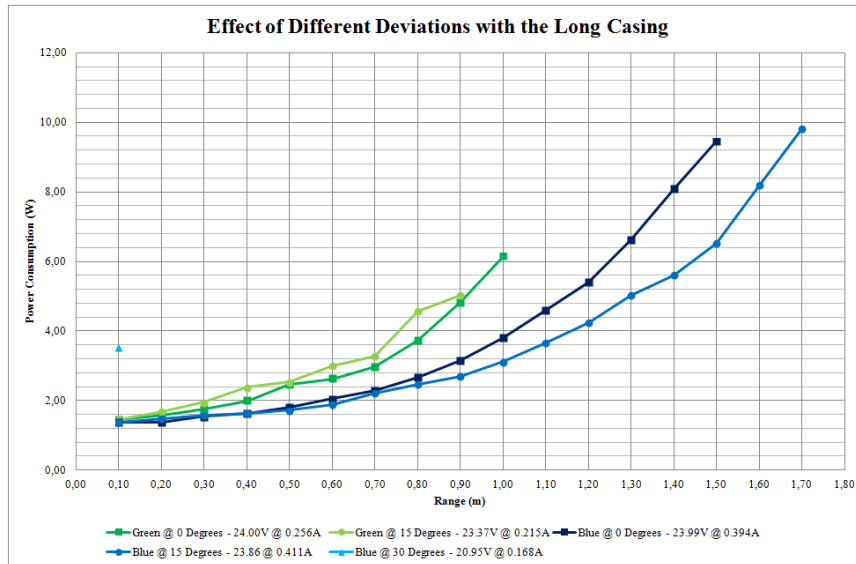
Figure 4.17: Results of the interference of different levels of ambient light

As it can be seen in the graphs 4.17, it maintained the similar performance, being the long casing trace thinner than the trace of the short case, due to the interference of light. The error is the green measurements at the default light level.

For next tests the performance of the modules will be tested by applying the deviations marked in the holder. Since the previous workbench tests, the best range results were obtained when the

deviation was applied to the modules, and although the general performance of the system declines underwater, it is predicted that the best range results underwater will be obtained also by applying the deviation.

(a) Long Tx



(b) Casing Tx

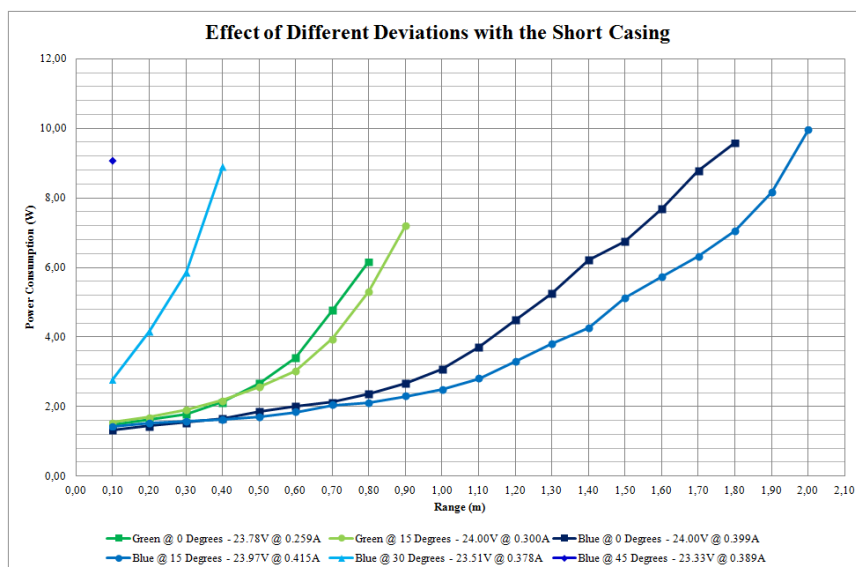


Figure 4.18: Results of the different module deviations.

In the graphs 4.18, more precisely in the 4.18a, the signal of the green light with no deviation, that was assumed like an error measurement, looks like an output response of the already deviated light. In 4.18b, also the green does not represent a big deviation like it should show, which may indicate that the green light is more influenced by the water than the blue light, which is a bit attenuated, but not in a such significant difference.

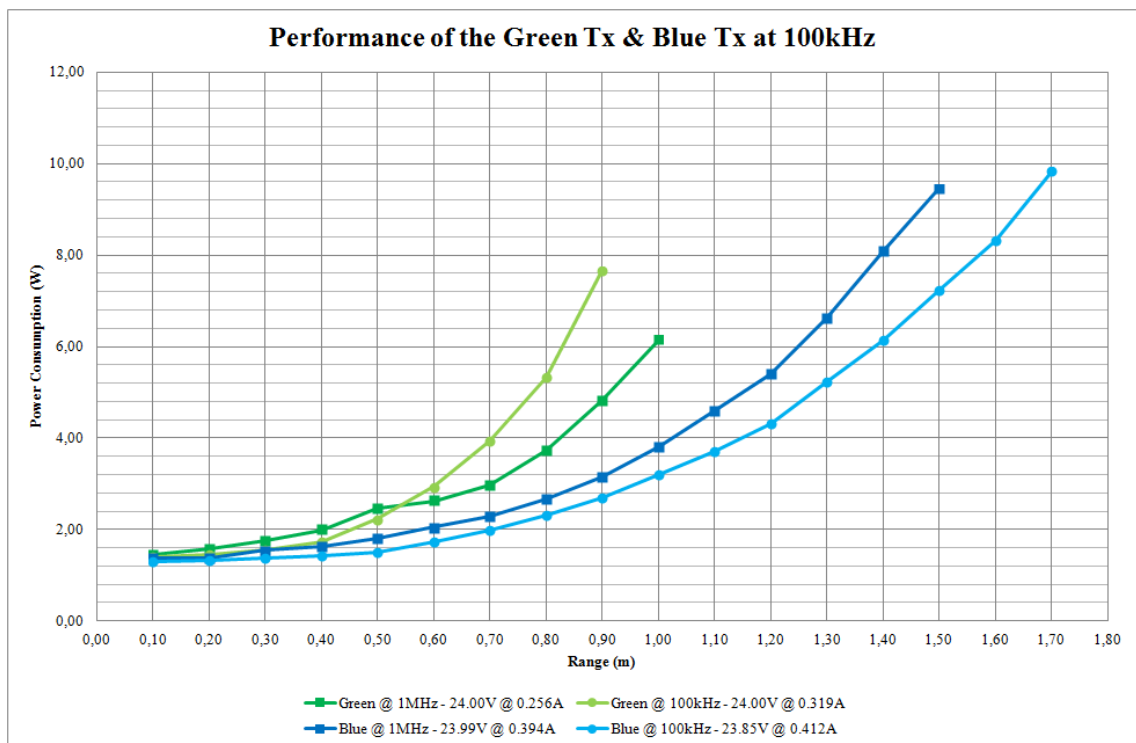


Figure 4.19: Test results using different transmission frequencies of 100kHz and 1MHz.

In this last case, as shown in the graph 4.19 the transmission in 100kHz using blue light, against the normal tendency shown by the past experiments, is reaching higher ranges with lower consumption. The green light presents a very predictable behavior, but does not shown deviation flaws.

## 4.5 Summary

In this chapter, it was possible to test and analyze, even if briefly, the characteristics of the communication module. Although far from perfection some basic concepts were also validated, which contributed to the value of the work.

As some performance specifications, the prototype was able of transmitting up to 2.80 meters with a deviation of 15 degrees out of water, and was able of transmitting up to 2.00 meters with the same deviation of 15 degrees in underwater.

This tests enable the possibility of validating and fulfill the primary objective that is creating a prototype able of transmitting information underwater.

The recommended improvements and new ideas to increase the potential of all this project will be described in the future work section.



## Chapter 5

# Conclusions and Future Work

Finally, the conclusions chapter was reached, which will be an overview of the final status of the project, as well as the outline topics for future work.

### 5.1 Summary of the performed work

The fundamental objective of this dissertation focuses on the creation and the implementation of a physical module based on LEDs able to transmit information through light, in order to overcome some limitations imposed by some existing transmission technologies. This prototype is composed by a physical casing and some PCBs that should be used as a basis to develop a solution that could eventually be adopted. In order to achieve this objective, the following steps were followed:

- A study about the challenges and restrictions that the underwater communication was conducted as well as the tracking technologies that would enable to better perform the necessary operations;
- Secondly the layout of the system was selected. In this process some choices took place for the type of components that will be needed to implement the circuit and their features;
- Some circuits were designed to determine components values and to prove concept ideas;
- Once those circuits were designed, the process of creating the PCB for testing the proposed solution. At this point the PCB was designed and produced;
- It was performed a set of tests in order to prove the concept and the proper functioning of the various parts of the circuit.

### 5.2 Concluded Objectives

Comparing the original objectives of the project and with the practical results obtained, it is possible to say that the core objective of this dissertation was accomplished.

As for the remaining objective, of testing the solution in an non control environment, in the ocean and river, it was not explored, due to complications with the hardware encountered during the production of the prototype which led to a more reduced test schedule.

However, it is possible to point out that the prototype offers vast possibilities for future work and improvements, being this one of its most valuable aspects.

### 5.3 Future work

Although it has been achieved the implementation of the functional prototype, it is still possible to determine improvements to be added to it. Regarding this subject, it is possible to draw two groups of future implementations - those that correspond to the Hardware improvement of the prototype and the others that correspond new possible work. At the hardware level we have:

- The cable that connects the prototype interior to the exterior, was one of the sources of noise, since it was not for this use and did not had proper isolation. A better choice would be a reinforced cable with protection against interference noise and other factors;
- To eliminate the problem regarding the MOSFET charge and discharge noisy operation that affected the Rx board signal acquirement, a solution could be by implementing two separate power supplies to the same module. By doing this the dual-communication option would become a more viable solution;
- As previously mentioned, the comparator of the Rx layer, was not robust enough for the operation that it has to perform, making it harder to determine a positive result from the tests. So that being, an improved comparator with hysteresis (also known as Schmitt trigger), is a solid option in order to avoid some ambiguous situations, where the received signal can be confused with the background noise;
- Other problem encountered, while testing using the casing, was the temperature that the module reached when transmitting at higher power rates. So alternative ways to dissipate the heat generate by the module such like, building a casing with a heat conductive material, like aluminum, and soaking the circuitry in a cooling fluid, would be some interesting ideas.
- Experimenting different focusing lens could improve the signal transmission and/or its reception, improving its range and subsequently its power consumption.
- Another idea, although not so feasible, would be to manufacturing the MCPCB for the LEDs itself, in order to create a more optimized design, were the PD could be attached behind the LEDs, improving the chances of having successful dual-transmission.

Finally, other points of future work would be to make the proposed tests in the outdoor in the Ocean and River, in order to see if the solution is robust enough for a real application. These tests would require to be done at different water and day time conditions. Also since this work



was only focused on developing a hardware solution, some software resources that would enable a quantification and qualification of the communication channel, should be developed, in order to make a more robust validation of the experiments. Additionally, it would be interesting to develop some case studies for a real application of this project.



## **Appendix A**

# **PCB Footprints and Schematics**

In this appendix there are provided the footprints and schematics of the designed PCBs. It is possible to see the versions that were created and its evolution through the development of the prototype. The PCB were all designed using the software, Eagle CAD. When needed there are presented the top and bottom layer of the footprints. Some of the values of the drawn components might differentiate from the actually used.



## A.1 Initial Version

### A.1.1 Tx Layer

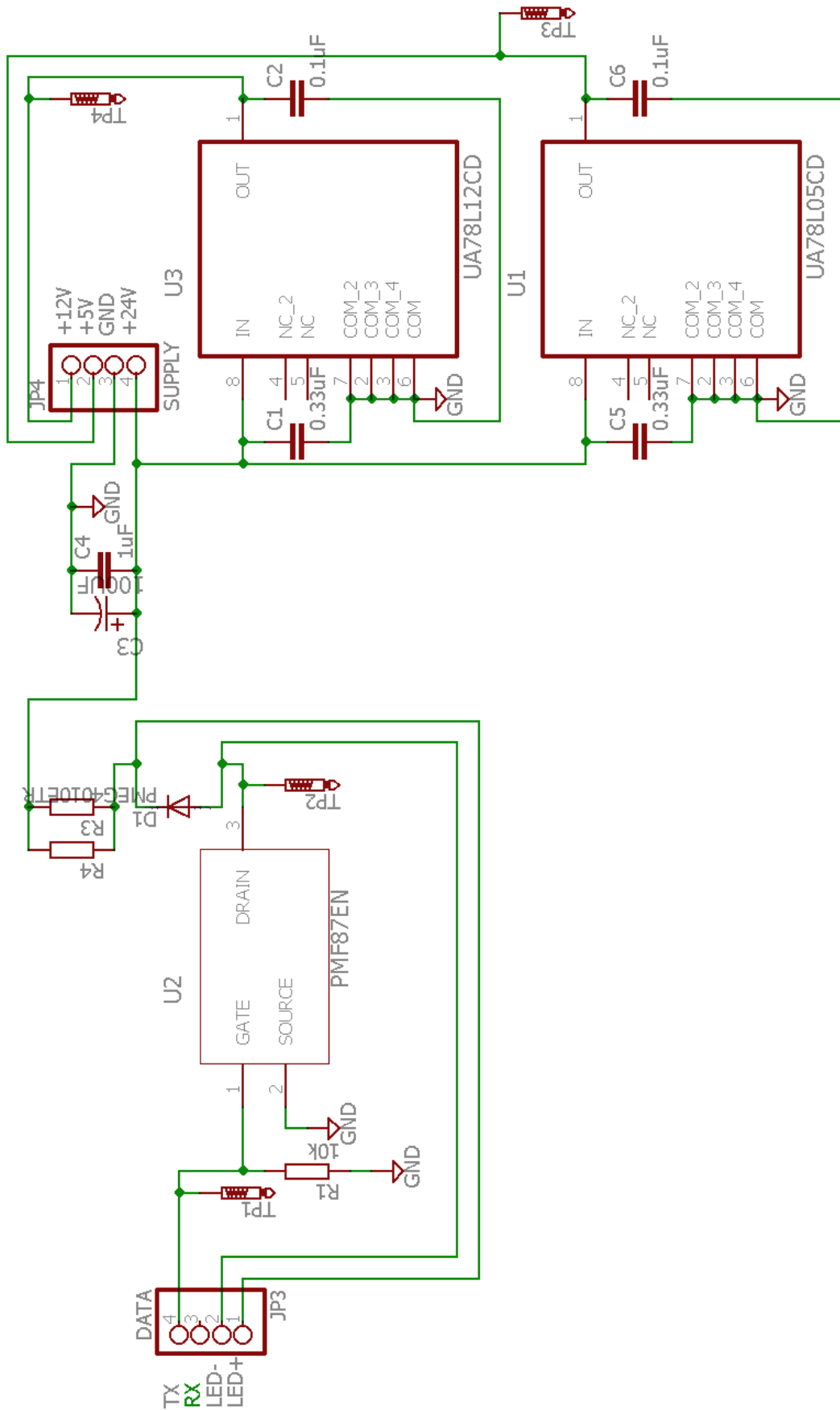


Figure A.1: Initial PCB Schematic - Tx layer.

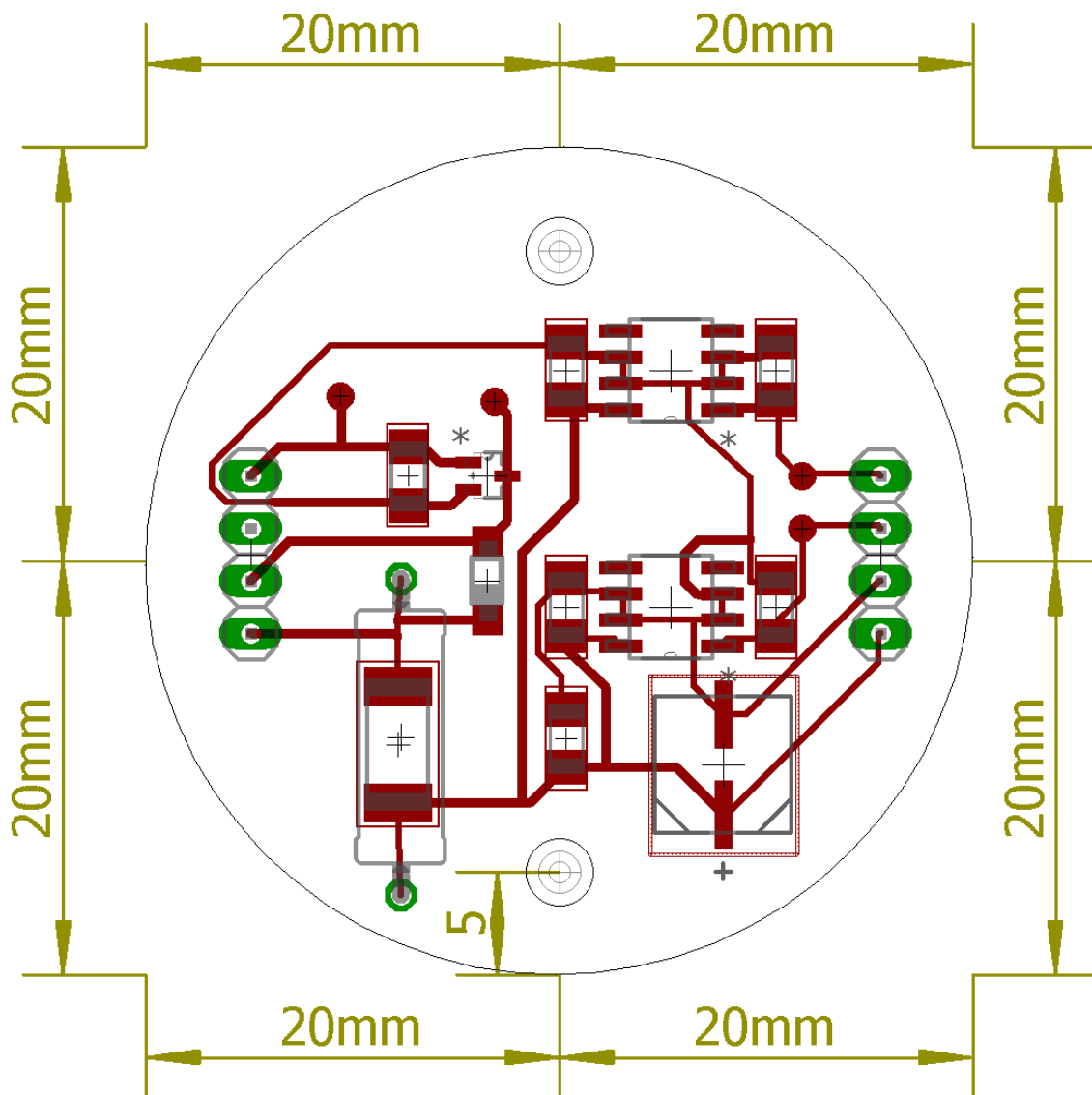


Figure A.2: Initial PCB Footprint - Tx layer (only top layer).



A.1.2 Rx Layer

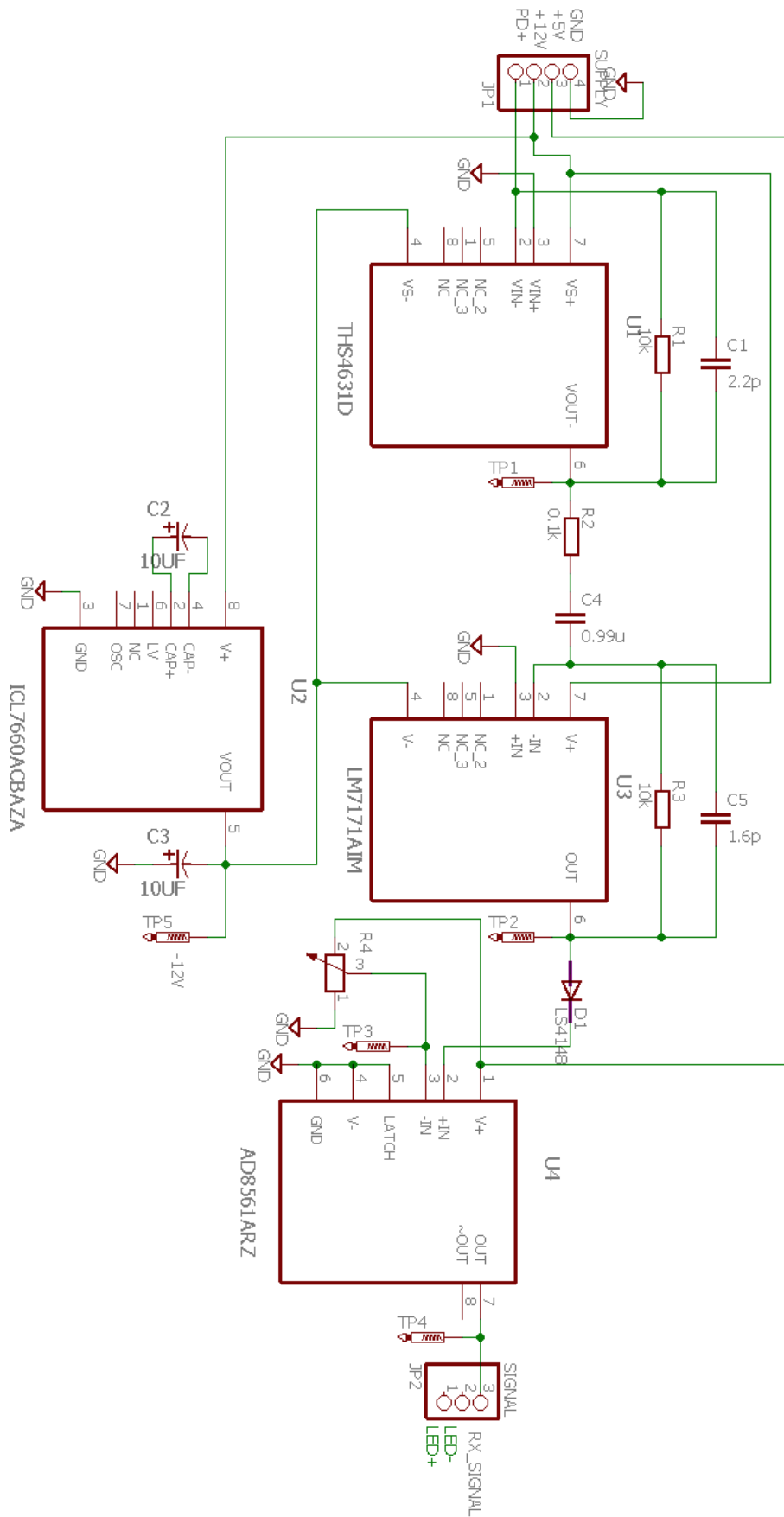


Figure A.3: Initial PCB Schematic - Rx layer.



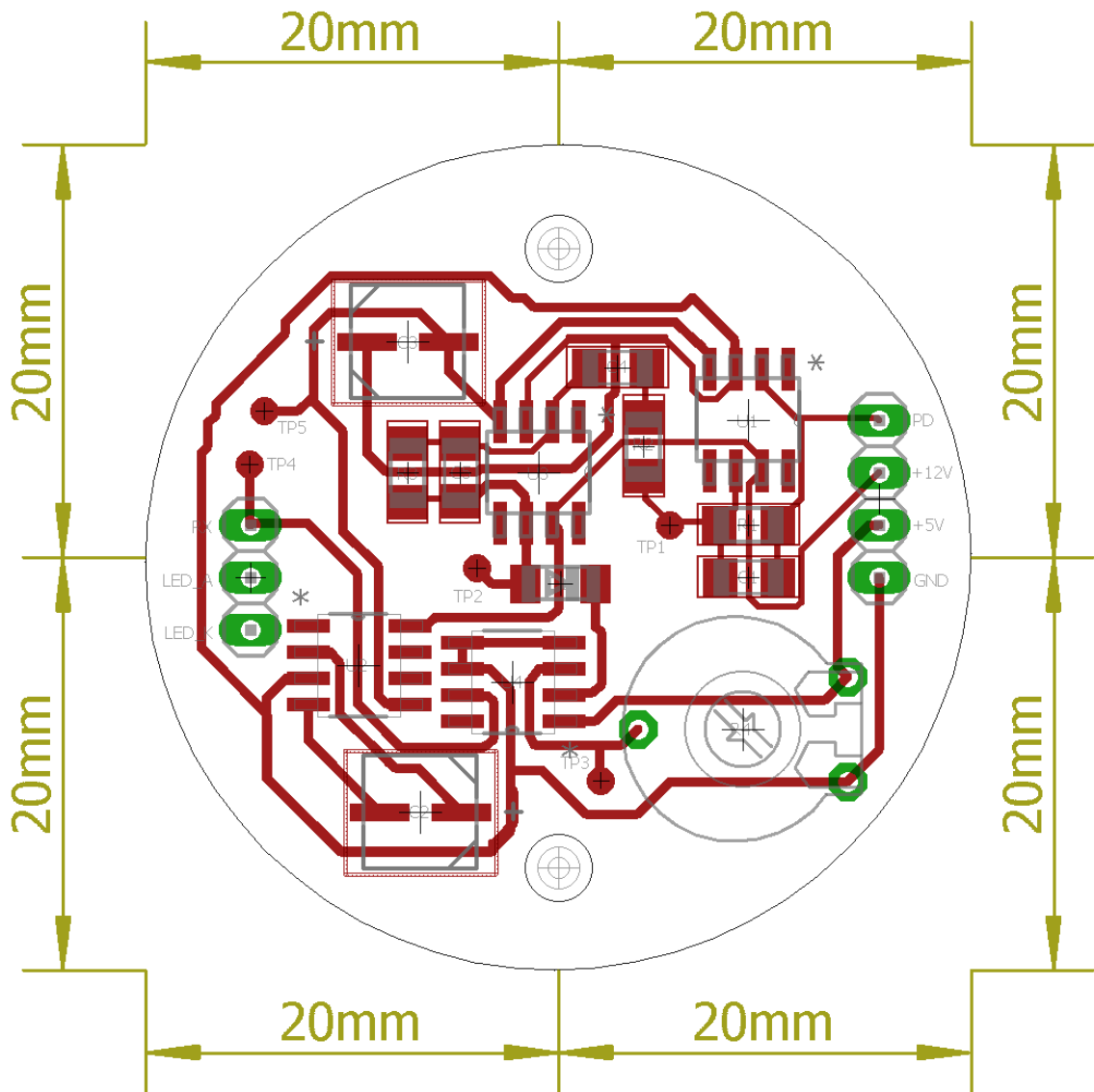


Figure A.4: Initial PCB Footprint - Rx layer (only top layer).



## A.2 Final Version

### A.2.1 Tx Layer

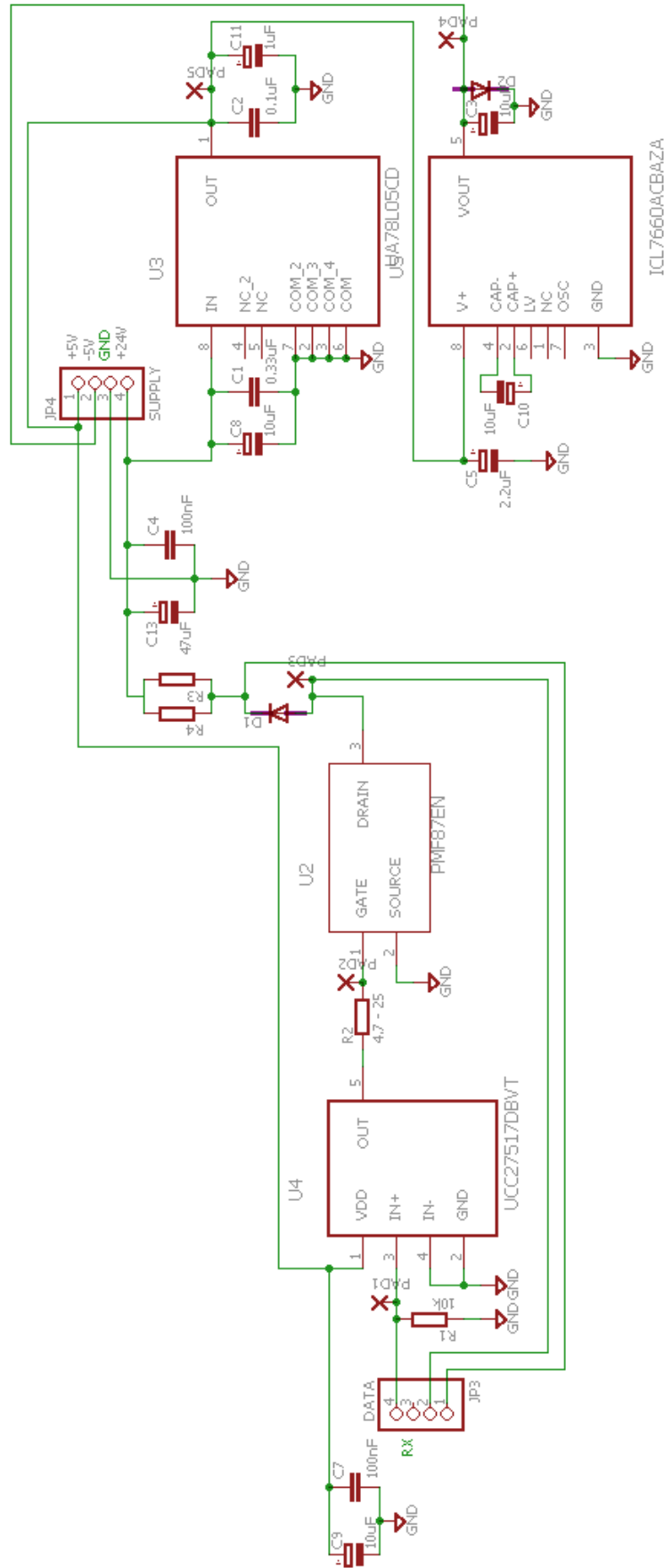


Figure A.5: Final PCB Schematic - Tx layer.

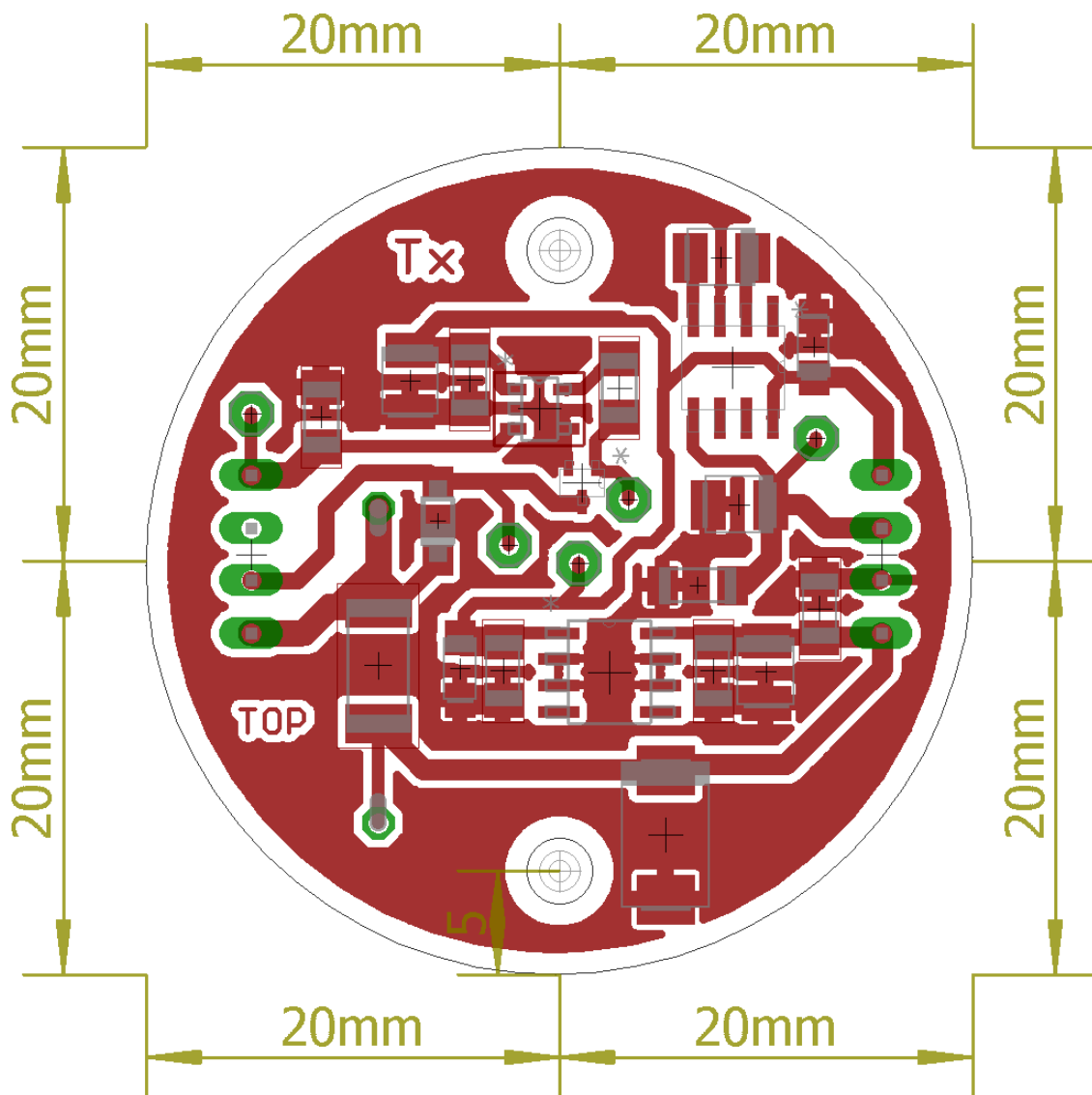


Figure A.6: Final PCB Footprint - Tx layer (only top layer).



### A.2.2 Rx Layer

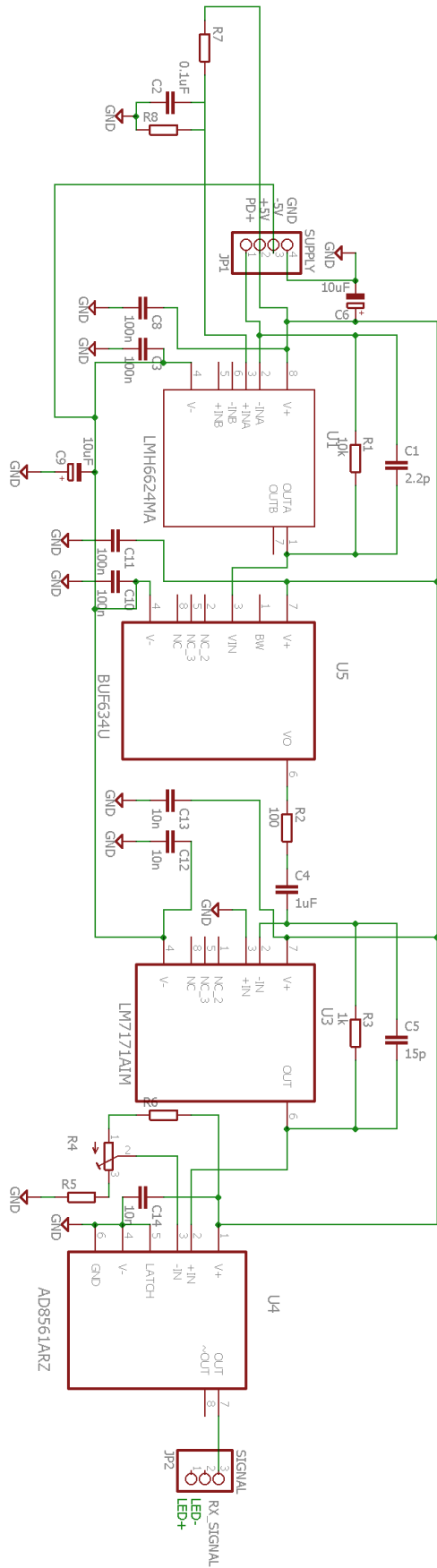


Figure A.7: Final PCB Schematic - Rx layer.

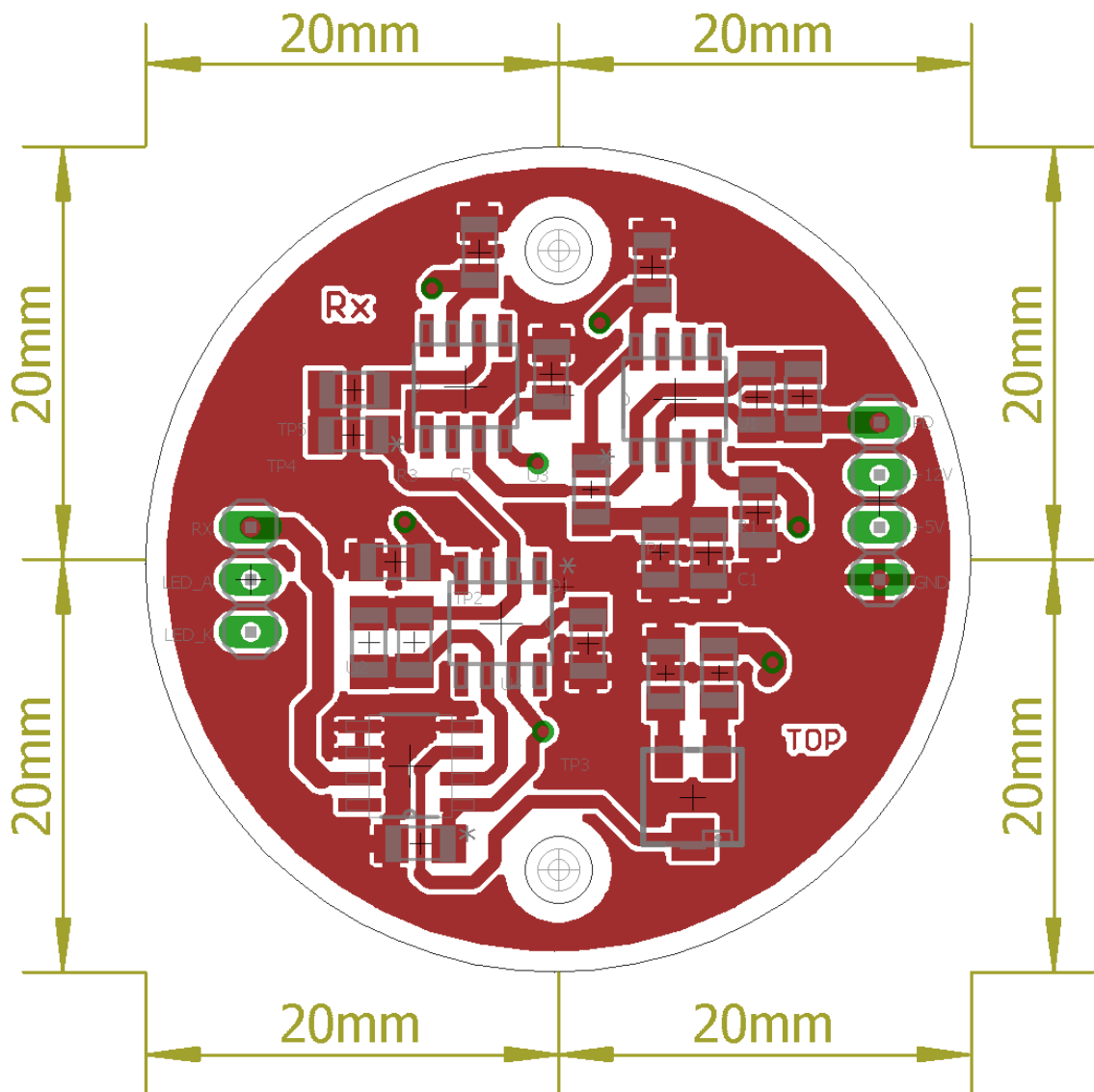


Figure A.8: Final PCB Footprint - Rx layer (Top)

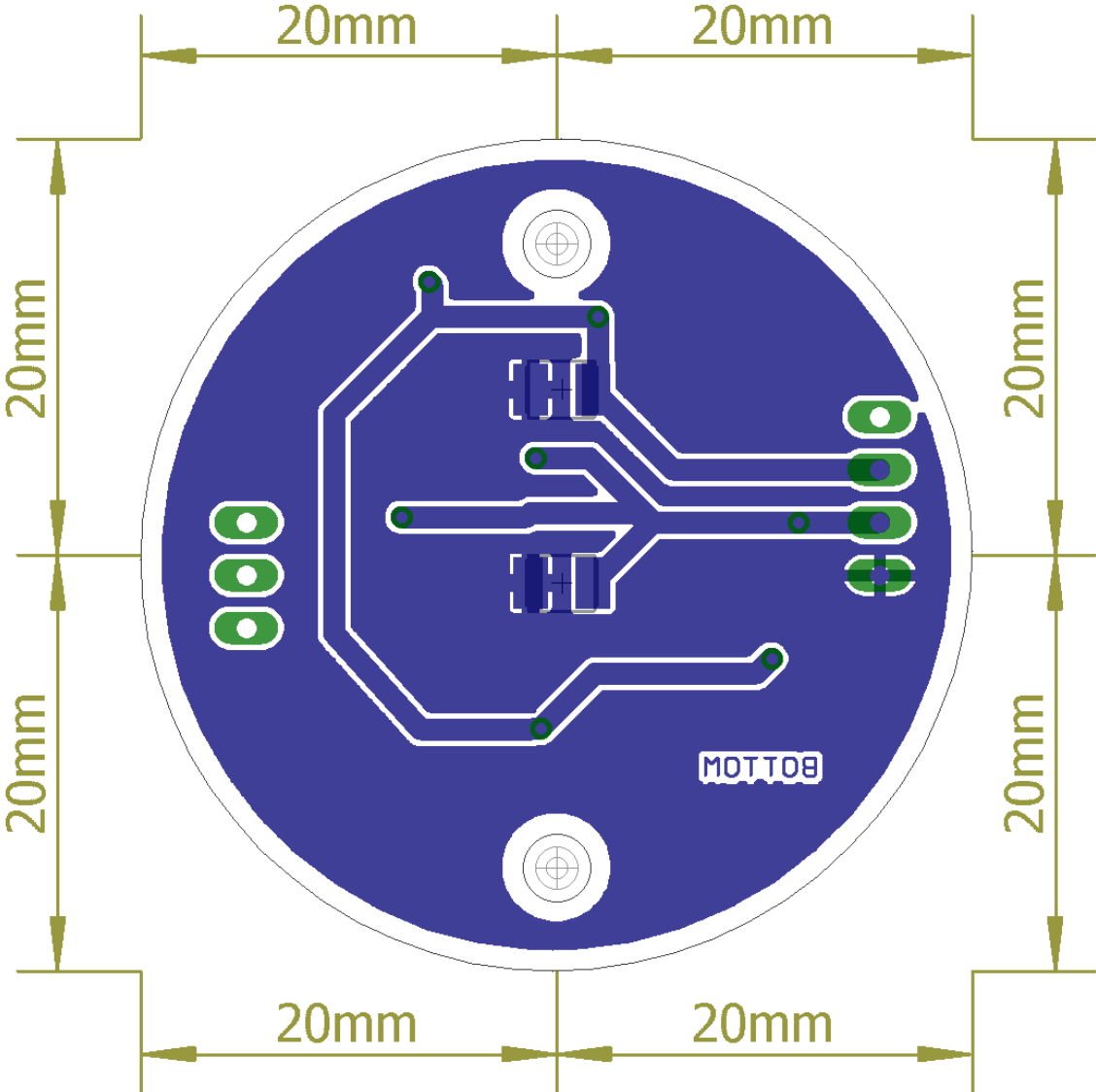


Figure A.9: Final PCB Footprint - Rx layer (Bottom)



# References

- [1] LJ Johnson and F Jasman. Recent advances in underwater optical wireless communications. *Underwater Technology*, 32, 2014.
- [2] William Charles Cox Jr. *Simulation, Modeling, and Design of Underwater Optical Communication Systems*. PhD thesis, North Carolina State University, 2012.
- [3] ST. Datasheet STP30NF10. <http://www.st.com/web/en/resource/technical/document/datasheet/CD00002440.pdf>, 2006. [Online; accessed 23/February/2015].
- [4] Fairchild Semiconductor. Datasheet BS170. <https://www.fairchildsemi.com/datasheets/bs/bs170.pdf>, 2010. [Online; accessed 23/February/2015].
- [5] ON Semiconductors. Datasheet MGSF1N02L. [http://www.onsemi.com/pub\\_link/Collateral/MGSF1N02LT1-D.PDF](http://www.onsemi.com/pub_link/Collateral/MGSF1N02LT1-D.PDF), 2013. [Online; accessed 23/February/2015].
- [6] Pierre-Philippe J. Beaujean, Edward A. Carlson, John Spruance, and Dion Kriel. HERMES - A high-speed acoustic modem for real-time transmission of uncompressed image and status transmission in port environment and very shallow water. In *OCEANS 2008*, pages 1–9. IEEE, 2008.
- [7] Sonardyne. AvTrak 6 Type 8220. <http://www.sonardyne.com/products/positioning/avtrak-6.html>. [Online; accessed 13/February/2015].
- [8] AquaSeNT. Acoustic Modems — Aquatic Sensor Network Technology. <http://www.aquasent.com/acoustic-modems/>. [Online; accessed 13/February/2015].
- [9] Teledyne Benthos. Dashboard - Teledyne Benthos Acoustic Modems. [https://teledynebenthos.com/product\\_dashboard/acoustic\\_modems](https://teledynebenthos.com/product_dashboard/acoustic_modems). [Online; accessed 18/February/2015].
- [10] EvoLogics. Underwater Acoustic Modems. <http://www.evologics.de/en/products/acoustics/index.html>. [Online; accessed 13/February/2015].
- [11] LinkQuest Inc. Underwater Acoustic Modem Models. <http://www.link-quest.com/html/models1.htm>. [Online; accessed 13/February/2015].
- [12] Felix Stephan Schill. *Distributed Communication in Swarms of Autonomous Underwater Vehicles*. PhD thesis, The Australian National University, 2007.
- [13] William C. Cox, Jim a. Simpson, Carlo P. Domizioli, John F. Muth, and Brian L. Hughes. An underwater optical communication system implementing reed-solomon channel coding. In *Oceans 2008*, 2008.

- [14] William Charles Jr. Cox. *A 1 Mbps Underwater Communication System Using a 405 nm Laser Diode and Photomultiplier Tube*. PhD thesis, North Carolina State University, 2008.
- [15] Heather Brundage. *Designing a Wireless Underwater Optical Communication System*. Msc thesis, Massachusetts Institute of Technology, 2010.
- [16] L Lanbo, Z Shengli, and C Jun-Hong. Prospects and problems of wireless communication for underwater sensor networks. *Wireless Communications and Mobile Computing*, 8(8):977–994, October 2008.
- [17] Mohammad-Ali Khalighi, Chadi Gabriel, Tasnim Hamza, Salah Bourennane, Pierre Leon, and Vincent Rigaud. Underwater wireless optical communication; recent advances and remaining challenges. In *2014 16th International Conference on Transparent Optical Networks (ICTON)*, pages 1–4. IEEE, July 2014.
- [18] Brandon M. Cochenour, Linda J. Mullen, and Allan E. Laux. Characterization of the beam-spread function for underwater wireless optical communications links. *IEEE Journal of Oceanic Engineering*, 33(4):513–521, 2008.
- [19] WFS Technologies Ltd. Wireless for Subsea: Subsea Wireless Instrumentation and Control Solutions. <http://www.wfs-tech.com/index.php/products/seatooth/>. [Online; accessed 14/February/2015].
- [20] B Cochenour and L Mullen. Channel response measurements for diffuse non-line-of-sight (NLOS) optical communication links underwater. In *Oceans 2011*, pages 1–5. IEEE, 2011.
- [21] James W Bales and Chryssostomos Chryssostomidis. High-bandwidth, Low-power, Short-range Optical Communication Underwater. In *Proceedings of the 9th International Symposium on Unmanned Untethered Submersible Technology*, pages 406–415, Durham, New Hampshire, USA, 1995.
- [22] Mark Alan Chancey. *Short Range Underwater Optical Communication Links*. Msc thesis, North Carolina State University, 2005.
- [23] N. Farr, a. Chave, L. Freitag, J. Preisig, S. White, D. Yoerger, and P. Titterton. Optical Modem Technology for Seafloor Observatories. In *Proceedings of OCEANS 2005 MTS/IEEE*, pages 1–7. IEEE, 2005.
- [24] N. Farr, a. D. Chave, L. Freitag, J. Preisig, S. N. White, D. Yoerger, and F. Sonnichsen. Optical modem technology for seafloor observatories. In *Oceans 2006*, pages 1–6. Woods Hole Oceanogr. Instn., MA, September 2006.
- [25] Brandon Cochenour, Linda Mullen, and Alan Laux. Phase coherent digital communications for wireless optical links in turbid underwater environments. In *Oceans Conference Record (IEEE)*, pages 1–5. IEEE, 2007.
- [26] Greg Baiden and Yassiah Bissiri. High bandwidth optical networking for underwater untethered telerobotic operation. In *Oceans Conference Record (IEEE)*, pages 1–9. IEEE, 2007.
- [27] Greg Baiden, Yassiah Bissiri, and Andrew Masoti. Paving the way for a future underwater omni-directional wireless optical communication systems. *Ocean Engineering*, 36(9-10):633–640, July 2009.

- [28] Ambalux. High-Bandwidth Underwater Transceivers. <http://www.ambalux.com/underwater-transceivers.html>. [Online; accessed 13/February/2015].
- [29] Frank Hanson and Stojan Radic. High bandwidth underwater optical communication. *Applied Optics*, 47(2):277, 2008.
- [30] Clifford Pontbriand, Norman Farr, Jonathan Ware, James Preisig, and Hugh Popenoe. Diffuse high-bandwidth optical communications. In *Oceans 2008*, pages 1–4. IEEE, 2008.
- [31] M. Doniec, I. Vasilescu, M. Chitre, C. Detweiler, M. Hoffmann-Kuhnt, and D. Rus. AquaOptical: A lightweight device for high-rate long-range underwater point-to-point communication. In *OCEANS 2009, MTS/IEEE Biloxi - Marine Technology for Our Future: Global and Local Challenges*, pages 1–6. IEEE, 2009.
- [32] J.a. Simpson, B.L. Hughes, and J.F. Muth. A spatial diversity system to measure optical fading in an underwater communications channel. In *OCEANS 2009, MTS/IEEE Biloxi - Marine Technology for Our Future: Global and Local Challenges*, pages 1–6, 2009.
- [33] Jim A. Simpson, William C. Cox, John R. Krier, Brandon Cochenour, Brian L. Hughes, and John F. Muth. 5 Mbps optical wireless communication with error correction coding for underwater sensor nodes. In *OCEANS 2010 MTS/IEEE SEATTLE*, pages 1–4. IEEE, September 2010.
- [34] Marek Doniec and Daniela Rus. BiDirectional optical communication with AquaOptical II. In *2010 IEEE International Conference on Communication Systems*, pages 390–394. IEEE, November 2010.
- [35] N. Farr, A. Bowen, J. Ware, C. Pontbriand, and M. Tivey. An integrated, underwater optical/acoustic communications system. In *OCEANS 2010 IEEE-Sydney*, pages 1–6. IEEE, May 2010.
- [36] N. Farr, J. Ware, C. Pontbriand, T. Hammar, and M. Tivey. Optical communication system expands CORK seafloor observatory’s bandwidth. In *OCEANS 2010 MTS/IEEE SEATTLE*, pages 1–6. IEEE, September 2010.
- [37] Jim A. Simpson, Brian L. Hughes, and John F. Muth. Smart Transmitters and Receivers for Underwater Free-Space Optical Communication. *IEEE Journal on Selected Areas in Communications*, 30(5):964–974, June 2012.
- [38] Marek Doniec, Michael Angermann, and Daniela Rus. An end-to-end signal strength model for underwater optical communications. *IEEE Journal of Oceanic Engineering*, 38(4):743–757, October 2013.
- [39] G. Cossu, R. Corsini, A. M. Khalid, S. Balestrino, A. Coppelli, A. Caiti, and E. Ciaramella. Experimental demonstration of high speed underwater visible light communications. In *2013 2nd International Workshop on Optical Wireless Communications (IWOW)*, pages 11–15. IEEE, October 2013.
- [40] Penguin ASI. Penguin Automated Systems Inc. <http://www.penguinasi.com/>. [Online; accessed 16/February/2015].
- [41] SA Photonics. Neptune underwater optical communications. <http://www.saphotonics.com/high-bandwidth-optical-communications/underwater>, 2013. [Online; accessed 16/February/2015].

- [42] Sonardyne. BlueComm Underwater Optical Modem. <http://www.sonardyne.com/products/all-products/instruments/1148-bluecomm-underwater-optical-modem.html>. [Online; accessed 13/February/2015].